POLITECNICO DI MILANO

Master of Science in Biomedical Engineering

Department of Electronics, Information and Bioengineering

Biomechanical model to analyze countermeasure exercises performed on ISS and risks related to incorrect executions

Supervisor: Prof. Giancarlo Ferrigno

Co – supervisor: Prof.ssa Alessandra Pedrocchi

Master Thesis of

Martina Ravizza

Student ID: 874030

Anno accademico 2018/2019

A Mamma e Chiara,

alla nostra Forza.

RINGRAZIAMENTI

Un ringraziamento speciale va al professore Giancarlo Ferrigno, per la stimolante collaborazione di questi mesi che ha permesso di ampliare le mie conoscenze in svariati ambiti, alimentando la mia passione e la mia curiosità.

Ringrazio la professoressa Alessandra Pedrocchi per avermi indirizzata nella scelta di questo percorso.

Ringrazio John DeWitt, biomeccanico del NASA Jhonson Space Center, per i consigli dati durante la programmazione degli esperimenti e per la revisione dei protocolli adottati.

Ringrazio la professoressa Veronica Cimolin per la messa a disposizione del Laboratorio di Analisi della Postura e del Movimento "Luigi Divieti" e per il prezioso aiuto durante la fase di acquisizione dei dati.

ABSTRACT

State of art and aims

During space missions, astronauts are inserted in environment that significatively differs from that on Earth. Weightlessness induces a series of human body changes and adaptations, which involve different systems: cardiovascular, respiratory, visual and musculo-skeletal. The unloading of bones and muscles in microgravity produces rapid and severe mineral loss and reduction of muscle mass and muscle strength. Bone density drops at over 1% per month; the decrease of muscle strength is compared with studies of bed rest that show a diminution of 50% in the first two weeks. Currently, space agencies are planning long-duration missions (LDMs) to flight on Moon and Mars. Unlike the current flights, in which recovery time is not critical, on LDMs these physiological effects must be considered. To prevent this deconditioning, crewmembers follow a specific training protocol pre, during and post-flight. On the International Space Station (ISS), countermeasures exercise devices are present, to allow to perform both cardiovascular and resistive training. Cycle Ergometer with Vibration Isolation and Stabilization (CEVIS) and treadmill COLBERT are used for health of cardiovascular system; the Advance Resistive Exercise Device (ARED) is used to prevent muscle atrophy and bone mineral loss. It simulates the use of free weights in microgravity by generating a constant load, which can be changed from 0 to 272.5 Kg. It permits to perform different target exercises, including normal stance squat, wide stance squat and deadlift. However, the efficacy of these countermeasures is inadequate and the optimal training protocol planning is difficult given that internal bone and muscle forces in microgravity are unknown.

Two aspects have to be considered: firstly, in microgravity body weight is not perceived, so a percentage of body weight has to be applied directly on the shoulders by the ARED bar, causing discomfort and back pain; furthermore, the countermeasures are not

personalized for each astronaut and performance is without neither online nor offline supervision.

This Thesis is inserted in two research projects: "MARcatori biologici e funzionali per la biomedicina aStronautica di PREcisione – MARS-PRE", proposed by Italian Space Agency (ASI) and "ARED Kinematics – Biomechanical quantification of bone and muscle loading to improve the quality of microgravity countermeasure prescription for resistive exercise", which involves European Space Agency (ESA), Neuroengineering and Medical Robotics Laboratory (NearLab) of Politecnico di Milano, Jhonson Space Center (JSC) of National Aeronautics and Space Administration (NASA) and Kayser Italia. The first one aims to find biological and functional anticipatory makers of musculo-skeletal damage, which can occur as a consequence of target exercises performed with incorrect techniques. Then, a system able to automatically detect wrong executions and to correct astronaut in real-time will be developed. ARED Kinematics project wants to improve the subject specific effectiveness of daily exercises on flight by estimating internal body loads. To reach these goals, data collection using motion capture system and force plates pre, during and post flight is needed, as well as biomechanical analysis and statistical comparison of these data.

Currently, no inertial sensor data of exercises performed with ARED are available, but only kinematic and dynamics ones obtained by using a motion capture system and force plates. For this reason, a biomechanical model is needed to simulate sensors placement on body and to extract analog data.

Thus, this work was focused on the validation of a biomechanical model through the OpenSim software with the following purposes: (1) to simulate target exercises in microgravity and with different body weight replacements (BWRs) in order to evaluate the optimal one; (2) to conduct a biomechanical analysis of correct and incorrect techniques of normal stance squat, wide stance squat and deadlift, comparing kinematics and dynamics to evaluate risk of injuries and/or inefficacy of training; (3) to simulate inertial sensors in different body points, obtaining acceleration signals related to correct and wrong exercise techniques. These analyses were carried out with data collected at

Luigi Divieti laboratory at Politecnico di Milano with a barbell and weight and it will be extended to data collected at NASA JSC, whose transfer has ended in the writhing phase of the Thesis.

Experimental protocol

The optoelectronic system used to acquire motion data is SMART DX 400 (BTS Bioengineering S.p.A, Milan, Italy), composed by 8 TV cameras with 100 Hz sampling frequency; ground reaction forces (GRFs) were measured by two force plates (AMTI, USA). A total of 43 retro - reflective markers were placed on body, excluding upper limbs, plus 2 on the extremities of the bar. Data collection was carried out on two subjects (S1 – male, 30 years old, 65 kg, 175 cm; S2 - female, 25 years old, 54 kg, 164 cm), who performed one set of 4 repetitions of normal squat, wide stance squat and normal deadlift with correct executions, similarly to that collected at NASA JSC. Additionally, they performed one set of each kind of incorrect exercise with a number of repetitions varying from 2 to 4 basing on the individual sensation, to avoid injuries. Wrong techniques were proposed and approved by specialists of NASA JSC. External loads were in the range of 60-80% of maximal isometric strength (ISO-MAX) as follow: S1 - 50 kg for squat and wide squat; 80 kg for deadlift; S2 - 40 kg for squat and wide squat; 50 kg for deadlift.

Data processing and biomechanical simulations

Smart Tracker is the software used to track raw data, so to label each marker with specific name and to obtain three-dimensional marker trajectories over time. The open-source software utilized to conduct the biomechanical analysis and the microgravity simulations was OpenSim. Matlab R2018b was used to pre-process data and to create files in formats compatible with OpenSim. Raw data were interpolated with a cubic spline function to fill gaps and filtered with a Butterworth low pass filter with a cut-off frequency of 5 Hz. External loads were added by considering a constant vertical force applied on the shoulders of the model, on the mid-point of the barbell computed basing on the two markers put on the extremities of the bar. For weightlessness simulation, the percentage of body weight chosen was added to the vector that identified the bar and the complementary percentage was divided for two and subtracted to the left and right GRFs. Obtained files needed, the first step for the biomechanical analysis was the model scaling

basing on the anthropometry of each subject. For this scope, a standing position was acquired. Then, inverse kinematics, inverse dynamics, residual reduction algorithm and compute muscle control OpenSim tools were used to obtain joint angles, joint moments and to estimate muscle forces, for each subject and each type of exercise execution.

Regression model to evaluate optimal BWR

A linear regression model algorithm was developed in Matlab R2018b in order to identify the relation between the different BWR loads and joint moments in weightlessness. The inverse dynamics was computed in 0g by incrementing the BWR with step of 10%, ranging from 40% to 100%, in addition to simulation with 0% of body weight. Thus, the dependent variable of the regression model was a vector containing peak or mean joint moments for each BWR and the independent variable a vector with the BWRs.

Inertial sensors simulation and classifier development

Analyses Tool of OpenSim was used in order to simulate inertial sensors, so to extract accelerations data in different body points, related to each kind of training exercise and execution. The chosen points were sternum, sacrum, mid-thigh and mid shank. These data were opportunely elaborated and different features, both in time and frequency domains, were extracted. Principal component analysis (PCA) was used to reduce the feature set and two supervised learning methods were developed and tested to perform a binary classification, so to distinguish correct and incorrect exercises. Methods were feed-forward artificial neural network (ANN) and support vector machine (SVM).

Results and conclusions

Biomechanical comparison between correct and wrong exercise performances - the hypothesis of not equality in terms joint angles and joint moments was statistically demonstrated ($p < 0.05$). Therefore, the chosen categories of incorrectness can be considered suitable to characterize biomarkers, which will anticipate the risk of musculo-skeletal damage due to joint overloading and risk of training inefficacy caused by joint underloading

Optimal BWR - squat results were compared with the ones found in literature, sustaining that current BWR (70-75%) used is suitable for hip joint, but it might underload knee and

ankle joints and overload lumbar joint. The same results were obtained for wide squat and deadlift, but they showed higher BWR for hip joint. Overall, it was observed that optimal BWR changes considering different joints and between subjects. This suggests that find a single load usable for all astronauts and all training exercises could be not adequate. Thus, it may be opportune to create a biomechanical model for each crewmember and to perform simulations to reach the individual optimal BWR. Additionally, think to another way to better distribute the load over the body without applying it only on shoulders might be a solution.

Performance classification based on acceleration signals - PCA reduced the original dataset composed by 302 features to 12 for squat, 9 for wide squat and 10 for deadlift. ANN and SVM accuracies of binary classifications were respectively: 83.3% and 88% for squat; 75% and 71.4% for wide squat; 60% and 85.7% for deadlift. Further investigations are needed to enlarge the dataset and refine the classifier, but these preliminary results could be seen as incentive to consider this approach as working solution.

Outlines of Thesis

The present work is structured as follow:

- Chapter 1: description of physiological adaptations that occur during space missions; review and state of art of countermeasures and motion capture systems used on ISS; aim of the thesis.
- Chapter 2: description of the software used for biomechanical modeling and to conduct the simulations.
- Chapter 3: description of the set-up data collection and their processing; description of the regression model used to find optimal body weight replacement; description of the procedure used for the inertial sensors simulation; development and validation of a primordial classifier.
- Chapter 4: results and discussions.
- Chapter 5: conclusions and future works.
- Appendix A

SOMMARIO

Stato dell'arte e obiettivi

Durante le missioni spaziali, gli astronauti si ritrovano in un ambiente che differisce notevolmente da quello terrestre. L'assenza di gravità provoca una serie di cambiamenti e adattamenti fisiologici del corpo che coinvolgono diversi sistemi: cardiocircolatorio, respiratorio, visivo e muscolo scheletrico. In microgravità le ossa e i muscoli non vengono sollecitati, questo causa una rapida e significativa demineralizzazione ossea e riduzione della forza muscolare. La densità dell'osso diminuisce dell'1% ogni mese; la perdita della forza muscolare è stata comparata con studi di "bed rest", ovvero di riposo forzato a letto, che ne hanno rivelato un calo del 50% nelle sole prime due settimane. Attualmente, le agenzie spaziali stanno pianificando missioni a lunga durata (LDMs) che hanno come obiettivo viaggi sulla Luna e su Marte. Le missioni correnti richiedono durate relativamente brevi, in cui il tempo di recupero non è critico; in visione dei viaggi a lunga durata, invece, gli effetti fisiologici devono essere considerati. Per prevenire il decondizionamento muscolo-scheletrico, i membri dell'equipaggio seguono un protocollo di allenamento specifico prima, durante e dopo la missione. Sulla Stazione Spaziale Internazionale (ISS) sono presenti diversi dispositivi che consentono di effettuare esercizi sia aerobici che resistivi. Sono a disposizione un cicloergometro (CEVIS) e un treadmill (COLBERT) per il mantenimento della salute del sistema cardio vascolare e l'Advance Resistive Exercise Device (ARED) per prevenire l'atrofia muscolare e la perdita di minerali ossei. ARED simula l'uso di pesi esterni generando un carico costante che può variare da 0 a 275.5 Kg. Consente di eseguire diversi esercizi target, tra cui il normal stance squat, il wide stance squat e il deadlift. Tuttavia, l'efficacia di queste contromisure non è adeguata e la pianificazione di un programma di allenamento ottimale è complesso in quanto non si conoscono le forze interne agenti durante gli allenamenti a bordo della ISS.

Due aspetti devono essere particolarmente presi in considerazione: innanzitutto, in microgravità il peso del corpo non è percepito, per cui una percentuale dello stesso deve essere aggiunta direttamente sulle spalle mediante la barra di ARED, risultando scomodo e doloroso per le spalle e causando dolori alla schiena; inoltre, le contromisure non sono personalizzate per ogni astronauta e gli allenamenti non vengono monitorati, né online, né offline.

Questa tesi è inserita in due progetti di ricerca: "MARcatori biologici e funzionali per la biomedicina aStronautica di PREcisione – MARS-PRE", proposto dall'Agenzia Spaziale Italiana (ASI) e "ARED Kinematics – Biomechanical quantification of bone and muscle loading to improve the quality of microgravity countermeasure prescription for resistive exercise", che coinvolge l'Agenzia Spaziale Europea (ESA), il laboratorio di Neuroingegneria e Robotica Medica (NearLab) del Politecnico di Milano, il Jhonson Space Center (JSC) della National Aeronautics and Space Administration (NASA) e l'azienda Kayser Italia. L'obiettivo del primo progetto è quello di fornire marcatori funzionali personalizzati di correttezza dell'esecuzione degli esercizi di contromisure. Verrà quindi sviluppato un sistema di machine learning basato su sensori inerziali utilizzabili in microgravità che sarà in grado di riconoscere automaticamente le esecuzioni scorrette degli esercizi e di fornire un feedback correttivo in real-time. Il progetto ARED – Kinematics mira invece al miglioramento dell'efficacia degli allenamenti individuali stimando le forze interne in gioco. Per raggiungere questo scopo, verranno acquisiti dati cinematici e dinamici utilizzando un sistema di cattura del movimento e delle piattaforme di forza. Le prove verranno effettuate prima, durante e dopo le missioni e verranno quindi condotte delle analisi biomeccaniche e dei confronti statistici tra i risultati.
Attualmente, dati provenienti da sensori inerziali collezionati durante l'esecuzione degli esercizi con ARED non sono a disposizione, sono invece disponibili dati cinematici e dinamici acquisiti con un sistema di cattura del movimento e con piattaforme di forza. Per questo motivo, è necessario sviluppare un modello biomeccanico in modo da simulare il posizionamento dei sensori sul corpo e per estrarre dati analoghi.

Dunque, questo lavoro si è focalizzato sulla validazione di un modello biomeccanico attraverso il software OpenSim con i seguenti propositi: (1) simulare gli esercizi target in

microgravità e con diverse percentuali di peso corporeo per trovare quella ottimale; (2) condurre analisi biomeccaniche delle esecuzioni corrette e scorrette di squat, wide stance squat e deadlift, confrontandone la cinematica e la dinamica per valutare il rischio di infortuni e/o l'inefficacia dell'esercizio; (3) simulare i sensori inerziali posizionati in diversi punti del corpo, al fine di ottenere segnali di accelerazione relativi alle tecniche corrette e scorrette di esecuzione degli esercizi. Queste analisi sono state effettuate con dati acquisiti presso il laboratorio Luigi Divieti del Politecnico di Milano con un bilanciere e dei pesi, ma verranno estese a dati acquisiti al NASA JSC il cui trasferimento si è concluso in fase di stesura della tesi.

Protocollo sperimentale

Il sistema optoelettronico utilizzato per le acquisizioni è SMART DX 400 (BTS Bioengineering S.p.A, Milan, Italia), composto da 8 telecamere con una frequenza di campionamento di 100 Hz; le forze di reazione al terreno (GRFs) sono state misurate con due piattaforme di forza (AMTI, USA). Sono stati posizionati 43 marker passivi su tutto il corpo, ad esclusione degli arti superiori, e due sono stati aggiunti alle estremità del bilanciere. I dati sono stati acquisiti su due soggetti (S1 – maschio, 30 anni, 65 kg, 175 cm; S2 - femmina, 25 anni, 54 kg, 164 cm) che hanno eseguito un set di 4 ripetizioni di squat, wide stance squat e deadlift in configurazione corretta dell'esercizio, in modo analogo a quanto fatto al NASA JSC. In aggiunta, hanno eseguito un set per ogni tipo di scorrettezza, con un numero di ripetizioni che è variato da 2 a 4 in base alle sensazioni individuali, per evitare infortuni. Le scorrettezze sono state proposte e approvate dagli specialisti del NASA JSC. Il carico esterno utilizzato è stato all'interno del range di 60-80% della massima forza isometrica (ISO-MAX) come segue: S1 - 50 kg per squat e wide squat; 80 kg per deadlift; S2 - 40 kg per squat e wide squat; 50 kg per deadlift.

Elaborazione dei dati e simulazioni biomeccaniche

Smart Tracker è il software utilizzato per il tracking dei dati grezzi, quindi per etichettarli con un nome specifico e per ottenere le traiettorie tri-dimensionali dei marker nel tempo. Il software open source usato per condurre le analisi biomeccaniche e le simulazioni in microgravità è OpenSim. Matlab R2018b è stato invece utilizzato per il pre-processing dei dati e per creare file in formati compatibili con OpenSim. Le traiettorie dei marker sono

state interpolate con una funzione cubica spline e filtrati mediante un filtro Butterworth passa-basso con una frequenza di taglio di 5 Hz. I carichi esterni sono stati aggiunti considerandoli come force costanti verticali applicate sulle spalle del modello, nel punto medio del bilanciere calcolato considerando i marker posti alle sue estremità. Per le simulazioni in assenza di gravità, la percentuale di peso corporeo da aggiungere al carico è stata addizionata al vettore identificativo della forza espressa dalla barra e la percentuale complementare è stata divisa per due sottratta alle GRFs di entrambi i lati. Ottenuti i file necessari, il primo step per l'analisi biomeccanica è stato quello di scalare il modello sulla base dell'antropometria del soggetto. A questo proposito, è stata acquisita una posizione statica per alcuni secondi. Dopodiché, sono stati utilizzati appositi tool di OpenSim per ottenere angoli articolari, momenti articolari e stimare le forze muscolari in gioco, per ogni soggetto e per ogni tipologia d'esercizio.

Modello di regressione per valutare il BWR ottimale

Per identificare la relazione tra le diverse percentuali di peso da aggiungere al carico esterno (BWR) e i momenti articolari, è stato sviluppato un modello di regressione con Matlab R2018b. La cinematica inversa è stata calcolata in 0g incrementando il BWR dal 40% al 100% con step di 10%, in aggiunta alle simulazioni effettuate considerando lo 0% del peso corporeo. Quindi, la variabile dipendente del modello di regressione è stato un vettore contenente le medie o i picchi dei momenti articolari per ogni BWR e la variabile indipendente un vettore contenente le diverse percentuali di peso considerate.

Simulazione dei sensori inerziali e sviluppo del classificatore

Il tool di OpenSim sfruttato per simulare i sensori inerziali è stato Analyse Tool, grazie al quale sono state estratte le accelerazioni nei punti del corpo desiderati e relative a ogni tipologia d'esercizio. I punti scelti sono stati lo sterno, il sacro, mezza coscia e mezza tibia. I dati sono stati opportunamente elaborati e da essi sono state estratte variabili nel dominio del tempo e delle frequenze. L'analisi delle componenti principali (PCA) è stata utilizzata per ridurre la dimensione del dataset e due metodi di apprendimento supervisionato sono stati sviluppati e testati per effettuare una classificazione binaria, quindi per distinguere le esecuzioni corrette da quelle errate. Gli algoritmi di machine

learning considerati sono stati una rete neurale artificiale (ANN) feed-forward e il support vector machine (SVM).

Risultati e conclusioni

Confronto tra la biomeccanica degli esercizi corretti e scorretti – l'ipotesi di disuguaglianza tra angoli articolari e momenti articolari è stata statisticamente dimostrata ($p < 0.05$). Dunque, le categorie di scorrettezza scelte possono essere considerate adatte per la caratterizzazione dei biomarcatori che anticiperanno il rischio di danneggiamento muscolo-scheletrico dovuto a un sovraccarico dell'articolazione o il rischio di inefficacia dell'allenamento dovuto a una sollecitazione insufficiente.

BWR ottimale – i risultati ottenuti per lo squat sono stati confrontati con i dati presenti in letteratura, sostenendo che il BWR attualmente utilizzato (70-75%) è adeguato per l'articolazione dell'anca, ma troppo basso per ginocchio e caviglia ed eccessivo per la lombare. Le analisi del wide squat e del deadlift hanno supportato queste considerazioni, ma hanno mostrato un BWR più alto per l'articolazione dell'anca rispetto allo squat. I risultati suggeriscono che l'utilizzo di un unico valore per tutti gli astronauti e indipendentemente dall'esercizio potrebbe essere inadeguato. Sarebbe invece opportuno creare un modello biomeccanico per ogni membro dell'equipaggio ed effettuare delle simulazioni personalizzate per il calcolo del BWR ottimale. Inoltre, si potrebbe pensare a una via alternativa per la distribuzione del carico in modo omogeneo lungo il corpo, evitando quindi di applicarlo interamente sulle spalle.

Classificazione della performance basata su segnali di accelerazione – con la PCA i dataset originari includenti 302 variabili sono stati ridotti a 12 per lo squat, 9 per il wide squat e 10 per il deadlift. Le accuratezze dell'ANN e del SVM per la classificazione binaria sono state rispettivamente: 83.3% e 88% per lo squat; 75% e 71.4% per il wide squat; 60% and 85.7% per il deadlift. Sono necessarie ulteriori analisi per aumentare la dimensione dei dataset e per rifinire il classificatore, ma questi risultati preliminari possono essere visti come incentivanti per considerare questo approccio come possibile soluzione.

Struttura della tesi

Il lavoro presentato è strutturato come segue:

- Capitolo 1: descrizione degli adattamenti fisiologici che avvengono durante le missioni spaziali; review e stato dell'arte delle contromisure e dei sistemi di cattura del movimento adottati a bordo della ISS; scopo della tesi.
- Capitolo 2: descrizione del software utilizzato per la modellizzazione biomeccanica e per effettuare le simulazioni.
- Capitolo 3: descrizione del set-up adottato per l'acquisizione dei dati e della loro elaborazione; descrizione del modello di regressione utilizzato per il calcolo della percentuale del peso corporeo ottimale da aggiungere al carico; descrizione della procedura di simulazione dei sensori inerziali; sviluppo e validazione di un classificatore primordiale.
- Capitolo 4: risultati ottenuti e discussioni.
- Capitolo 5: conclusioni e sviluppi futuri.
- Appendice A

LIST OF CONTENTS

LIST OF FIGURES

LIST OF TABLES

LIST OF ABBREVIATIONS

ANN	Artificial Neural Network
ARED	Advanced Resistive Exercise Devices
ASCR	Astronaut Strength, Conditioning and Rehabilitation
ASI	Agenzia Spaziale Italiana
ASIS	Anterior Superior Iliac Spine
BWR	Body Weight Replacement
CMC	Compute Muscle Control
CNN	Convolutional Neural Network
CO	Correct
ESA	European Space Agency
FFT	Fast Fourier Transform
GRF	Ground Reaction Force
HB	Hyperextended Back
ID	Inverse Dynamics
IK	Inverse Kinematics
IMU	Inertial Measurement Unit
IR	Infra-Red
iRED	interim Resistive Exercise Device
ISO-MAX	Maximal Isometric Strength

ISS	International Space Station
JSC	Johnson Space Center
KOT	Knees Over Toes
LDM	Long Duration Missions
LOSOCV	Leave One Site Out Cross Validation
MARS-PRE	MARcatori biologici e funzionale per la biomedicina aStronautica di PREcisione
MOCAP	MOtion CAPture
NASA	National Astronautics and Space Administration
PCA	Principal Component Analysis
PSIS	Posterior Superior Iliac Spine
RB	Rounded Back
RH	Raised Heels
RoM	Range of Motion
RRA	Residual Reduction Algorithm
SB	Shoulder behind Bar
SVM	Support Vector Machine
TVC	TeleVision Camera
VIS	Vibration Isolation System
VK	Valgus Knees
WP	Word Package

CHAPTER 1
INTRODUCTION

1.1 Physiological adaptation during long-duration space missions

From 1961, when Yuri Gagarin completed a single orbit of the Earth for the first time, over five hundred people have flown in space. Nowadays, astronauts participate frequently in long-duration missions (LDM), which last approximately six months. Data collected in this period allowed to understand that the space is an extreme environment for human body due to a prolonged exposure to different stimuli such as acceleration forces, radiations and weightlessness. In the last fifty years, several studies about physiological adaptations during spaceflights revealed alterations of different systems: cardiovascular, respiratory, visual and musculo-skeletal (Demontis *et al.*, 2017; Macias *et al.*, 2015; Prisk *et al.*, 2014).

During missions, astronauts are exposed to galactic cosmic rays, which include charge ions, and to solar proton events. In a first time, these can cause nausea, vomiting and falling blood count (Donnelly *et al.*, 2010); in long-term, there are serious risks for carcinogenesis and degenerative diseases (Cucinotta *et al.*, 2006). Currently, only short-time mission data are available to conduct studies and, consequently, risks related to future long-term lunar or Mars missions are not clearly defined. Now, only simple countermeasures such as shielding or radio protective drugs are adopted to avoid these

problems, but probably these could not be enough to safeguard human, so further investigations are needed (Cucinotta *et al.*, 2013).

The immediate effect of microgravity regards a different blood and fluid distribution in the body. On Earth, the arterial pressure is higher in the feet and lower in the head, 200 mmHg and 70 mmHg respectively. In orbit the situation changes: the gradient of pressure is almost absent, so the brain is subjected to a higher pressure than that in normal conditions (figure 1).

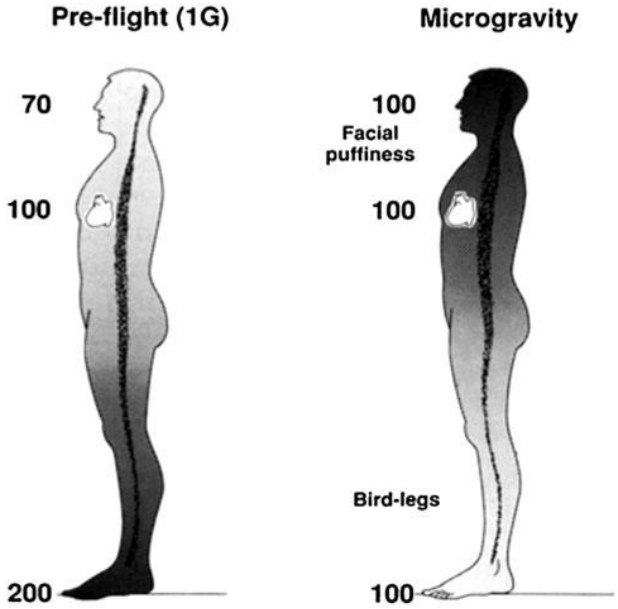

Figure 1: Hypotetical arterial blood pressure in 1-G (left) and microgravity (right) (from Hargens *et al.*, 2012).

It was demonstrated that this shift leads to facial edema and to increase intracranial brain pressure, which may push in the back of eyes causing vision problems resulting from anatomical alterations (Kramer *et al.*, 2012). As reported, several tests before and after missions are conducted in order to recognize such structural deformations. A large amount of ophthalmic procedures and imaging technology were initiated, finding that, actually, a large proportion of subjects do not show change in visual acuity, suggesting that genetic polymorphisms factors may play a role in developing eye problems in weightlessness (Zwart *et al.,* 2012). Furthermore, after few minutes of exposition to microgravity, crewmembers can suffer from the space adaption syndrome, called also space motion sickness. This is due to an alteration in the response of baroceptor, nervous

and endocrine systems in absence of gravity. The vestibular and the visual systems send different signals to the brain and the result is disorientation, nausea, vomiting, headache and general sickness; the symptoms gradually disappear over 48-72 h. In addition, cardiovascular dysfunctions were documented. Space missions could generate anemia, hemolysis (Markin *et al.*, 1998) and variations in red blood cell membrane phospholipid composition (Rizzo *et al.*, 2012).

Regarding the ventilatory system, data collected during Spacelab missions 1 and 2 showed that weightlessness induces a rising of the respiratory frequency and a reduction of the dead space (Donnelly *et al.*, 2010). Other studies based on 6-months stay on ISS demonstrated a lower O_2 consumption and CO_2 production (Prisk *et al.*, 2014). This probably happens because of a diminution of muscle work and to the fact that the different perfusion between upper-right and left-lower regions might require less frequent and deep ventilation by the respiratory muscles (Demontis *et al.*, 2017).

The unloading of the musculo-skeletal system in weightlessness condition produces a remodeling of that system, which shows a progressive resorption of bone and a reduction of both muscle mass and strength. In normal gravity, tissue mass is maintained thanks to a continuous cellular turnover; in space this equilibrium is perturbated, evoking a bone's density dropping at over 1% per month due to mineral losing. The rate of bone loss was compared with that of elderly men and women, which range from 1% to 1.5% per year, demonstrating the presence of risk of osteoporosis-related fractures later in life of the astronauts without an appropriate rehabilitation after returning to Earth (Abadie *et al.,* 2015). Regarding the muscle atrophy, the main reason is a decrease in proteins synthesis. To better understand many physiological responses to microgravity, uninterrupted bed rest was found to be a suitable model to simulate the behavior. These researches showed a 50% reduction in skeletal muscle protein synthesis during the first two weeks of bed rest (Ferrando *et al.,* 1996). Furthermore, it was demonstrated that the muscles located in the trunk and legs are the main subjected to atrophy, especially the ones involved in supporting the body weight in normal gravity, that are the ones located in correspondence with lumbar spine, femoral neck, trochanter, pelvis, calcaneus and leg. Focusing on the spine, in absence of gravity it is stretched and this causes lower back pain. As a consequence of muscle loss, crewmembers manifest weakness post-flight, muscle fatigue, lack of coordination and low back ache.

It is evident how it is important to have specific training plans pre-flight, in-flight and post-flight. Pre-flight exercises have multiple scopes: (a) to support astronauts in maintaining an over-all fitness level, (b) to collect data in order to individually tailor the in-flight training protocols and (c) to prepare them by replicating the ISS exercise countermeasures. Post-flight exercise reconditioning is necessary to correct any alteration resulting from the microgravity adaptation and the re-adaptation to Earth's gravity. A special attention needs to be given to the in-flight exercises training.

1.2 In-flight countermeasures on ISS

The International Space Station (ISS) (figure 2) is a low Earth orbital space facility used as habitat for crew. It is used as an orbital microgravity laboratory, a life-sciences one, a test area for new technologies and a platform for astronomical and Earth observations.

Figure 2: International Space Station (ISS).

It has a modular structure which is reconfigurable basing on the crewmembers' needs. Especially, it presents 3 nodes: node 1 (Unity) connects U.S.A and Russian segments of the ISS; node 2 connects U.S.A, European and Japanase laboratories; node 3 (Tranquillity)

provides habitation functions including hygiene, sleeping and training compartments. The last one, is the most modern of ISS, it was built by the European Space Agency (ESA) and the Italian Space Agency (ASI) and it hosts the training area of the Station (figure 3).

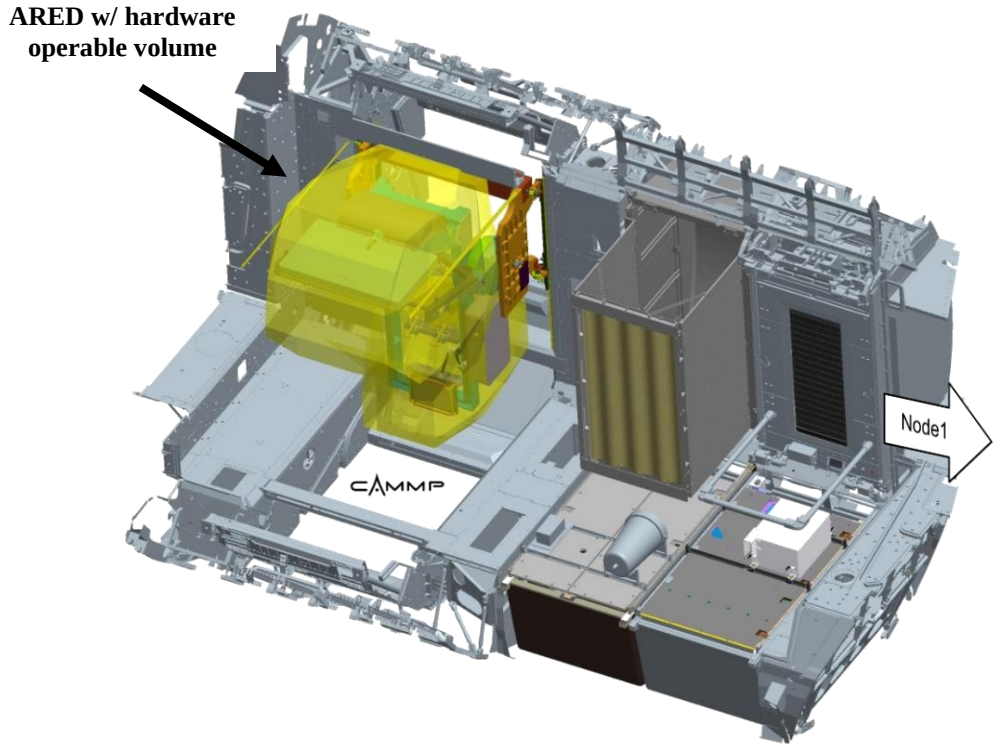

Figure 3: Node 3 configuration with the Advanced Resistive Exercises Devices (ARED) system.

In-flight countermeasures exercises devices have changed over time as shown in table 1.

Table 1: Historical overview of exercise countermeasure hardware available on ISS for ESA's eight long-duration missions to the International Space Station (ISS) (from Petersen *et al.*, 2016).

Year	Hardware used by ESA crew on ISS	ESA mission
2000 – 2009	Treadmill (TVIS, SB-1)	LDM 1-3
2000 – 2009	iRED	LDM 1-3
2009 -	Treadmill (T2), ARED	LDM 3-8
2013 -	Treadmill BD-2	LDM 6-8
2001 -	Cycle ergometer (CEVIS, VELO)	LDM 1-8

Two cycle ergometers and two treadmills are available for cardiovascular exercises. The Cycle Ergometer with Vibration Isolation and Stabilization (CEVIS) and the VELO-ergometer provide workloads from 25-350 Watts and 100-250 Watts respectively. The 2nd generation of the treadmill, called COLBERT or T2, and the D-2 treadmill provide motorized speed up to 20.4 km/h and 20 km/h respectively.

Resistance exercise was previously performed by using the interim Resistive Exercise Device (iRED), which was substituted by the Advanced Resistive Exercise Device (ARED) (figure 4) in 2009 because of its inefficacy on maintaining muscle mass, muscle strength and bone mineral density (Lang *et al.,* 2004; Trappe *et al.,* 2009).

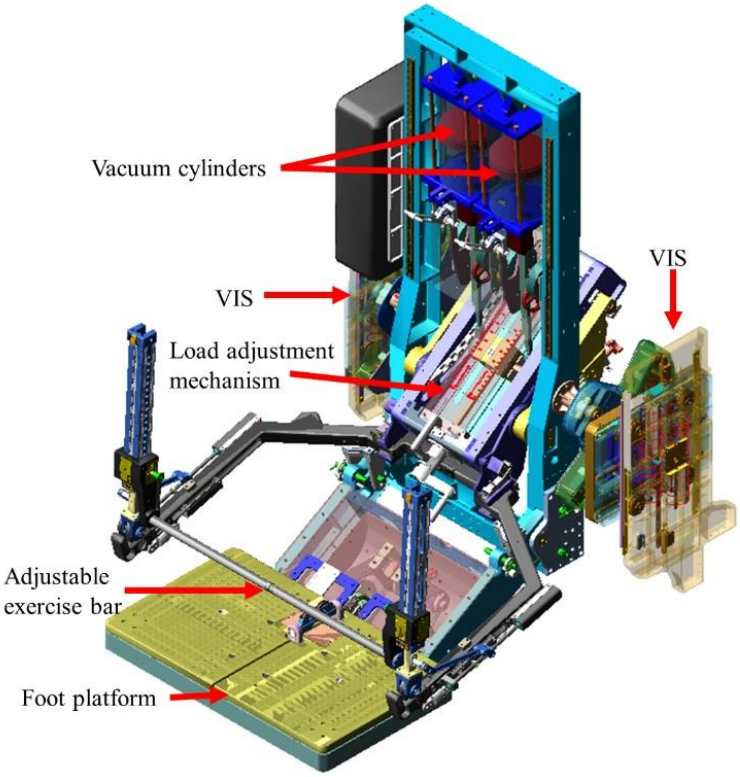

Figure 4: ARED/VIS module (from Appel Knowledge Services, 2012). Foot platform provides the docking station to perform exercises and incorporates two force plates used to measure Ground Reaction Forces (GRFs). Vacuum cylinders provide the force to the adjustable exercise bar, which includes the wishbone arm and the lift bar components. Loads are modified by turning a load adjustment handle in the load adjustment mechanism. Vibration Isolation System (VIS) avoids any transmission of vibrations to the ISS by absorbing shocks.

ARED simulates the use of free weights in microgravity by generating a constant load. The resistive force is supplied by two piston-driven vacuum cylinders with an adjustable load: from 0 to approximately 2670 N (0 to 272.5 Kg on Earth) for bar exercises. To avoid any transmission of forces to the ISS during exercising, the ARED is attached to the station with a Vibration Isolation System (VIS), which absorbs shocks thanks to springs and dampers.

ARED consents to carry out up to 29 exercises including squat, wide stance squat, single leg squat and deadlift. These exercises are performed by adding an external load as a percentage of individual maximal isometric strength (ISO-MAX) tested before flight. Currently, training approach is planned specifically for each astronaut and includes three phases (Petersen *et al*., 2016) in which the load is gradually increased:

I. Adaptation phase: starting from the second day after arrival on ISS, it takes 2-3 weeks during which cycle ergometer exercises are performed, beginning from 1 h per day and with an increase up to 2.5 h per day. The intensity is relatively low.
II. Main phase: for 130 – 250 days, resistance exercise load has to be increased, so each week it is incremented by 3-5% of ISO-MAX reaching at least its 80%. Running and cycling speeds are augmented basing on the individual performance.
III. Preparation for re-entry phase: during the last 3-4 weeks of flight the loads of resistive exercises are maintained high.

A critical aspect to consider in microgravity is that the body weight is not perceived as on Earth due to the reduced or absent gravity acceleration. For this reason, all load must be applied via the ARED bar. At the moment, a replacement of almost 70-75% of body weight is used, basing on the personal experience and feedback of astronaut.

DeWitt *et al* (2011) and Mummidivarapu *et al.* (2017) conducted a quantitative analysis to determine the suitable body weight replacement for squat exercise. The first study assumed that the joint work was positively related to BWR load and concluded that a replacement of 66.77±4.92% for hip, 88±4.17% for knee and 96.05±1.26% for ankles are appropriate to replicate the 1G behavior; in the second study they conducted the same analysis, but considering joint moments, joint loads and muscle forces and computing a weighted sum of the resulting percentage for each joint. They showed an optimized BWR of 71% for joint moment, of 84% for muscle forces and 75% for joint reaction loads.

Until now, no investigation has been explored about the optimal BWR for deadlift and wide stance squat and the same percentage has been applied for each exercise; therefore, one of the objectives of this thesis was to extend this analysis to the other mentioned techniques, as better explained in Chapter 2.

1.2.1 Target exercises on ISS

Standard exercises performed during each training session are normal stance squat, wide stance squat and deadlift. Subjects have to undertake extensive training to guarantee correct performance with ARED in order to avoid any injury or inefficacy. Following, it is presented an explanation of the optimal techniques of these exercises, reviewed and approved by the NASA Astronaut Strength, Conditioning, and Rehabilitation (ASCR) specialists.

Normal stance squat and wide stance squat

Squat is one of the main exercises used in training and rehabilitation, able to strengthen lower limb muscles and to assess ranges of motion. It is a closed kinetic chain motion task that involves hip flexion, knee flexion and angle dorsiflexion. It requires a great joint mobility and synergy between several muscle groups, each which contracts and relaxes in specific phases of the movement. Beginning from a standing position and maintaining a straight trunk, knees are flexed to reach an angle equal or greater than 90° and then extended to return to the starting position.

Wide stance squat is a variation of the normal stance squat and it involves more muscles than the first one. The main difference regards the placement of feet, that is closer for the normal squat, which requires a separation like that of the shoulders, and more distant for the wide stance squat, with a separation 1.5-2 times larger. In both cases, if they are performed with an inappropriate technique, they can cause inefficacy of training and/or injuries, especially at levels of trunk and lower limb joints.

To minimize risk of trauma and ensure maximal lower limb muscles activation, optimal squat technique (figure 5) requires: heels in contact with the floor, to prevent forward lean of the trunk; upright trunk to maintain spine in a neutral position, with a slightly lordotic lumbar spine (pelvic anteversion); knees tracking over the toes, so without bring

them closer and avoiding to overcome the vertical lines of the toes; tibiae parallel to the upright torso; gaze forwards or upwards (Comfort *et al,* 2018; Braidot *et al.,* 2007; Lorenzetti *et al.,* 2018; Myer *et al.,* 2014).

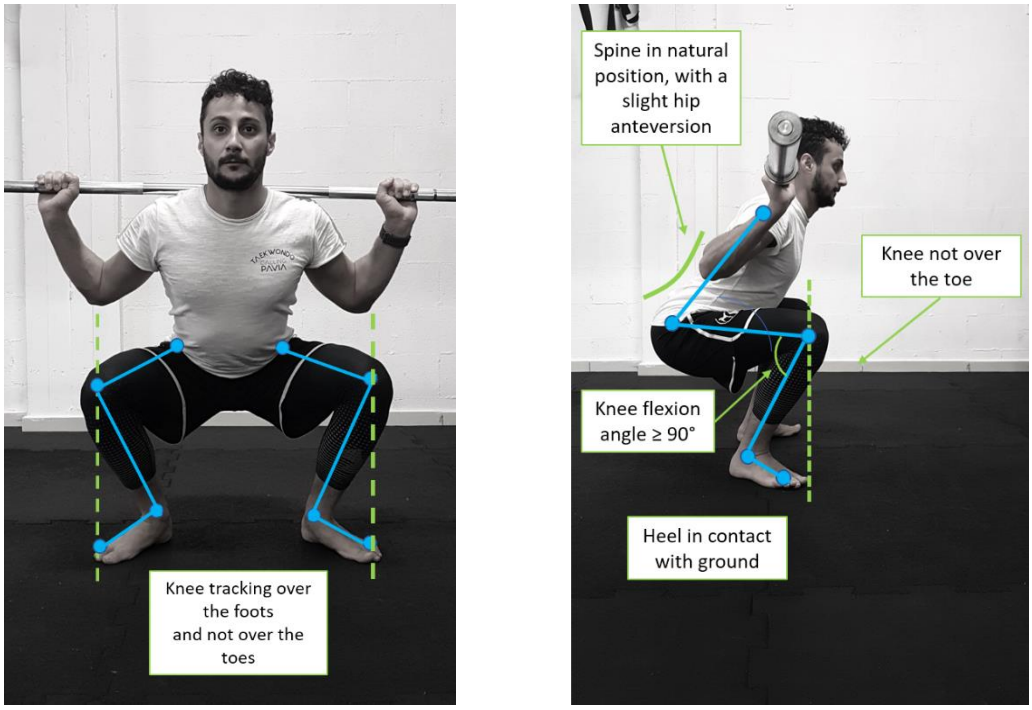

(a) (b)

Figure 5: frontal (a) and lateral (b) views of correct squat position. Dashed green lines show the vertical lines which originate from toes. In frontal plane, knee joints remain laterally in respect to the lines; in sagittal plane, they stay behind the lines. Solid green line highlights the natural lordotic lumbar curve, which has to be maintained during squatting. Knee angle should be ≥ 90°. (Photos are acquired at A.S.D. Taekwondo Calling Pavia).

Deadlift

Deadlift is a training exercises used to develop strength of trunk muscles. It is a complex movement with high risk of back injury if performed wrongly. The optimal deadlift technique (figure 6) requires a starting position in partial squatting, with natural width of feet and with arms coming down outside the legs to reach the bar. Then, hip and shoulders have to be lifted at the same time maintaining a natural position of the spine. Also in this case, it is necessary to respect some features to avoid inefficacy of training and/or injuries: hip joints higher than knees, to prevent forward lean of the trunk; upright trunk to maintain spine in a neutral position; shoulder blades adduced, slightly in front of

bar; gaze forwards; knees tracking over the toes, so without bring them closer and avoiding going over the vertical lines of the toes.

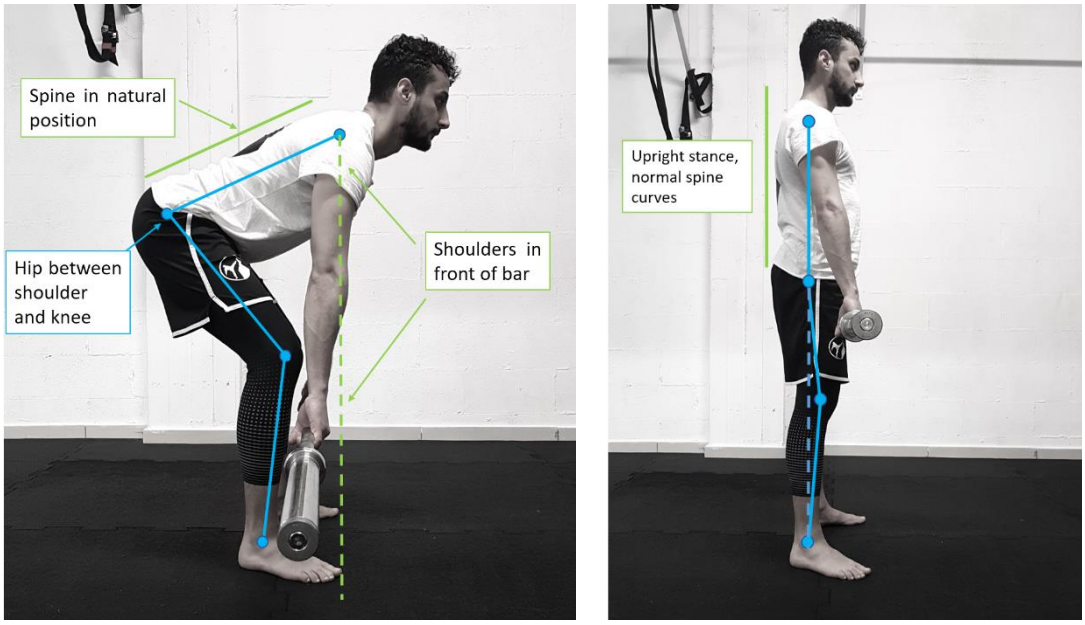

(a) (b)

Figure 6: lateral view of correct starting (a) and ending (b) positions of deadlift. Dashed green line represents the vertical line coming from the shoulder; bar must not pass that line. Solid green line shows the correct upright position of trunk to maintain during lifting, instead dashed blue line points out the correct alignment of shoulder, hip and knee at the end of exercise. (Photos are acquired at A.S.D. Taekwondo Calling Pavia).

1.3 Need of real-time coaching

Currently the ARED Photo/TV system (figure 7) is used in order to have a real time audio/video communication between ground team and astronaut during the training session. This was thought to allow astronaut to receive feedback recommendations. However, the more the distance from the Earth, the longer the communication delays, so exercise feedback becomes more difficult to receive (Linh Vu *et al.*, 2018). It would be necessary a tool that can provide real-time instruction and correction feedback for the subject in the absence of human coaching to prevent injuries and optimize overall muscle strength outcomes.

Figure 7: standard ARED Photo/TV system field of view on ISS (from Ferchette *et al.,* 2017).

To achieve this purpose, it could be combined a system which should have the peculiarities of tracking movements, comparing them with standardized ones and giving real-time corrective biofeedback.

1.3.1 Motion capture system on ISS

Motion capture (MOCAP) is a technique which allows to track and digitize movements of people, animals and objects with large applications in several areas comprising entertainment, sport, medicine and robotics. This method permits to acquire kinematics data, that are mainly joint positions, velocities, accelerations and angles, from which it is possible to analyze quantitatively human motion, so to obtain biomechanical information of the musculoskeletal system during the execution of a motor task.

Technologies used to carry out human motion tracking exploited for a whole body and/or specific body part acquisition can be grouped into three different categories: (1) Marker-based systems; (2) depth camera-based systems; (3) sensor-based systems.

The first ones use optoelectronic measurement systems (OMSs) and markers placed on specific body points. Markers are little spheres which can be passive, so coated with reflective substances, or active, thus able to emit lights by themselves. Considering passive systems, OMSs are composed by a set of television cameras (TVCs) surrounded by a ring of light emitted diodes (LED) coaxial with the camera optical devices. Infrared (IR) light

is emitted with a specific frequency (wavelength of around 800-850 micrometers) and retro-reflected by the passive markers. If active markers are used, ring of LED is not needed because light is directly emitted by them. Retro-reflected rays are then captured by the TVC sensors in which markers are projected, so the representation of their position in each sensor of each camera is obtained. To reconstruct the 3D position of each marker, it is required a proper calibration of the TVCs before the acquisition; this allows to compute 3D coordinates via triangulation. Examples of OMSs used to monitor astronauts, on Earth and/or on ISS, are ELITE-S2, CODAmotion and BTS-SMART (figure 8).

Figure 8: TVC of BTS-SMART system.

Depth camera-based systems do not use reflective markers, but light patterns projected on the subject. The reconstruction could be based on two principles: pattern projection or Time-Of-Flight (ToF). In the first case, a known infrared pattern is projected into the scene and out of its distortion the depth is computed. The reconstruction in 3D is based on triangulation. The IR projector is an IR laser that passes through a diffraction grating and turns into a set of IR dots. The relative geometry between the IR projector, the IR camera and the projected IR dot pattern are known. By matching a dot observed in an image with a dot in the projected pattern, it is possible to reconstruct the image by triangulation. The TOF technology uses an infrared light beam to illuminate the scene and then measures the phase lag between the waves sent by the transmitter and the ones received by the receiver device. Microsoft Kinect and Intel ® RealSense™ are the main low-cost products on market belonging to this kind of systems.

The last ones, sensor-based systems, do not utilize cameras, but sensors based on the principle of inertia. The most common inertial sensors used for motion capture are accelerometers, gyroscopes and magnetometers, especially a combination of them to form the Inertial Measurement Units (IMU). Accelerometers measure accelerations along its axes and convert them into displacements; gyroscopes lead a measurement of orientation and its rate of change; magnetometers detect Earth magnetic field along their axes from which orientation is computed.

The first MOCAP system installed on board the ISS was ELITE-S2 (Ferrigno *et al.,* 2003). Now, it is thought that the moment to substitute it with a more recent technology has come. For this purpose, the BTS-Smart system was chosen as valid successor. Figure 9 shows the placement of the old system and a first arrangement of the new one.

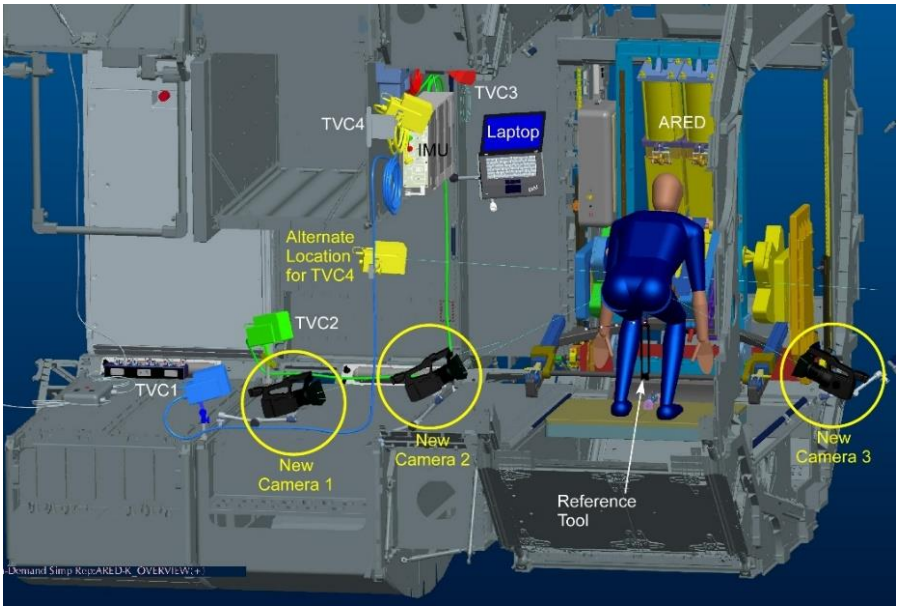

Figure 9: previous Elite-S2 camera placement (TVC1, TVC2, TVC3, TVC4) and available HD cameras (New Camera 1, New Camera 2, New Camera 3).

However, NASA is planning to add a second toilet on the left of the subject (figure 10), where TVCs would have to be installed. A new arrangement is needed because the working volume will be reduced. At the moment, the procurement and certification of a new COTS MOCAP system to be adopted to support on board data collection are in progress.

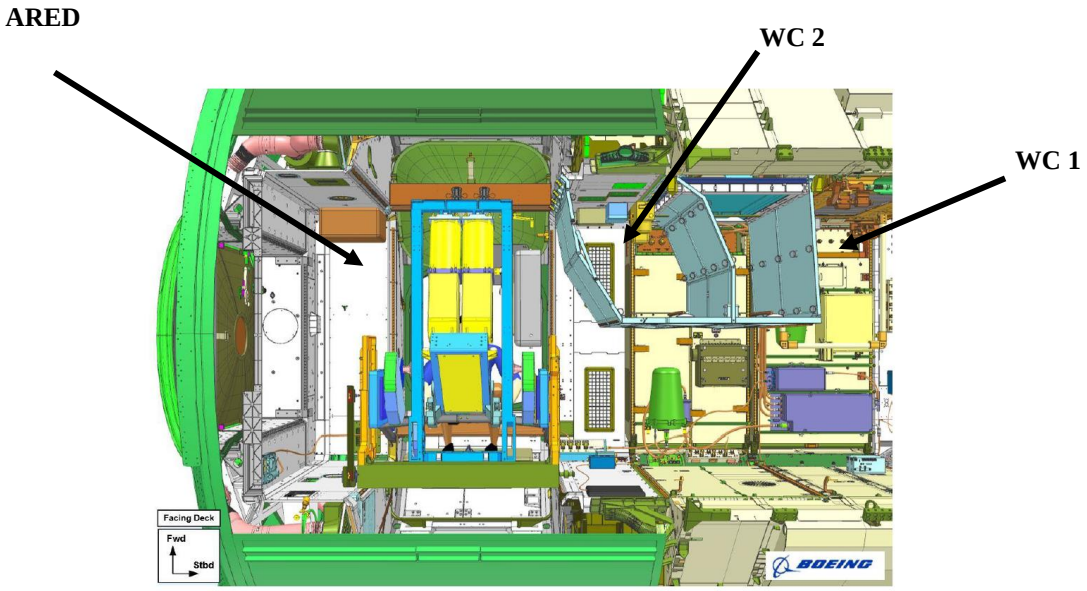

Figure 10: future Node3 configuration with ARED and the new toilet (WC2).

1.4 Aim of the Thesis

This thesis is inserted in the research project "MARcatori biologici e funzionali per la biomedicina aStronautica di PREcisione – MARS-PRE", proposed by Italian Space Agency (ASI) and structured in 21 Work Packages (WPs). The general aim is to explore biological markers to characterize human adaptation to different gravity conditions, such as biochemical measures of fluids, structural and physical properties of tissues, functional test of muscular strength and biomarkers of sensory-motor behavior. Nodo 1700 has been assigned to Politenico di Milano, whose WP is entitled: "Marcatori personalizzati del programma di contromisure attraverso machine learning e sensori indossabili per biofeedback". The purpose is to design a system able to monitor astronaut training performed with ARED on ISS. The system should provide a real-time biofeedback in order to correct exercises executions so that any injury and/or inefficacy of the training will be avoided. It has to be based on the use of a small set of wearable sensors, so on acceleration signals correlated to the movement and not on kinematics variables as joint positions and joint angles. These sensors should provide information about biomechanical variables considered relevant to evaluate the correctness/incorrectness of

the performance. Both a biomechanical model including muscular actions and a machine learning algorithm are required to reach the aforesaid scope. The model must be inserted in a virtual environment where target exercises, proposed on ISS, can be simulated both in Earth gravity and microgravity conditions. Executions in different configurations, both correct and incorrect ones, are needed so that biomechanical variables associated with a musculoskeletal risk should be extracted. These parameters ought to be associated with measures detectable by using a set of wearable sensors easy to install and based on accelerometers and/or gyroscopes suitable in weightlessness. Corrective information must be provided with different types of biofeedback easy to interpret.
This system could have other interesting applications on Earth in the area of rehabilitation, to allow continuity of care with reliable and simply technologies. Furthermore, it could be thought to monitor training in order to optimize the performance of subjects or athletes.

The biomechanical model would be also used in the contest of project "ARED Kinematics – Biomechanical quantification of bone and muscle loading to improve the quality of microgravity countermeasure prescriptions for resistive exercise", which involves ESA, NearLab at Politecnico di Milano, NASA JSC and Kayser Italia. The aim is to investigate internal forces during resistance exercise performed on ISS with ARED to optimize resistance exercises prescriptions, maximizing their effectiveness and minimizing the required time. To do this, kinematics and dynamics data will be collected from each astronaut while performing exercises on the ARED before, during and after flight, with three different load levels. In this context, the model would be used to analyze data and to compare results, in particular specific goals are:

- Goal 1: Characterize differences in squat and deadlift kinematics before, during and after spaceflight;
- Goal 2: Characterize the differences in squat and deadlift joint and muscle forces before, during, and after spaceflight.

Assuming that:

- Hypothesis 1 (per goal 1): In-flight ankle, knee, and hip kinematics will be different from pre- and post-flight.

- Hypothesis 2 (per goal 2): In-flight ankle, knee, and hip joint toques will be different from pre- and post-flight.
- Hypothesis 3 (per goal 3): In-flight lower extremity muscle activity will be different from pre- and post-flight.
- Hypothesis 4 (per goal 4): In-flight ankle, knee, and hip joint torques will be directly related to applied resistance loads.

My work was focused on the validation of a biomechanical model through the OpenSim software with the following aims:

1) Biomechanical analysis of correct and incorrect techniques of normal stance squat, wide stance squat and deadlift in order to evaluate risk of injuries and/or inefficacy of training. This evaluation was carried out by comparing kinematics, joint moments and muscle forces of different exercise executions, highlighting risk of injuries and/or inefficacy of training. This wants to support the definition of the classes that the machine learning algorithm will have to distinguish. The mistakes were proposed and approved by the NASA ASCR specialists.

2) Simulation of target exercises performed on ISS both in normal gravity and zero gravity conditions. For weightlessness simulations, different BWRs were considered to quantitative evaluate the optimal one in order to replicate joint moments obtained on Earth.

3) Extraction of accelerations of different body points for both correct and wrong exercises techniques. These data want to reproduce output that we can obtain from inertial sensors placed on these body points. They will support the future development of a machine learning algorithm (e.g. Artificial Neural Network or Support Vector Machine), which will be able to detect bad executions of exercise in real time. These body points will be identified as anticipatory biomarkers of muscle-skeletal damage.

Up to now, the OpenSim model has been validated by using data collected at the Luigi Divieti Laboratory at Politecnico di Milano of two subjects, who performed target exercises with barbell and weights in both correct and incorrect configurations.. The protocol used to acquire data at Politecnico di Milano was reviewed and approved by ASCR NASA JSC. Right in the final writing phase of the Thesis, data collected at NASA JSC have been transferred. These include kinematics and dynamics data of six subjects, three males and three females, who performed squat, wide squat and deadlift with ARED. They will permit to expand dataset of the correct executions and to verify the adherence of the model developed in the thesis to the data collected with ARED.

In the following page it is shown a scheme which explains the project.
Motion of astronaut during training will be tracked using inertial sensors suitable for microgravity. These sensors will provide acceleration signals related to the body points on which they will be attached. These data will be elaborated in order to allow the software based on machine learning algorithm to classify motions between correct and wrong, distinguishing different levels of incorrectness. Then, a real-time biofeedback will be delivered to the subject in order to correct the technique.
Currently, no IMU data are available, but only kinematics and dynamics ones obtained by using a motion capture system and force plates. For this reason, a biomechanical model with OpenSim software is used to simulate IMU placement on body and to extract analog data. This model permits also to simulate exercises in different gravity conditions and to conduct a biomechanical analysis of target exercises proposed on ISS.

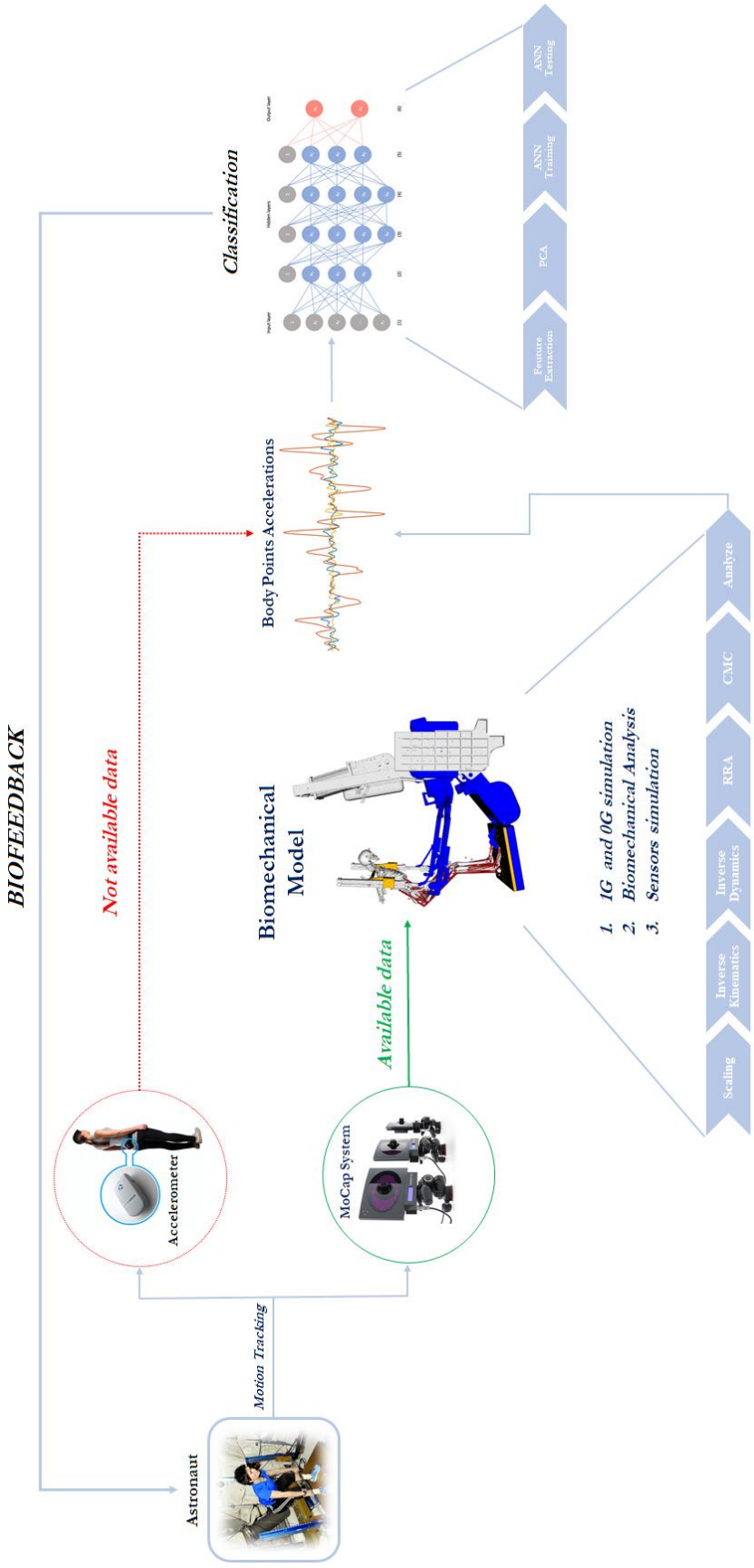
BIOFEEDBACK
Astronaut
Motion Tracking
Accelerometer
MoCap System
Not available data
Available data
Biomechanical Model
Body Points Accelerations
Classification
Feature Extraction
PCA
ANN Training
ANN Testing
1. IG and 0G simulation
2. Biomechanical Analysis
3. Sensors simulation
Scaling
Inverse Kinematics
Inverse Dynamics
RRA
CMC
Analyze

CHAPTER 2
OPENSIM 3.3 ®

OpenSim is an open-source software used for modeling human, animals, robots and environments, to simulate motions and to analyze neuro-musculo-skeletal system. It is written in ANSI C++ and the graphic unit interface (GUI) in Java, so that the software can be used on all common operating systems. OpenSim provides a musculoskeletal models library containing a set of validated musculoskeletal models, which can be used to conduct own simulations and analyzes. The software permits also to create and/or edit a model of a broad range of musculoskeletal structures. Muscles are modeled considering Hill-type muscle models, which include active and passive forces that define muscle properties; these models are based on well-tested models of muscle-tendon dynamics.

2.1 OpenSim models

In an OpenSim model each component corresponds to parts of the physical system. Skeleton is made up of rigid bodies interconnected by joints that define how body can move with respect to another one. Muscles are modeled as specialized force elements that act at points connected to rigid bodies. Force depends on muscle fibers, tendon lengths, the rate of change of the fibers and the level of muscle activation. In addition, it is possible to add some constraints to limit the movement between segments. OpenSim permits also to change the vector describing the acceleration due to gravity and to apply external loads,

including GRFs. Each model is described by XML file where tags identify and manage information. Figure 11 shows an example of the structure.

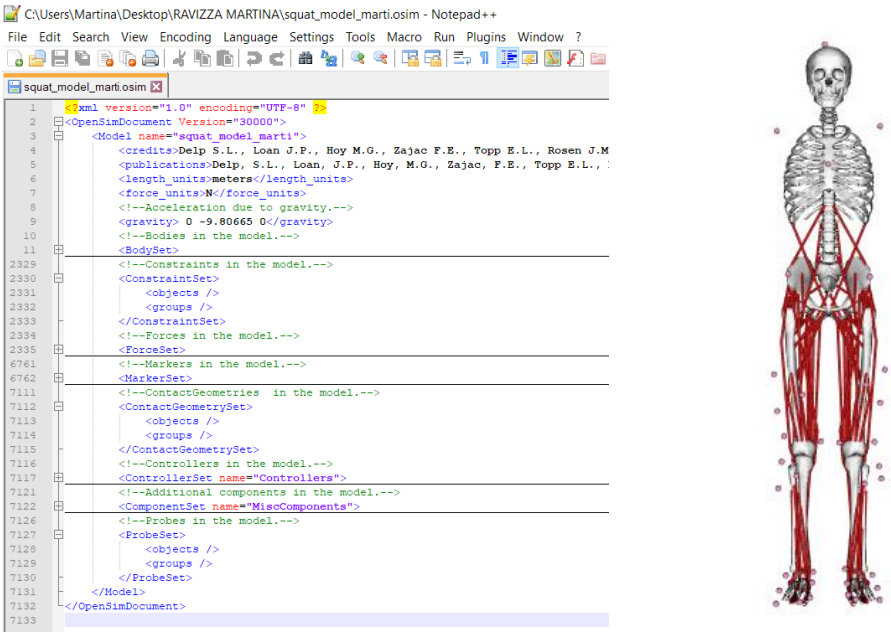

Figure 11: (a) example of XML code structure of OpenSim model. (b) Example of OpenSim model available in library; in red modeled muscles; in pink markers on body

2.2 OpenSim workflow

OpenSim includes robust tools able to execute biomechanical simulations of musculo-skeletal system during motor gestures and to analyze them. Among the tools, those relevant for this work are model scaling, inverse kinematics (IK) and inverse dynamics (ID) problems resolution, muscle forces estimation, plotting results, creating video and capturing screenshots of model during simulation.

The following step are needed to analyze experimental data collected in laboratory:

I. Preparing kinematics and dynamics data in specific formats;

II. Choosing/creating a model and put on it virtual markers in order to reproduce the same marker set-up used during data acquisition;

III. Scaling the model basing on anthropometry of the subject;

IV. Computing the IK problem to obtain joint angles that better reproduce movement captured with the MOCAP system;

V. Solving the ID problem to determine joint torques;

VI. Reducing residuals to minimize errors deriving from modeling, so due to the simplification of the system, and marker data processing. This leads to make generalized coordinates more consistent with GRFs and joint moments computed;

VII. Generation of muscle excitations.

2.2.1 Preparing data

Firstly, to allow OpenSim to work, it is necessary to input trajectories of markers in Track Row Column (.trc) file format. This file specifies positions of markers placed on body in each time instant during the movement performed and acquired with the MOCAP system. A fragment of this file is presented in figure 12. The first three rows form the header, followed by two rows containing marker names, which will have to be the same of the virtual marker placed on the OpenSim model, and their components (X, Y, Z). Then, there are the rows data. Each row data specifies frame number, time value and coordinates of each marker in this sequence. Considering the header, *DataRate* is the acquisition frequency in Hertz, hence, the sampling frequency of the MOCAP system; *NumFrames* represents the number of frames, *NumMarker* the number of makers and *OrigDataStartFrame* the number of the first frame.

	A	B	C	D	E	F	G	H	I
1	PathFileType	4	(X/Y/Z)	C:\Users\Martina\Desktop\RAVIZZA MARTINA\Marti_squat\Correct\motion_squat_marti.trc					
2	DataRate	CameraRa	NumFrames	NumMarker	Units	OrigDataRate	OrigDataSta	OrigNumFrames	
3	100.0	100.0	1515,00	44,00	mm	100.0	1,00	1515,00	
4	Frame#	Time r_head		l_head			c_head		
5	X1	Y1	Z1	X2	Y2	Z2	X3	Y3	Z3
6	1,00	0.0	617,47	1055,28	170,90	639,66	1044,26	-406,57	322,37
7	2,00	0.01	617,90	1053,22	168,58	641,24	1042,56	-408,65	381,81
8	3,00	0.02	620,29	1050,55	165,89	643,57	1041,06	-537,42	426,47
9	4,00	0.03	621,54	1050,98	163,53	646,25	1040,36	-571,62	453,24
10	5,00	0.04	624,56	1051,42	161,25	652,01	41,46	-58323,00	464,35
11	6,00	0.05	628,16	1051,44	158,45	652,25	1043,54	-572,10	462,89

Figure 12: first rows of .trc file containing time history of marker coordinates.

Then, external forces must be specified in a .mot file (figure 13). The first row of *header* indicates the name of the file and its format. The next lines express the total number of rows and columns. Optional comments could be added before the final line *endheader,* after which data section begins. The first row should contain labels for each column that usually starts with time and continues with force data. These data include X, Y, Z components of GRFs collected with force plates, the center of pressure and torques. In addition, any other forces applied on the body can be added; an example could be the load coming from a barbell with weights during training, as needed in this work. Each group of force (force_v), point of application (force_p) and torque (force_torque) columns must have a common prefix. For example, to specify GRFs, labels should be:

- time
- r_ground_force_vx, r_ground_force_vy, r_ground_force_vz
- r_ground_force_px, r_ground_force_py, r_ground_force_pz
- l_ground_force_vx, l_ground_force_vy, l_ground_force_vz
- l_ground_force_px, l_ground_force_py, l_ground_force_pz
- r_ground_torque_x, r_ground_torque_y, r_ground_torque_z
- l_ground_torque_x, l_ground_torque_y, l_ground_torque_z

	A	B	C	D	E	F	G	H	I	J	K	L	M	N	O	P
1	force_squat_marti.mot															
2	version=1															
3	nRows=3021															
4	nColumns=25															
5	inDegrees=yes															
6	endheader															
7	time	r_ground_	r_ground_	r_ground_	r_ground_	r_ground_	r_ground_	l_ground_	l_ground_	l_ground_	l_ground_	l_ground_	l_ground_	r_ground_	r_ground_	r_ground_
8	0	-2,65E+07	3,81E+08	-7,82E+07	2,65E+05	8,98E+03	-2,02E+05	3,30E+07	4,65E+08	6,81E+07	1,90E+05	4,65E+03	-6,84E+05	4,44E+04	8,86E+06	-6,40E+04
9	5,00E+03	-2,65E+07	3,78E+08	-7,79E+07	2,66E+05	8,98E+03	-2,02E+05	3,31E+07	4,66E+08	6,83E+07	1,90E+05	4,65E+03	-6,84E+05	4,43E+04	8,83E+06	-6,38E+04
10	1,00E+04	-2,65E+07	3,75E+08	-7,75E+07	2,67E+05	8,98E+03	-2,02E+05	3,32E+07	4,66E+08	6,84E+07	1,90E+05	4,65E+03	-6,84E+05	4,41E+04	8,80E+06	-6,35E+04
11	1,50E+04	-2,64E+07	3,72E+08	-7,71E+07	2,68E+05	8,98E+03	-2,01E+05	3,31E+07	4,67E+08	6,84E+07	1,89E+05	4,66E+03	-6,84E+05	4,40E+04	8,76E+06	-6,33E+04
12	2,00E+04	-2,62E+07	3,69E+08	-7,65E+07	2,68E+05	8,98E+03	-2,01E+05	3,30E+07	4,67E+08	6,85E+07	1,89E+05	4,66E+03	-6,84E+05	4,39E+04	8,75E+06	-6,32E+04

Figure 13: first rows of .mot file containing time history of external forces applied to the model.

2.2.2 Scaling model

The first operation is the scaling of the model basing on the anthropometry of the subject under examination. This consents to obtain a personalized biomechanical model, which represents that subject. For this purpose, it is required a .trc file containing marker coordinates that correspond to a static position of the subject. This data could be obtained

by acquiring standing position during data collection and by averaging marker coordinates across a desired time range. Furthermore, virtual markers (pink markers in figure 14) must be placed on the virtual model with the same disposition of the experimental markers (blue markers in figure 14) put on the subject during acquisitions.

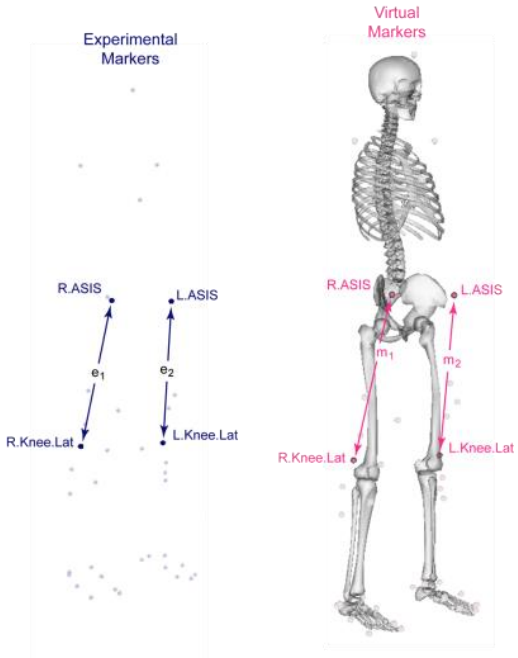

Figure 14: experimental marker positions are computed with MOCAP system (blue markers); virtual markers are placed manually on biomechanical model in anatomical correspondence (pink markers). Distances between experimental markers (e_i) relative to the distances between virtual markers (m_i) are used to compute scale factors.

OpenSim Scale Tool rescales each segment in the model so that the distance between the virtual markers matches the distance between experimental markers, computed by the MOCAP system. By this way, each scale factor (s_i) is computed using one or more marker pairs as: $s_i = \frac{e_i}{m_I}$, where e_i is the i-th experimental marker and m_i the i-th virtual one. Then, the overall scale factor S is computed as the average of the scale factors due to all of the pairs: $s = \frac{\sum_{i=1}^{N} s_i}{N}$, where i is the i-th scale factor related to the i-th marker pair and N is the total number of marker pairs. The overall scale factor S is then used to scale any segment in the model along X, Y and Z axes. Additionally, mass of each segment is adjusted considering that the total sum of the masses of the segments must be equal to

the total mass of the subject. In the end, also muscle lengths and ligament lengths are updated.

Input and output of the Scale Tool are showed in figure 15. Please, see the Appendix A for specifications about content of each file.

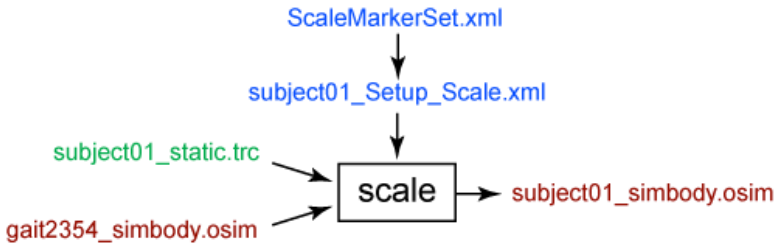

Figure 15: input and output of the scale tool. Experimental data are in green, OpenSim files (.osim) are in red; setting files are in blue. Names are only as examples.

2.2.3 Inverse kinematics

Kinematics is the study of motion of one or more bodies without considering forces and moments that cause the movement. The IK is a process that determines joint parameter that provides a desired position of the end-effectors. Considering biomechanical simulations, this procedure is applied to induce model to perform a desired movement; this means to find joint angles and body segment positions that better reproduce the movement of the real subject. To solve the IK problem, OpenSim IK Tool analyzes each single frame of motion and computes generalized coordinates that best match the positions of the experimental markers for that time step. This means to resolve a weighted last mean squares problem in order to minimize marker and/or coordinate errors. Marker error is the distance between experimental marker and the corresponding marker on the model; coordinate error is the difference between experimental coordinate value and the coordinate value computed by IK. Coordinate values could be joint angles obtained directly from a MOCAP system or computed by other algorithms.

The weighted last mean square solved by IK is represented by equation 1:

$$\min_{q,\theta}\left[\sum_{i\in marker} w_i\left\|x_i^{exp}-x_i^{mod}(\theta)\right\|^2+\sum_{j\in coordinate}\omega_j\left(q_j^{exp}-q_j^{mod}\right)^2\right] \quad \text{Eq. (1)}$$

Where $x_i^{exp}-x_i^{mod}(\theta)$ is the i-th marker error between the i-th experimental marker position and the i-th virtual marker position; $q_j^{exp}-q_j^{mod}$ is the j-th coordinate error between the j-th experimental coordinate and j-th virtual coordinate; w_i and ω_j are weights given to different markers and joint angles. q_j^{exp} value is predicted by the algorithm. The result is a set of coordinates over time, which describes virtual marker positions and joint angles of the model so that it reproduces the actual movement performed by the subject. The output being saved in a .mot fie.
Input and output of the IK Tool are showed in figure 16. Please, see the Appendix A for specifications about content of each file.

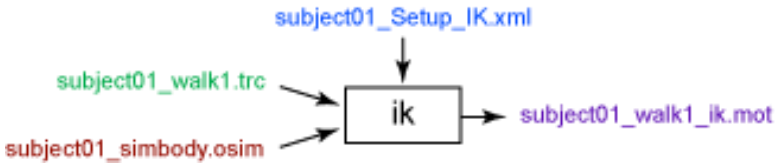

Figure 16: input and output of IK tool. Experimental data in green; OpenSim files are in red; setting file are in blue; output of IK is in purple. Names are as example.

2.2.4 Inverse dynamics

Dynamics is the study of motion of one or more bodies considering forces and moments that cause the movement. The ID is a process that determines forces and moment of forces of a body segment, given its kinematics and its inertial properties. In biomechanics, this means to find joint moments responsible for a given movement, considering kinematics coming from MOCAP system and GRFs deriving from the force plates. In addition, any external force applied to the body needs to be considered, such as a barbell

with weights used in this study. The scheme below describes the workflow starting from measured data, passing through IK and ID to obtain joint moments.

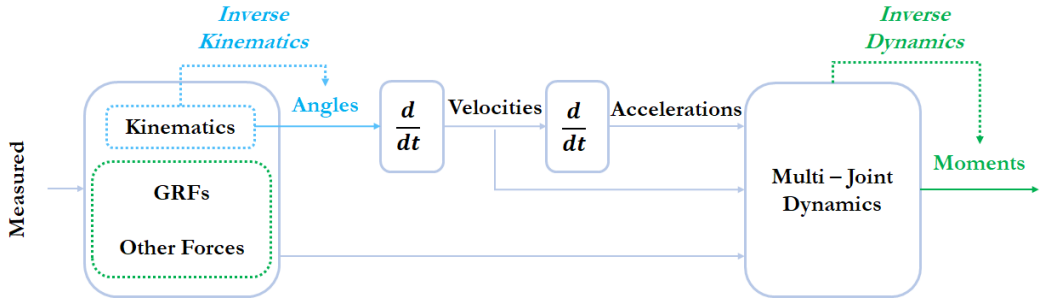

This is done considering kinematics and external forces acting on the subject and by solving Newton - Euler equations of motion based. For each joint, classical equations can be written as:

$$\sum F_x = m\ddot{x} \qquad \sum M_x = I_x\ddot{q_x}$$
$$\sum F_y = m\ddot{y} \qquad \sum M_y = I_y\ddot{q_y} \qquad \text{Eq. (2)}$$
$$\sum F_z = m\ddot{z} \qquad \sum M_z = I_z\ddot{q_z}$$

Terms $\ddot{x}, \ddot{y}, \ddot{z}$ and $\ddot{q}$ are linear and angular accelerations along each axis coming from the IK problem resolution; F are forces, M are moments, m is mass of segment and I are inertial moments in respect to specific axis.

Input and output of the IK Tool are showed in figure 17. Please, see the Appendix A for specifications about content of each file.

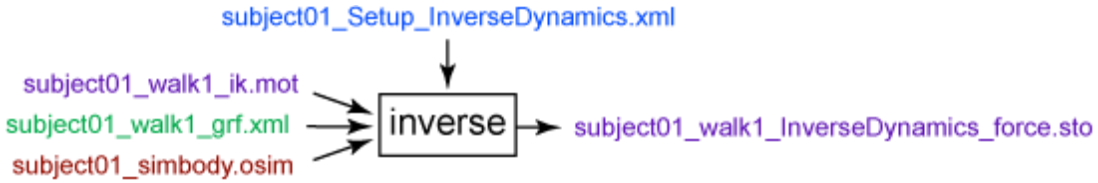

Figure 17: input and output of IK tool. Experimental data in green; OpenSim files are in red; setting file are in blue; output of IK and ID are in purple. Name are as example.

2.2.5 RRA

Residual Reduction Algorithm aims to minimize errors deriving from modeling and data processing, which could generate non-physical compensatory forces called residuals. Typically, considering those errors, Newton's Second Law is not satisfied, so:

$$F_{ext} \neq ma \qquad F_{ext} = \sum_{i=1}^{N} m_i a_i - F_{residual} \qquad \text{Eq. (3)}$$

Where F_{ext} is the experimental external force, N is the total number of segments, a_i is the acceleration of the Center of Mass (CoM) of i-th body segment, m_i is the mass of the same segment and $F_{residual}$ represents a residual force, which could be equal to zero in absence of errors. RRA computes residuals taking small steps in time and choosing the actuator forces that minimize an objective function. Then, model masses are adjusted basing on the residual average values computed for each actuator. The adjusted model is saved in an .osim file.

Input and output of the RRA tool are shown in figure 18. Please, see the Appendix A for specifications about content of each file.

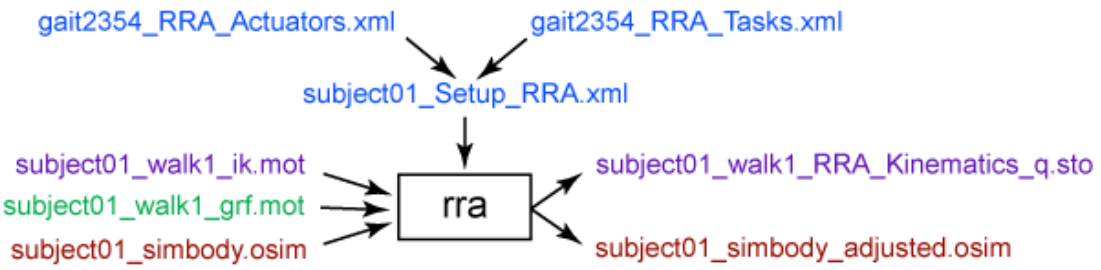

Figure 18: input and output of RRA tool. Experimental data are in green; OpenSim files are in red; setting file are in blue; output of IK and RRA are in purple. Name are as example.

2.2.6 CMC

Compute Muscle Control Tool calculates a set of muscular excitations that drive the musculo-skeletal dynamic model to track a desired kinematics. This is done by using a proportional-derivative control and a static optimization (figure 19).

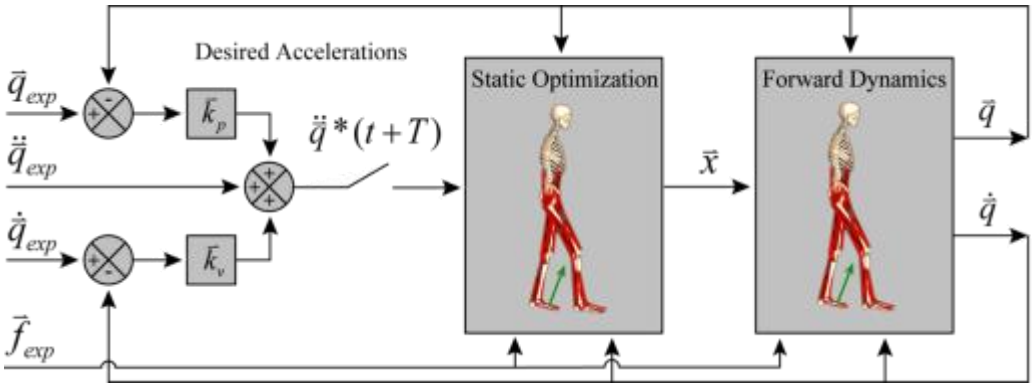

Figure 19: scheme of CMC algorithm.

Before starting, initial states of the model are computed, which are the initial values of joint angles q, initial velocities $\dot{q}$ and other states, including muscle levels of activation and fiber lengths. Angles and velocities can be taken from kinematics, instead muscular activations and fiber lengths are unknown, so CMC is initially applied to the first 0.03 seconds of the desired movement to set them. Once this is done, the algorithm starts.

Firstly, a set of desired accelerations $\ddot{\vec{q}}^*$ is computed using the following PD control law:

$$\ddot{\vec{q}}^*(t+T) = \ddot{\vec{q}}^*{}_{exp}(t+T) + \vec{k}_v\left[\dot{\vec{q}}_{exp}(t) - \dot{\vec{q}}(t)\right] + \vec{k}_p\left[\vec{q}_{exp}(t) - \vec{q}(t)\right] \qquad \text{Eq. (4)}$$

$\vec{k}_v$ and $\vec{k}_p$ are gains of position and velocity coordinates respectively. $\vec{k}_v$ is chosen so that $\vec{k}_v = 2\sqrt{\vec{k}_p}$. The desired accelerations, when reached, drive the model coordinates $\vec{q}$ toward experimental coordinates $\vec{q}_{exp}$ end errors between model coordinates and experimental ones drive to zero.

The next phase is the static optimization in which actuator controls $\vec{x}$, which are muscle forces, are obtained to achieve the desired accelerations $\ddot{\vec{q}}^*(t+T)$. It is defined static

because it computes quantities in each time instant. Static optimization works basing on two formulations: the first one (Eq. 5), called slow target, minimizes and distributes loads across actuators and the model accelerations toward the desired accelerations; the second one (Eq. 6), called fast target, is the sum of squared controls augmented by a set of constraints $C_j = 0$ that require the desired accelerations to be achieved within the tolerance set for the optimizer. The last one is faster and produce better tracking, but if constraints can not be met, it fails.

$$J = \sum_{i=1}^{n_x} x_i^2 + \sum_{j=1}^{n_q} \omega_j \left(\ddot{q}^*_j - \ddot{q}_j \right)^2 \qquad \text{Eq. (5)}$$

$$J = \sum_{i=1}^{n_x} x_i^2 \qquad C_j = \ddot{q}^*_j - \ddot{q}_j \quad \forall j \qquad \text{Eq. (6)}$$

In the end, CMC computes controls to conduct a standard forward dynamic simulation over time, so that muscle excitations are estimated.

The scheme in figure 20 describes the workflow starting from measured data, passing through IK, ID and CMC to obtain muscle forces.

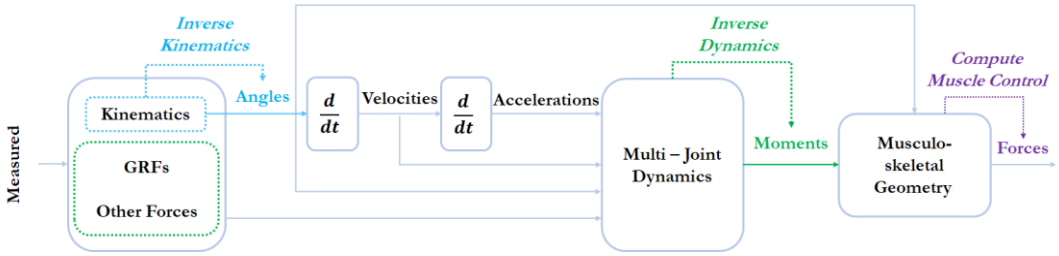

Figure 20: from left to right it is shown the workflow to obtain muscle forces starting from data acquisition using MOCAP system and force plates. Kinematics data measured with MOCAP system (markers' coordinates over time) are in light blue and they are used to compute IK, so that joint angles are obtained. Force data (GRFs and external forces) utilized to resolve the ID problem, which needs also joint angular accelerations obtained by deriving twice joint angles, are in green. In the end, complex algorithms estimate control actuators (muscle forces) using data obtained in the step before.

Input and output of the IK Tool are showed in figure 21. Please, see the Appendix A for specifications about content of each file.

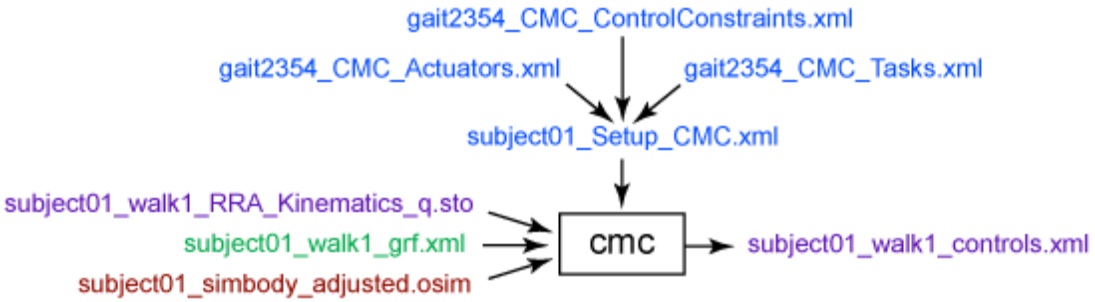

Figure 21: input and output of RRA tool. Experimental data are in green; OpenSim files are in red; setting file are in blue; output of IK and RRA are in purple. Name are as example.

2.2.7 Analyses tool

This Tool permits to analyze model or simulation basing on different kinds of input. Available analyses include:

- Kinematics: records generalized coordinates, speeds and accelerations of each body segment;
- BodyKinematics: records CoM position and orientation of each body, as well as their linear and angular velocities and accelerations. It records also the overall CoM, its velocity and acceleration;
- Actuation: records generalized force, speed and power of each actuator of the model;
- JointReaction: reports joint reaction loads;
- PointKinematics: computes trajectory, linear and angular velocities and accelerations of body points properly specified by user. To do this, it is needed to specify the coordinates of the points involved, the name of the segment in which they are located and the reference system in which they are expressed (figure 22). This feature was used to simulate inertial sensors on body.

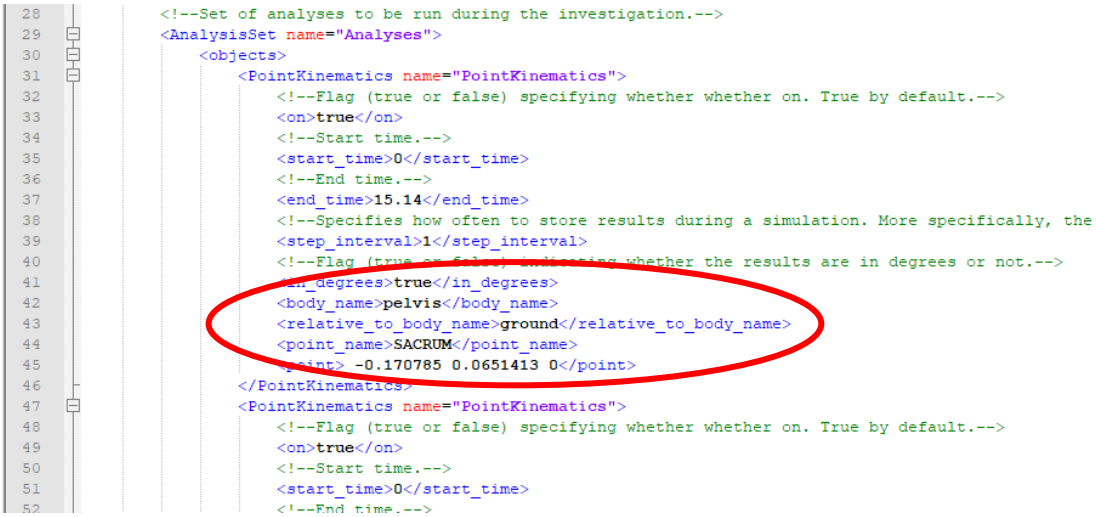

Figure 22: example of set-up file for analyzing kinematics of desired points. Circled in red, specification of selected point on sacrum for which coordinates relative to global reference frame are specified.

CHAPTER 3
MATERIALS AND METHODS

3.1 Protocols

Waiting for the transfer of on-ground data collected at NASA JSC with ARED, we reproduced analog experiment at Politecnico di Milano. Given that ARED was not available, we used a barbell with weights. Data collection was carried out on two subjects (S1 – male, 30 years old, 65 kg, 175 cm; S2 - female, 25 years old, 54 kg, 164 cm), who performed target exercises proposed on ISS. Kinematics data were acquired at Posture and Movement Analysis Laboratory "Luigi Divieti" of the Electronic, Information and Bioengineering Department (DEIB) of Politecnico di Milano.

3.1.1 Hardware set-up

The optoelectronic system used to acquire motion data is SMART DX 400 (BTS Bioengineering S.p.A, Milan, Italy), composed by 8 TVCs with 100 Hz sampling frequency; ground reaction forces were measured by two force plates (AMTI, USA).
A total of 43 retro - reflective markers were placed on body (figure 23) plus 2 on the bar as follow:

- 4 on each foot (medial distal first phalange, lateral distal fifth phalange, medial midfoot and most posterior aspect of calcaneus);
- 2 on each ankle (lateral and medial malleolus);
- Bank of 3 markers on each lateral thigh;

- 1 on each lateral knee;
- Bank of 3 markers on each lateral shank;
- 1 on each head of greater trochanter;
- 7 on pelvis (each ASIS, each PSIS, each iliac crest and sacrum);
- 1 on sternum (xiphoid process);
- 1 on each supraclavicular notch;
- 2 on spine (10th thoracic vertebrae T10 and vertebra prominems C7);
- 3 on head;
- 2 on the extremities of barbell;

(a) (b)

Figure 23: marker placement for data collection. Frontal (a) and lateral (b) views.

3.1.2 Exercises

Each subject performed one set of 4 repetitions of normal squat, wide stance squat and normal deadlift with correct executions, similarly to those performed at NASA JSC. In addition, they executed one set of each kind of incorrect exercise, as explained in the following paragraph, with a number of repetitions varying from 2 to 4 basing on the individual sensations, to avoid injuries. External loads were in the range of 60-80% of ISO-MAX, computed as the load with which each subject was able to perform ten repetitions maximum. Weights used are shown in table below:

Table 2: external loads used for each subject and each exercise.

SUBJECT	SQUAT	WIDE SQUAT	DEADLIFT
S1	50 kg	50 kg	80 kg
S2	40 kg	40 kg	50 kg

Incorrectness of exercises executions

NASA Astronaut Strength, Conditioning and Rehabilitation Specialists approved the main execution mistakes here below summarized.

Squat and wide stance squat

1) No straight trunk (figure 24a): it means to not maintain the natural lumbar curves, so to keep the pelvis in retroversion instead of in anteversion during squatting and then to rounding back during rising.
2) Valgus knees (figure 24b): in this case, knees do not follow feet directions, but they approach the medial line of the body.
3) Knee joints over the toes lines (figure 24c): knees do not remain behind the vertical lines passed through toes.
4) Heels not in contact with the floor (figure 24c): heels are risen at the end of squatting.
5) Shallow squat: knees flexion angles smaller than 90°.

For simplicity, techniques will be called CO (Correct), RB (Rounded Back), VK (Valgus Knees), KOT (Knees Over Toes), RH (Raised Heels) and SH (SHallow).

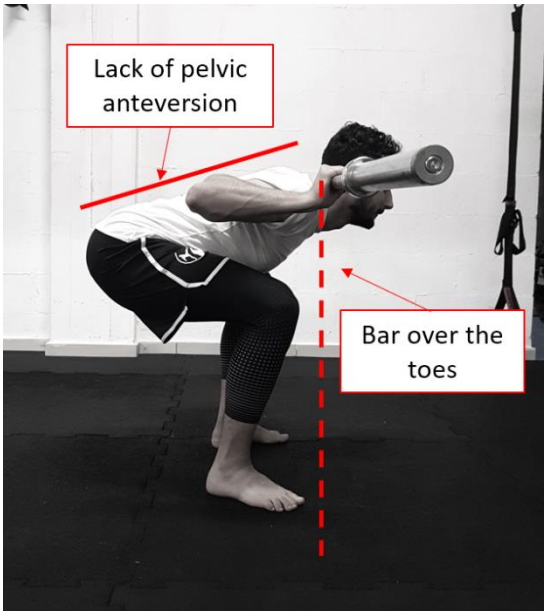

(a)

(b)

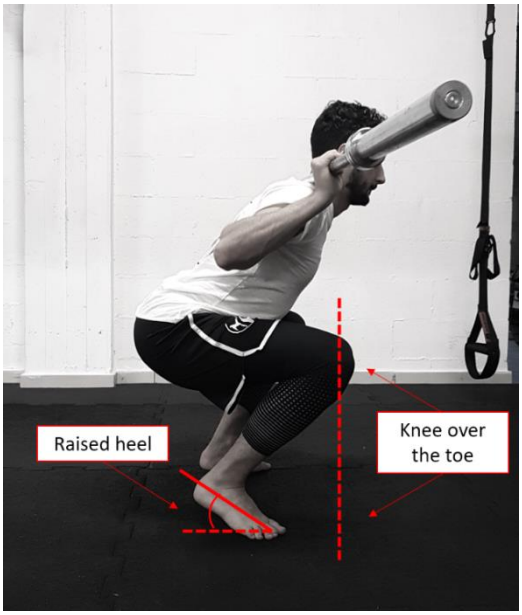

(c)

Figure 24: incorrectness of squat. (a) Trunk is not kept straight and this leads to bring the bar over the vertical lines of toes; dotted line projects shoulder joint on ground highlighting that line ends in front of toe. (b) Knees are brought closer; dotted lines show that knees and toes are not aligned. (c) Knees go over toes and heels are raised. Dotted line points out as knee overcomes toe.

Deadlift

1) Rounded back (figure 25a): trunk is not maintained in natural position, but it is bent forward.
2) Shoulders behind bar (figure 25b): bar is brought too far ahead at the start of exercise, overcoming the shoulders.
3) Hyperextended back (figure 25c): at the end of lifting, lumbar is overextended.

For simplicity, incorrect techniques will be named as RB, SB and HB respectively.

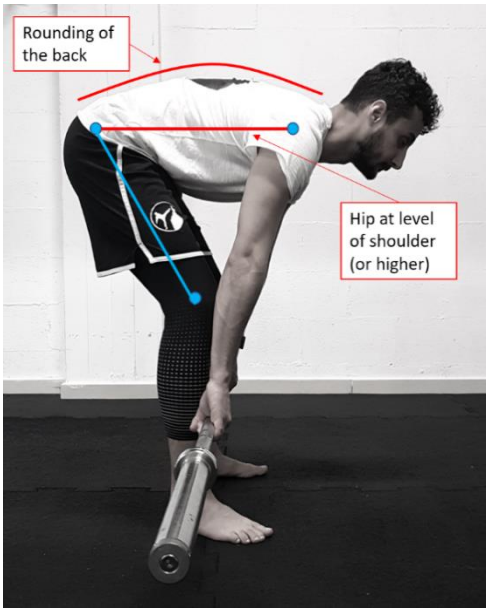

(a)

(b)

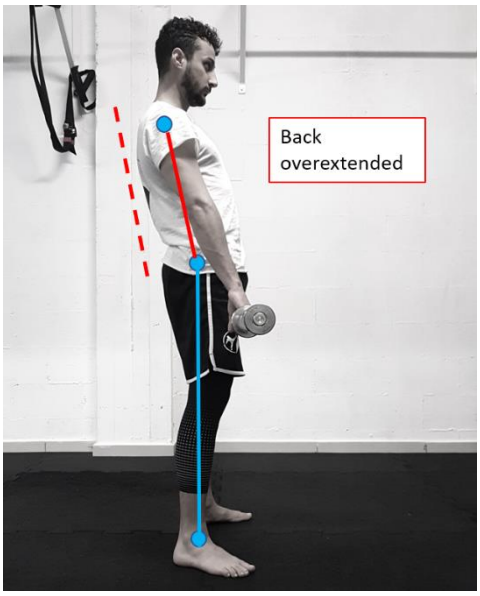

(c)

Figure 25: incorrectness of deadlift. (a) Trunk is rounded and this lends to start exercise with hip and shoulder at the same level instead of to have shoulder higher than hip. (b) Dotted line shows the vertical line passing from the shoulder; it is evident that exercise start with bar in front of that line. (c) At the end of lifting it is performed an excessive lumbar extension, so shoulder, hip and ankle are not aligned.

3.2 OpenSim models used

OpenSim provides different muscolo-skeletal models distributed and supported by the OpensSim Team. The most used and validated is gait2392_simbody. It reproduces lower extremity body with two legs and torso segment; it includes 23 degrees of freedom and 92 muscle-tendon actuators representing 76 muscles. The limitation is that it does not model upper limbs. Another interesting model is Full Body Running Model, provided by Leland Stanford Junior University, not by OpenSim Team, which has also upper limb extremities. Both models were tested in this work to simulate data collected at Politecnico di Milano. In the end, gait2392_simbody was chosen because no markers were placed on arms, so in the Full Body model they would have been fixed; furthermore, Inverse Kinematics using the Full Body model returned non-realistic hip flexion angles.
This model has seven rigid-body segments: pelvis, femur, patella, tibia/fibula, talus and foot (which includes calcaneus, navicular cuboid, cuneiforms and metatarsal) and toe. Each segment has a fixed reference frame. Hip is modeled as a ball-and-socket joint. Knee joint is simplified with a single-degree-of-freedom model, this to calculate extensor moment arm in a computationally inexpensive way. The model of ankle, subtalar and metatarsophalangeal joints is a frictionless revolute. Muscles are represented as red line segments with specific points of origin and insertion.
Model was modified by constraining a barbell with weights on the shoulders in order to make more realistic the simulation (figure 26a).

In addition, it was considered model developed by Fregly *et al* (2015) with ARED available online. They modeled the ARED kinematic structure starting from a three-dimensional computer-aided design (CAD) geometry of ARED components and connected a Full Body model to the structure (figure 26b). They created a joint between bar and shoulders and constrained feet on platform. This defined a kinematic structure including two closed kinematic chains. This model will be validated with data collected at NASA JSC to conduct a quantitative analysis; however, it was used to simulate motion with our data, but did not allow to obtain accurate kinematics results, but just a visive evidence to what happens during training with ARED.

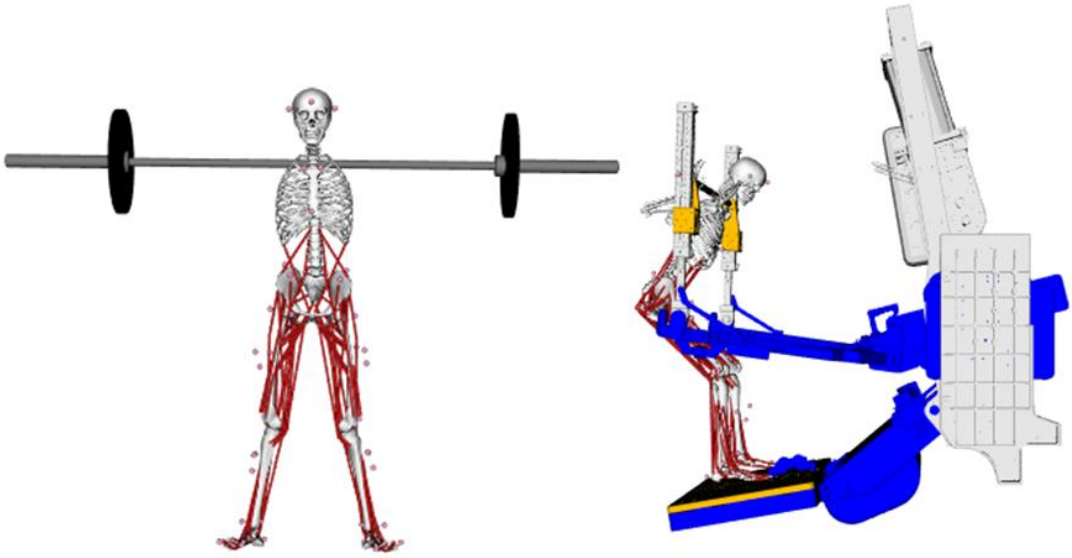

(a) (b)

Figure 26: (a) model used for simulation of motion collected at Politecnico di Milano; (b) model with ARED to validate with data collected at NASA JSC.

3.3 Data collection and data processing

Experimental data collection required a previous accurate calibration of the system, fundamental step to obtain good data, so to minimize systematic errors, which could affect the measures. Once markers were placed on each subject basing on the set-up described in section 3.1.1, the acquisition started. The software used in this step was BTS Smart Capture, provided by the producer, which returns a .trc file for each session of acquisition, which contains marker coordinates and GRFs along each axis and over time. Firstly, it was acquired a standing position of the subject in analysis to have information about its anthropometry. It was asked to maintain a static position, representative of the exercise considered, for few seconds and with each foot on each force plate. These data were later used to scale the biomechanical model as explained in 2.2.2. Subsequently, the subject performed both correct and incorrect techniques for each target exercises illustrated in 2.2.3. Smart Tracker was used to track raw data, so to label each marker giving it a specific name representative of the body point to which it was attached. The software required the creation of a model that recalled the positions of markers in space. For this purpose, it was created a model with 45 markers properly named and linked (figure 27). Tracked data related to each trial were exported in .tdf files.

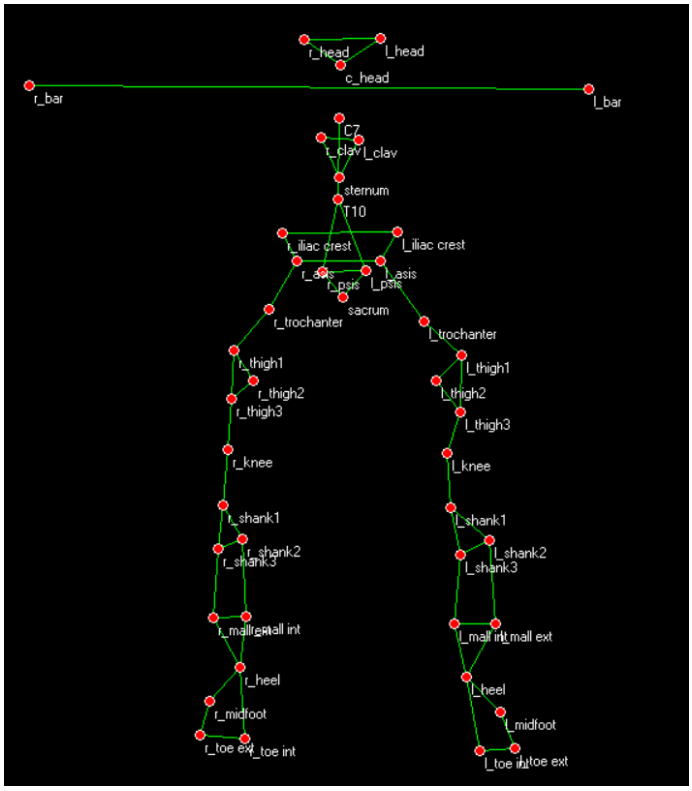

Figure 27: Markers' model built with Smart Tracker.

All subsequently data elaborations were done with Matlab R2018b.
An appropriate code was implemented to process raw data and to create files compatible with OpenSim. As explained in section 2.2.1, three files were needed: two .mot file containing kinematics data (marker coordinates) and one .trc file including dynamics data (external forces data, their points of application and, not mandatory, their torques).

To elaborate kinematics data, each marker trajectory along the three axes was interpolated with a cubic spline function to fill possible gaps; then, it was filtered with a Butterworth low pass filter with a cut-off frequency of 5 Hz. Furthermore, markers bad tracked were excluded basing on plots of their trajectories. In particular, markers put on ASISs were often subjected to occlusions, so they would have been useless for the next steps of the analysis. Static poses were extracted considering the mean of marker coordinates of the standing position. Then, two .trc file were created, one for Scale Tool and the other of IK Tool.

Special attention must be paid on force data files. From .tdf file of Smart Tracker it is possible to easily extract amplitudes, points of application and torques of GRFs; therefore, these information were opportunely written in the .mot file. Additionally, it was necessary to add external force due to the barbell. They were simulated different points of application in order to find the most suitable for OpenSim. The best one, which allowed to proceed with simulations without errors, was the midpoint of the barbell, so the point on shoulders where the load was mainly applied (figure 28).

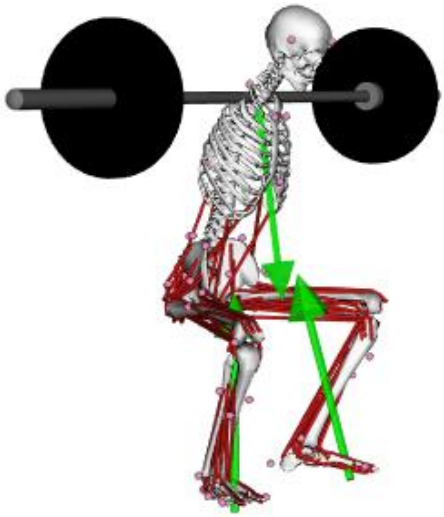

Figure 28: screenshot of the model during simulation of correct squat performed by S1. In green they are represented the GRFs applied to each foot and external force due to the barbell, applied to the torso.

Optoelectronic system and force plates worked with different frequencies, 100 Hz and 200 Hz respectively; thus, markers on the extremities of the bar were resampled in order to obtain the same number of frames as that of GRFs. Then, it was computed the midpoint for each instant of time and each axis. These data represented the points of application of the external force, frame per frame. Regarding the amplitude, it was considered only the vertical component, which was set equal to the loads used during the exercises under analysis, with negative sign and constant for the whole duration of the exercise:

$$F_{x_{bar}} = 0\ \text{N} \qquad F_{y_{bar}} = -\text{load} * g\ \text{N} \qquad F_{z_{bar}} = 0\ \text{N} \qquad \text{Eq. (7)}$$

where $F_{x_{bar}}, F_{y_{bar}}, F_{z_{bar}}$ are the components of the force acting on the shoulders, load is the weight used on ground with barbell and g is the gravity acceleration (9.81 m/s^2).

For example, considering S1, which performed normal stance squat with 50 kg, external vertical force was: $F_{y\_bar} = -50\ kg * 9.81 \frac{m}{s^2} = 490.50$ N.

Having created all files, it was possible to compute scaling, IK, ID, RRA and CMC with OpenSim following the workflow exposed in chapter 2.

3.3.1 Statistical analysis

Output coming from OpenSim software were elaborated with Matlab R2018b in order to compare results in terms of joint angles, joint moments and muscle forces between the different techniques. For each subject and exercise series, the singles repetitions were extracted. Starting and ending points were manually selected basing on plot of knee joint flexion angle and hip joint flexion angle (figure 29). For squat and wide squat one cycle begins and terminates with extension of hip and knee joints, for deadlift the opposite.

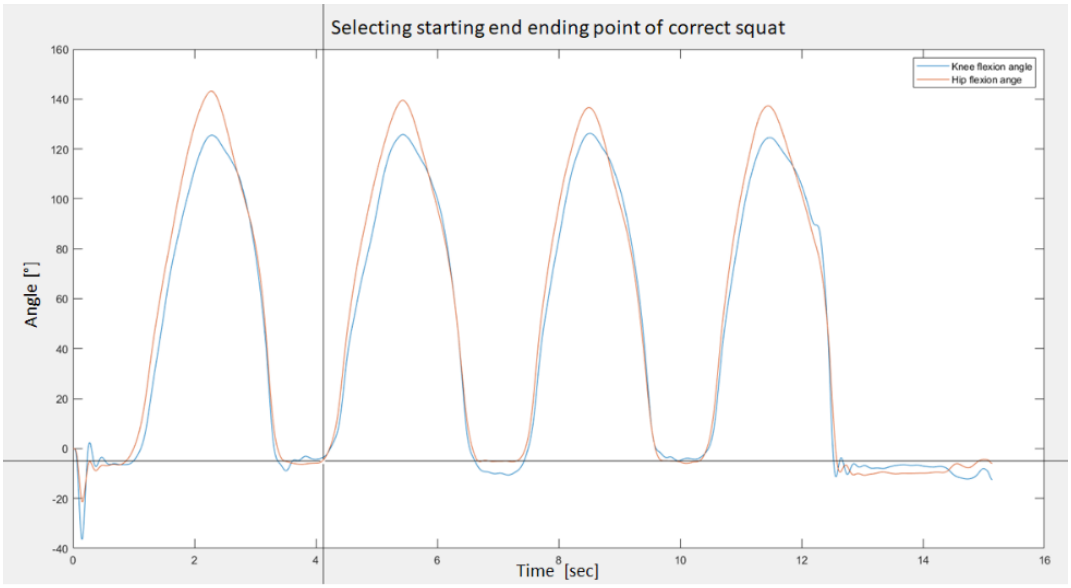

Figure 29: example of plot showing knee flexion angle (in blue) and hip flexion angle (in orange) of one series of 4 repetitions of correct squat. From this kind of plot, four start points and four stop points representative of singles repetitions were manually selected.

Then, repetitions were rescaled in time in order to have vectors with the same length and to distribute them in cycles spanning from 0% to 100%, regardless of the duration of the single repetition. Then, mid-trend and standard deviation were computed for each kind of exercise, considering the whole set of data, so including data of both subjects. In figure 30 it is possible to see an example of the resulted knee flexion joint angle of correct squat.

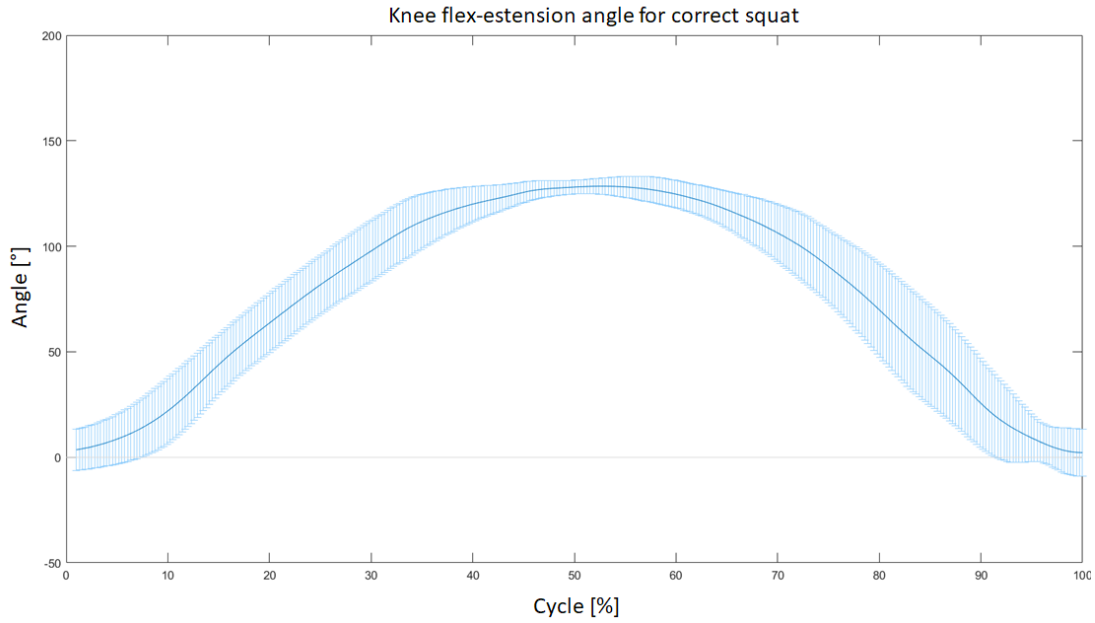

Figure 30: mid-trend and standard deviation of knee flexion-extension angle of correct squat (mean and standard deviation of all repetitions of all subject rescaled in time).

Obtained these data for each technique, the following statistics were computed:

- Correlation between right and left legs to check symmetry during execution;
- Max, range of motion (RoM) and mean of joint angles;
- Max and mean of joint moments, divided by body weight plus external load;
- Max and mean of muscle forces;
- Pairwise comparison with non-parametric test Wilcoxon-Mann-Whitney between correct and each kind of incorrect exercise (e.g. CO squat - RB squat), with the null hypothesis that the central tendencies were equal.

3.4 Weightlessness simulation

Different elaborations of force data were conducted to simulate exercises on ISS. In zero gravity conditions weight is lost, instead force due to the bar remains thanks to ARED, as described in 1.2. For this reason, body weight component was subtracted to the GRFs, which shifted lower by a constant then in 1G; the BW was equally distributed on each foot as follow:

$$\begin{aligned} \mathrm{GRF(i)_{y\_0g\_right}} &= \mathrm{GRF(i)_{y\_1g\_right}} - \left(\frac{\mathrm{BW}}{2} * \mathrm{g}\right) \mathrm{N} \\ \mathrm{GRF(i)_{y\_0g\_left}} &= \mathrm{GRF(i)_{y\_1g\_left}} - \left(\frac{\mathrm{BW}}{2} * \mathrm{g}\right) \mathrm{N} \end{aligned} \qquad \text{Eq. (8)}$$

Where i is the i-th value of GRF of the i-th frame, BW the body weight of the subject and g the gravity acceleration equal to $9.81 \frac{\mathrm{m}}{\mathrm{s}^2}$.

For example, considering again the S1, who performed squat with 50 kg and weights 65 kg, the x and z components of GRFs in 0g remained the same as in 1G and the vertical component became: $\mathrm{GRF(i)_{y\_0g\_right}} = \mathrm{GRF(i)_{y\_1g\_right}} - \left(\frac{65}{2} * 9.81\right) = \mathrm{GRF(i)_{y\_1g\_right}} - 318{,}825\ \mathrm{N}$ and the same for the left side.

In this part of simulation, also BWR had to be taken into account. As said in 1.2, astronauts perform exercises on ISS adding almost 70% of BW, so that the musculo-skeletal system is conditioned similarly then in 1G. For this reason, the desired percentage of BW was added to the vector that identified the bar and the complementary percentage was subtracted to the GRFs:

$$\begin{aligned} \mathrm{F_{y\_bar}} &= -(\mathrm{load} + \mathrm{BWR}) * \mathrm{g}\ \mathrm{N} \\ \mathrm{GRF(i)_{y\_0g\_right}} &= \mathrm{GRF(i)_{y\_1g\_right}} - \left(\frac{(1-\mathrm{BWR})}{2} * \mathrm{g}\right) \mathrm{N} \\ \mathrm{GRF(i)_{y\_0g\_left}} &= \mathrm{GRF(i)_{y\_1g\_left}} - \left(\frac{(1-\mathrm{BWR})}{2} * \mathrm{g}\right) \mathrm{N} \end{aligned} \qquad \text{Eq. (9)}$$

Where load is the weight used on Earth, BWR is the desired percentage of BW to add, (1-BWR) the complementary to subtract and g the gravity acceleration equal to $9.81\,\frac{m}{s^2}$..

For example, for S1, who weighs 65 kg, performed squat with 50 kg and choosing a BWR of 70%, values were: $F_{y\_bar} = -(50 + 0.7 * 65) * 9.81 = 936.855$ N, $GRF(i)_{y\_0g\_right} = GRF(i)_{y\_1g\_right} - \left(\frac{(0.3*65)}{2} * 9.81\right) = GRF(i)_{y_{1g_{right}}} - 95.6475$ N and the same for the left side.

In the end, vertical component of the gravity acceleration vector of the OpenSim biomechanical model was set to 0 before starting the simulation (figure 31).

```
<length_units>meters</length_units>
<force_units>N</force_units>
<!--Acceleration due to gravity.-->
<gravity> 0 0 0</gravity>
<!--Bodies in the model.-->
<BodySet>
    <objects>
        <Body name="ground">
            <mass>0</mass>
            <mass center> 0 0 0</mass center>
```

Figure 31: part of XML code of the .osim model in which is possible to change the gravity acceleration; in this case it was set equal to 0.

3.4.1 Regression model for computing optimal body weight replacement

Nowadays, the same BWR is used for all astronauts and for any exercises and quantitative analysis were conducted only for squat (DeWitt *et al* (2011) and Mummidivarapu *et al.*, 2017). The current work extended these considerations also for wide stance squat and deadlift. ID was computed in zero gravity by incrementing the BWR with step of 10% ranging from 40% to 100% in addition to simulation with 0% of BWR. Once having extracted each repetition, having rescaled in time and having obtained mid-trend as in 3.3.1, mean and peak moments were computed for each BWR. Thus, an algorithm was

developed in Matlab R2018b to identify the relation between the different BWR loads and joint moments using linear regression.

$$y = \beta_0 + \beta_1 x + \epsilon \qquad \text{Eq. (10)}$$

Where the dependent variable y is vector with peaks or mean of joint moments and the independent variable x is a vector with the BWRs. β_0 and β_1 are y-intercept and regression coefficient respectively and ϵ the error term. For each joint, $n = 8$ observed values of dependent and independent variables (x_1, y_1), …, (x_n, y_n) were given, where the n observations corresponded to the n percentages of body weigth used (0, 40, 50, 60, 70, 80, 90, 100).

In the end, to find the optimal BWR for each joint to replicate the 1G scenario, the weighted sums of least squared residuals between 0G regression line and 1G line were minimized. In figure 32 there is an example of the optimal hip joint BWR obtained considering flexion moment of correct squat performed by S1.

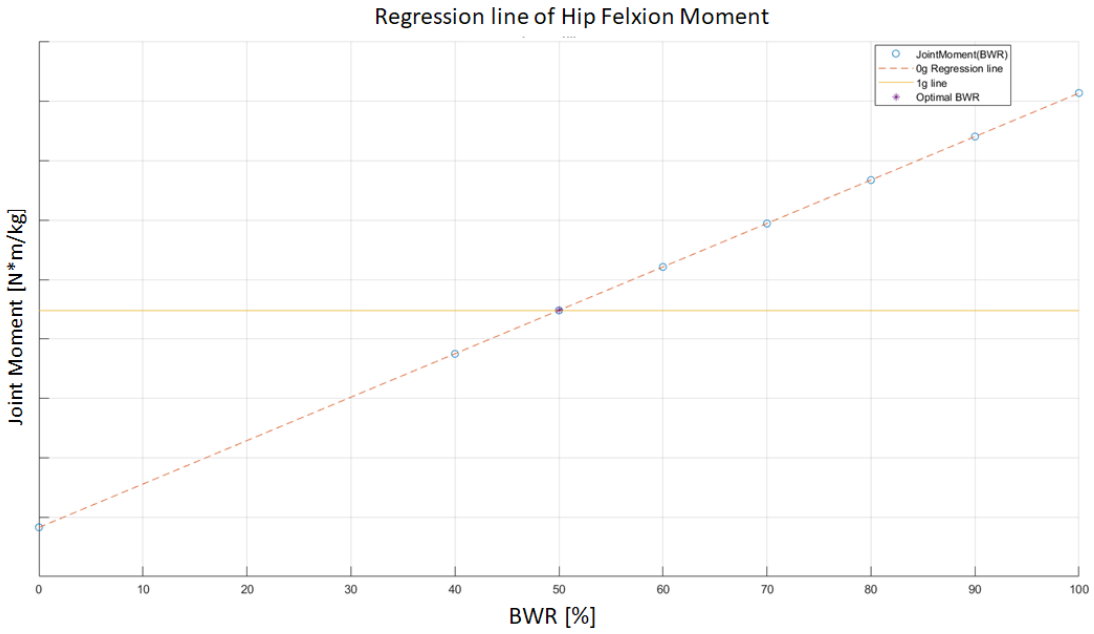

Figure 32: optimal BWR for hip joint of S1 during correct squat execution. Dotted line in orange is the regression line of max joint moments in 0G depending on BWR; yellow line is the max joint moment obtained in 1G. The intersection is the optimal BWR computed by minimizing the weighted sums of least squared residuals.

3.5 Inertial sensors simulation

Given that only kinematics data acquired with MOCAP system of exercises performed by astronauts with ARED are available, a way to extract accelerations data as the ones obtainable with inertial sensors is needed. For this scope, it was used the Analyses Tool of OpenSim; please, for any specification about how it works refer to 2.2.7.
The four body points chosen (figure 33) were: sternum, sacrum, mid-thigh and mid shank.

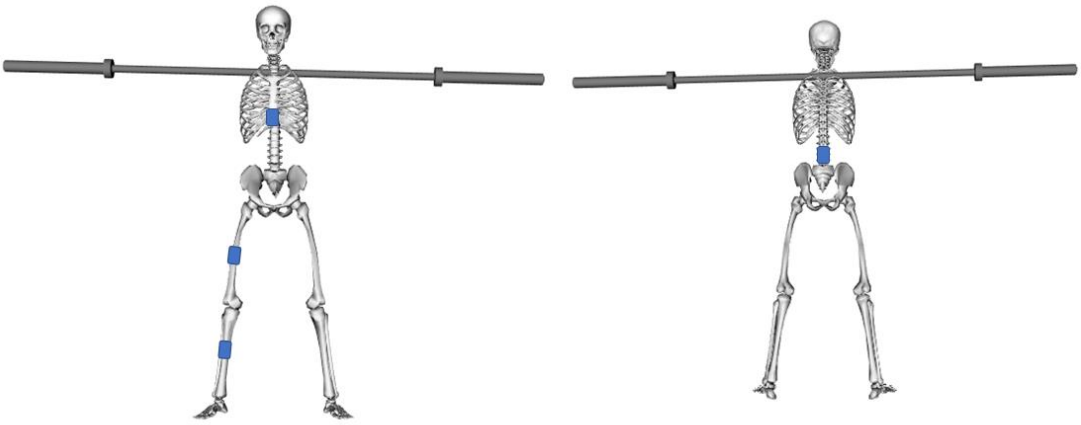

Figure 33: frontal (left) and back (right) view of model with virtual inertial sensors (in blue) placed on sternum, sacrum, mid-thigh and mid shank.

The software provided positions, linear and angular velocities, linear and angular accelerations of each point and saved the result in .sto file. However, it was observed an inexplicable drift of acceleration data, so they were computed via Matlab deriving velocities. An example of the result is shown in figure 34.

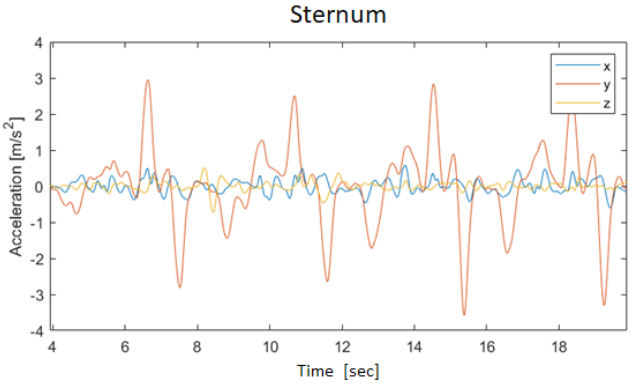

Figure 34: accelerations along the three axes of the virtual sensor put on sternum. Data are related to one set of 4 repetition of correct squat.

3.6 Approach to build the classifier

Despite the few acceleration data available, it was explored a method to build a classifier based on machine learning algorithm. In literature, there are many studies in which researcher classified human motion using inertial systems, especially IMUs.

The main area regards recognition of daily human activities, such as standing, walking, running and sitting (Yang *et al.,* 2008; Erdas *et al.,* 2016; Chernbumroong *et al.,* 2013; Sprager *et al.,* 2009; Farkas *et al.,* 2011; Farkas *et al.,* 2011). In clinics, they were used to detect fall of elderlies (Kazi *et al.,* 2014), to recognize stereotypical motor movements in autism spectrum disorder (Rad *et al.,* 2017), in gait analysis (Kavanagh *et al.* 2008) and medical monitoring (Zhang *et al.* 2009). Supervised learning methods were mainly used, in particular support vector machines (SVM) and artificial neural networks (ANN).

In sport, especially as concern training including exercises analyzed in this work, three studies are available. Soro *et al.* (2019) used a large amount of raw data coming from off-the-shelf smartwatches to classify ten typical CrossFit exercises using a convolutional neural network (CNN) and obtaining an accuracy of 99.96%. Similarly, Um *et al.* (2017) classified fifty gym exercises with CNN starting from large-scale motion data obtained from a forearm-worn wearable sensor. The accuracy was 92.1%. O'Reilly *et al.* (2015) classified seven induced deviations of squat performance with a single lumbar-worn IMU. They analyzed 22 subjects which performed squat correctly and with seven incorrectness. A total of thirty features in time domain and coming from each axis of accelerometer, gyroscope and magnetometer were extracted. This was done considering each single repetition of each single squat condition. A back-propagation neural network was chosen as suitable to label data. They performed both a binary classification, in order to distinguish correct and incorrect techniques, and multi-label classification. To test the algorithm, they used a leave one site out cross validation (LOSOCV). The results in terms of sensitivity, specificity and accuracy are shown in table 3.

Table 3: mean LOSOCV results of binary and multi-label classifier (O'Reilly *et al.* 2015)

	Binary Classification	**Multi-Label Classification**
Sensitivity (%)	64.41	59.65
Specificity (%)	88.01	94.84
Accuracy (%)	80.45	56.55

The same researcher group (2017) developed a classifier for detecting deadlift biomechanics using five IMUs placed on both sides of body (figure 35).

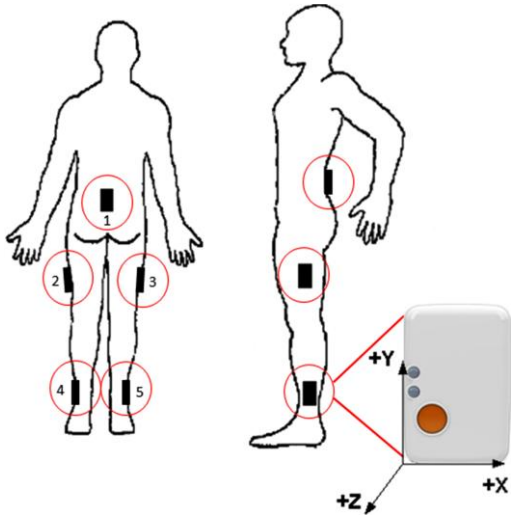

Figure 35: positions of five IMUs placed on body: lumbar spine, both thighs and both shanks (from O'Reilly et al., 2017).

They developed a system able to distinguish correct deadlift and 5 deviations of the technique. They collected more than 1800 repetitions distributed along the different executions from eighty healthy volunteers. They extracted 17 features from each signal related to each repletion coming from the five IMUs, obtaining a total of 1530 variables. They trained and tested a random forest classifier with LOSOCV for global analysis and Leave One Out Cross Validation (LOOCV) for personalized analysis. They also compared quality of classification when IMUs were worn in combination and isolated. As for squat, both binary and multi-label classifications were explored. The best results were obtained for binary personalized classification, considering the whole set of IMUs.

3.6.1 Methods chosen in this work

Due to the small dataset of accelerations, classification was limited to a binary classification in order to distinguish performance between correct and wrong, without differentiating the various mistakes. Two supervised learning methods were compared: Artificial Neural Network and Support Vector Machine.

Supervised algorithm usually begins with feature extraction. Starting from a set of measured data, non-redundant informative values are extracted. These features facilitate the subsequent learning and generalization steps. However, if the data set extracted is too large and may be redundant, it can be transformed and reduced in a subset by feature selection. The main statistical procedure used for selecting features is Principal Component Analysis (PCA), adopted in this project. The workflow can be seen in the scheme below.

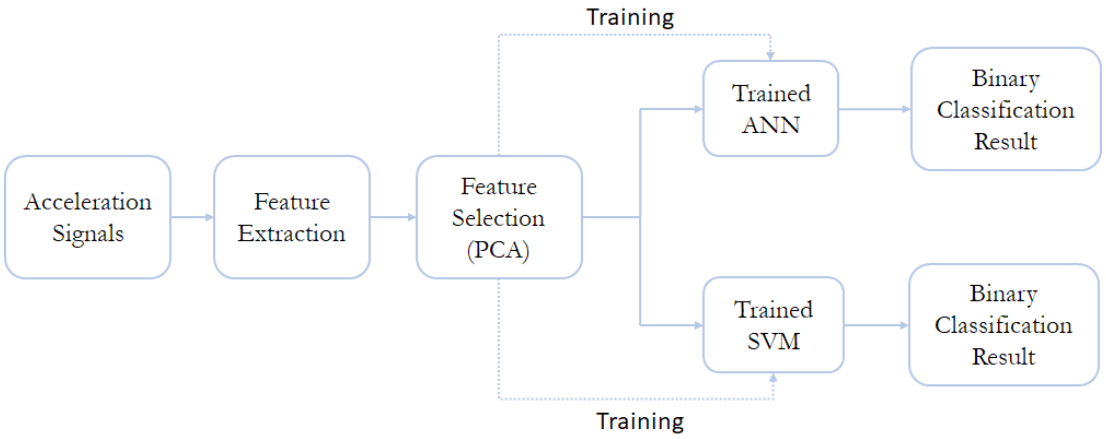

Feature extraction

Basing on previous cited works (Farkas *et al,* 2011; Erdas *et al.,* 2016), a total of 304 features for each kind of exercise were extracted. Values were computed considering signals coming from each axis of each virtual sensor. More in detail, four sensors were simulated, each one gave three acceleration signals, one per axis. Accelerations related to each repetition were extracted, filtered with a Butterworth low-pass filter with cut-off frequency of 2 Hz and rescaled in time. From the elaborated signals, features both in time and frequency domain were computed. To obtain the second ones, Fast Fourier Transform (FFT) was adopted. In table 4 there are all values listed.

Table 4: features extracted; each one is related to one axis of one sensor, apart from SMA and correlation, which combine values coming from two or three axis.

Name	**Formula**
Mean	$\bar{x} = \frac{\sum x_i}{N}$
Max	max(X)
Min	min(X)
Index of min	Index of min
Index of max	Index of max
Range max-min	max(X)-min(X)
Variance	$\sigma^2 = \frac{\sum(x_i - \bar{x})^2}{N}$
Standard Deviation	$\sigma = \sqrt{\frac{\sum(x_i - \bar{x})^2}{N}}$
Median	Median(X)
Root Mean Square (RMS)	$RMS = \sqrt{\frac{\sum {x_i}^2}{N}}$
Skewness	Skewness(X)
Kurtosis	Kurtosis(X)
Interquartile Range	Irq(X)
Mean Absolute deviation (MAD)	$MAD = \frac{\sum\|x_i - \bar{x}\|}{N}$
Signal Magnitude Area (SMA)	$SMA = \frac{1}{N}\left(\sum\|x_i\| + \sum\|y_i\| + \sum\|z_i\|\right)$
Correlation Between Axes (x-y, x-z, y-z)	$corr(x,y) = \frac{\sum(x_i - \bar{x})(y_i - \overline{y})}{\sigma_x \sigma_y}$
FFT Energy	$E = \sum\|x_i\|^2$
FFT Mean	mean(X)
FFT Max	max(X)
FFT Min	min(X)
FFT Band power	$E = \sum \frac{\|x_i\|^2}{N}$
FFT First Five Peaks	First five peaks

Principal Component Analysis

PCA is the most used technique of feature reduction. In general, it derives a transformation that allows to substitute the original data set with a lower number of new features obtained as their linear combination, without loss of useful information. This transformation can improve the accuracy of learning models subsequently used. Starting from n attributes of the dataset, PCA derives n orthogonal vectors named principal components (PCs). These components constitute a new base of the space $\mathbb{R}^n$. Generally, a subset of $q < n$ principal components describe equivalently the original dataset. Thus, the n original features are projected in a space with lower dimension q.

PCs are generated by applying iteratively an algorithm: the first PC is computed by solving an optimization problem so that it captures the maximum percentage of variance of the data. At each iteration, the next PC is chosen between orthogonal vectors of the PC already generated. In the end, PCs are listed in descending order with respect to the variance that they explained.

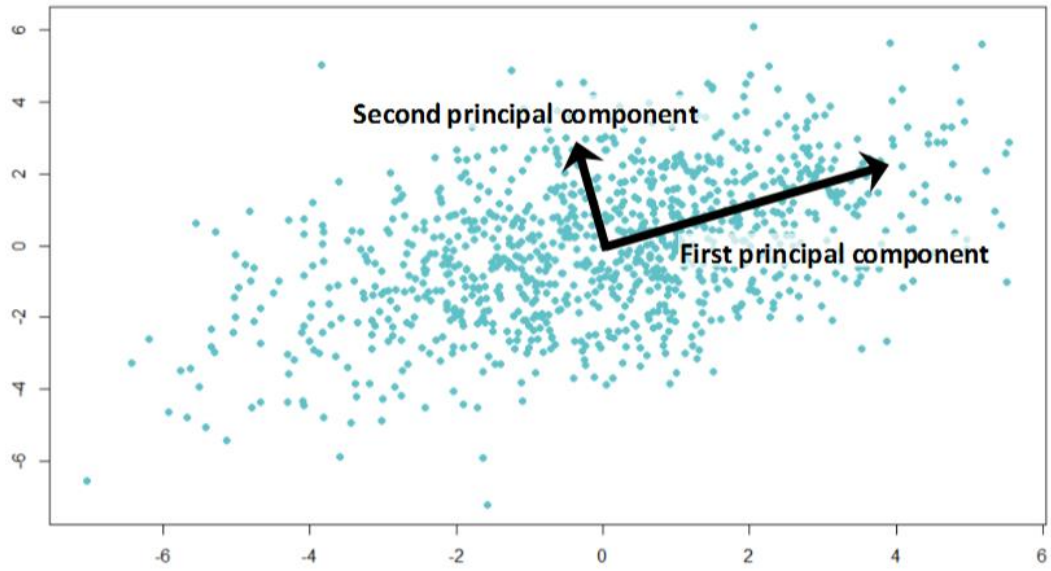

Figure 36: example of the result of PCA in which the first two PCs are plotted; it is evident as data are mainly distributed along the first PC and as the PCs are orthogonal.

First of all, data should be standardized to have all values in the same range and to have mean equal to 0. X is the matrix obtained with standardization and $\mathrm{V} = \mathrm{X}'\mathrm{X}$ its covariance matrix. $p_j, j \in N$ is the j-th PC, computed as $p_j = \mathrm{X}w_j$, where w_j are weights

to determine. A generic projection of a value x_i along the weight vector is $w_j' x_i$ and its variance is $w_j' V w_j$. The first PC p_1 is a vector in direction of maximum variance in the original space, so its weights can be obtained by solving the problem:

$$\max_{w_1} \{ w_1 V w_1 : w_1' w_1 = 1 \} \qquad \text{Eq. (11)}$$

This means to solve the system:

$$(V - \lambda_1 I) w_1 = 0 \qquad w_1' w_1 = 1 \qquad \text{Eq. (12)}$$

Where I is the identity matrix.

The solution to the maximization problem is $w_1 = u_1$, where u_1 is the eigenvector associated to the eigenvalue λ_1 of the covariance matrix V. Therefore, the first PC is $p_1 = X u_1$. The second PC is computed with the analog optimization problem of Eq. (11), with the addition of the orthogonality constraint to the first PC: $w_2' u_1 = 0$. Iteratively, it is possible to find all the PCs starting from the eigenvectors u_j of V ordered by non-increasing eigenvalues. The variance of each PC is given by $Var(p_j) = \lambda_j$.

The PC has the form:

$$p_h = u_{h1} a_1 + u_{h2} a_2 + \cdots + u_{hn} a_n \qquad \text{Eq. (13)}$$

Where u_{hj} is the weight of the attribute a_j in the determination of the principal component p_h. The higher u_{hj}, the more p_h is described by a_j. $Var(p_h) = \lambda_h$ is a measure of the total variance explained to the p_h. So, the index I_q measures the variance explained by the first q PCs.

$$I_q = \frac{\lambda_1 + \lambda_2 + \cdots + \lambda_q}{\lambda_1 + \lambda_2 + \cdots + \lambda_n} \qquad \text{Eq. (14)}$$

Usually, the number of PCs to consider is determined by choosing a threshold I_{min} and extracting the smaller number of PCs so that $I_q > I_{min}$.

For this work, the algorithm was developed in Matlab R2018b with the following steps:

- Standardization of data using z-score $Z = \frac{x_i - \bar{x}}{\sigma_x}$
- Computation of the covariance matrix $\mathrm{V} = \mathrm{X}'\mathrm{X}$
- Calculation of eigenvectors and eigenvalues of V, which represent respectively the directions of the PCs and their amplitudes
- Choice of the smallest number of PCs able to explain at least the 80% of the total variance

The algorithm was applied to each acceleration dataset related to each target exercise, considering both correct and incorrect techniques of all subjects. In the end, three reduced feature datasets were obtained: one for squat, one for wide stance squat and one for deadlift.

Feed-forward Artificial Neural Network

Artificial neural networks simulate the behavior of biological systems formed by neurons. They are largely used for prediction, classification and to estimate target attributes. An ANN is constituted by an oriented graph composed by nodes, which represent neurons. Nodes are connected by arcs that represent dendrites and synapses. A weight is associated to each arc and each node are defined with an activation function, which are applied to the input values corrected using weights.

A feed-forward ANN has different levels (figure 37):

- Input layer: it is formed by a number of neurons equal to the number of features present in the dataset.
- Hidden layer: it is composed by a chosen number of nodes connected with arcs to neurons of input and output layers. In this level, nodes compute transformations of the internal network values.

- Output layer: it has a number of neurons that differs basing on the type of classification desired.

Each arc has a weight, while each node has a coefficient and an activation function. The function could be for example linear, sigmoid or hyperbolic tangent. Additionally, feed forward neural network needs bias nodes to help its learning. They work as input nodes that produce a constant value, causing shifting of the output coming from the activation function. Equation 15 represents a single input sigmoid activation function f with weight w and bias b.

$$f(x, w, b) = \frac{1}{1 + e^{-(wx+b)}} \qquad \text{Eq. (15)}$$

The method which allows to determine weights is the backpropagation algorithm here explained. Weights are initialized with a random value and the input of the training set are examined using the current weights at each iteration. This permits to compute the prediction and the misclassification error. This error is then used to recursively correct the weights.

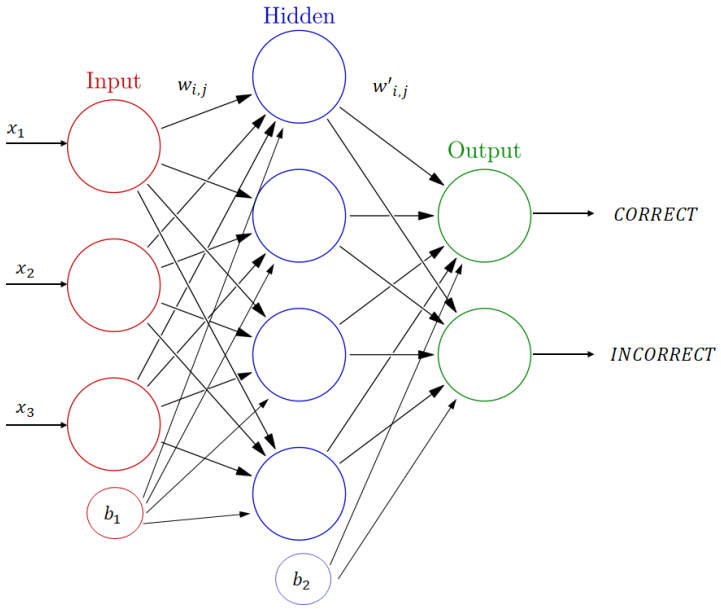

Figure 37: generic scheme representing a feed-forward artificial neural network; x_i are features in input; $w_{i,j}$ are weights and b_i are bias.

More in detail, calling the input q_i^{μ}, where μ are the p possible input configurations, the j-th unit of the hidden layer receives:

$$h_j^{\mu} = \sum_k w_{ij} q_k^{\mu} \qquad \text{Eq. (15)}$$

and produces as output:

$$V_j^{\mu} = g\left(h_j^{\mu}\right) = g\left(\sum_k w_{ij} q_k^{\mu}\right) \qquad \text{Eq. (16)}$$

Then, the i-th output unit receives in input:

$$h_j^{\mu} = \sum_k W_{ij} V_j = \sum_j W_{ij} g\left(\sum_k w_{ij} q_k^{\mu}\right) \qquad \text{Eq. (17)}$$

and produce as final output:

$$u_i^{\mu} = g\left(h_i^{\mu}\right) = g\left(\sum_j W_{ij} V_j\right) = g\left(\sum_j W_{ij} g\left(\sum_k w_{ij} q_k^{\mu}\right)\right) \qquad \text{Eq. (18)}$$

Error is the cost function:

$$E[w] = \frac{1}{2} \sum_{\mu i} \left[U_{di}^{\mu} - \mu_i^{\mu}\right]^2 \qquad \text{Eq. (19)}$$

Weights of the connections between hidden layer units and output layer units are modified basing on the gradient descend rule:

$$\Delta W_{ij} = -\eta \frac{\partial E}{\partial W_{ij}} = \eta \sum_{\mu} \left[U_{di}^{\mu} - \mu_i^{\mu}\right] g'\left(h_i^{\mu}\right) V_j^{\mu} = \eta \sum_{\mu i} \delta_i^{\mu} V_j^{\mu} \qquad \text{Eq. (20)}$$

Where

$$\delta_i^\mu = g'(h_i^\mu)[U_{di}^\mu - \mu_i^\mu] \quad \text{Eq. (21)}$$

To correct weights of the connections between input layer units and hidden layer units, the cost function is differentiated in respect to $w_{i,j}$:

$$\begin{aligned} \Delta W_{jk} &= -\eta \frac{\partial E}{\partial w_{jk}} \\ &= -\eta \sum_\mu \frac{\partial E}{\partial V_j^\mu} \frac{\partial V_j^\mu}{\partial w_{jk}} \\ &= \eta \sum_{\mu i} [U_{di}^\mu - \mu_i^\mu] g'(h_i^\mu) W_{ij} g'(h_j^\mu) q_k^\mu \\ &= \eta \sum_{\mu i} \delta_i^\mu W_{ij} g'(h_j^\mu) q_k^\mu = \eta \sum_{\mu i} \delta_i^\mu q_k^\mu \end{aligned} \quad \text{Eq. (22)}$$

Where

$$\delta_j^\mu = g'(h_j^\mu) \sum_i W_{ij} \delta_i^\mu \quad \text{Eq. (23)}$$

The two-layers feed-forward neural network used was developed using Matlab Neural Network Toolbox. Input layer was composed by a number of nodes depending on the result of PCA, which varies for each exercise. The number of hidden neurons was selected basing on the minimum error on validation sets. The output layer needed two neurons to classify correct and incorrect exercises. The activation function was the sigmoid. A matrix was created in order to define the target classification of each entries of the input matrix. Each row was labeled as [1 0] for correct performance and as [0 1] for the wrong one. The percentage of the reduced feature dataset to create subsets for training, validation and testing were respectively 80%, 5% and 15%. Confusion matrix and accuracies for each testing subset were obtained.

Support Vector Machine

Support Vector Machines represent a separation method for classification and estimation. They allow to identify a set of features, called support vectors (SVs), which are representative of the target classes. They are more important than the original features because SVs determine the position of the separation surface obtained from the classifier in the feature space.

In binary classification, SVM create N-dimension hyperplane which optimally separates data into two groups. The separation margin represents the distance between the pairs of canonic hyperplanes, parallel to the separation surface. The points collocated at the minimum distance to the hyperplane of separation are the support vectors (figure 38).

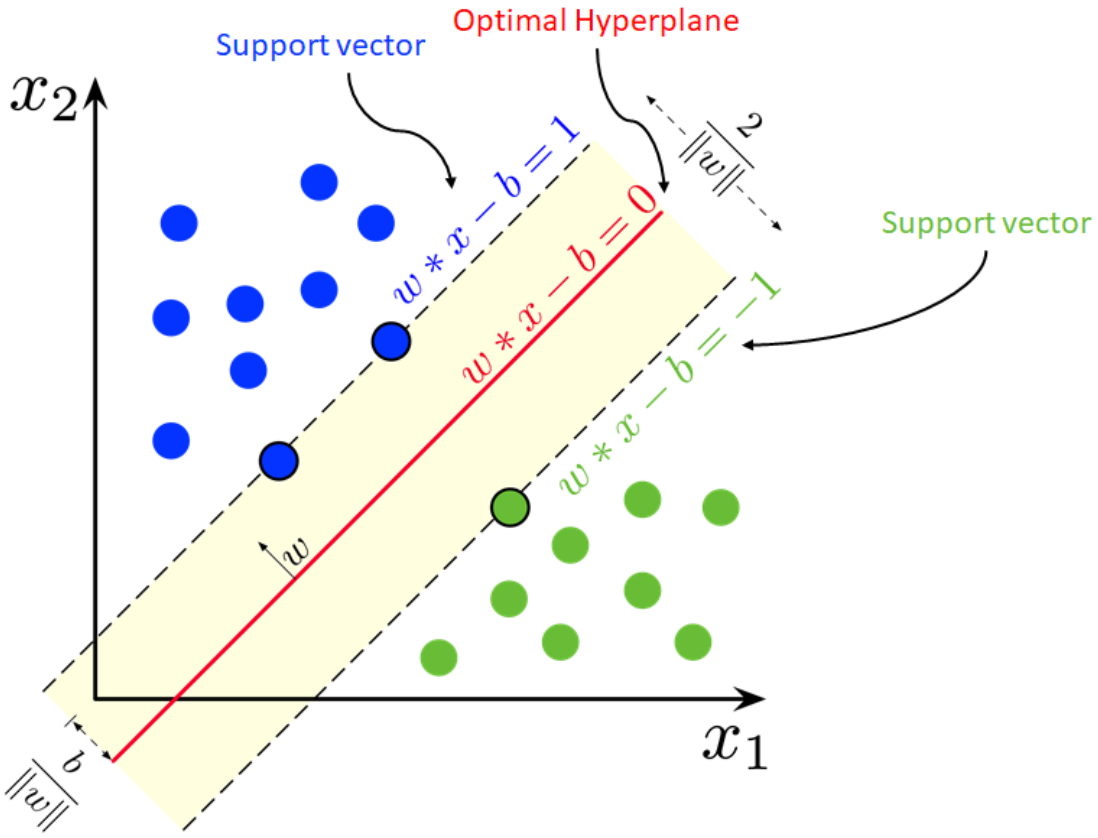

Figure 38: example of the separation surface of the maximum margin obtained with SVM applied for linearly separable data. In red is shown the optimal hyperplane; in yellow is represented the maximum margin; black dotted lines identify the support vectors for linearly separable data, whose formulas are expressed in blue and green. The two colors distinguish data belonging to the two classes.

Calling w the angular coefficient of the separator hyperplane and b the known term, the equation of the hyperplane is:

$$\mathrm{w}'\mathrm{x} = \mathrm{b} \qquad \text{Eq. (24)}$$

while the equations of the canonic hyperplanes are:

$$\mathrm{w}'\mathrm{x} - \mathrm{b} = 1 \qquad \mathrm{w}'\mathrm{x} - \mathrm{b} = -1 \qquad \text{Eq. (25)}$$

The separation margin δ is:

$$\delta = \frac{2}{\|\omega\|} \qquad \|w\| = \sqrt{\sum_{j \epsilon N} \omega_j^2} \qquad \text{Eq. (26)}$$

The goal of SVM is to maximize the separation margin with constraints, which impose that each point x_i stays in the half-space corresponding to the class y_i. In particular, if data are linearly separable, the optimization problem is:

$$\min_{w,b} \left\{ \frac{1}{2} \|\omega\|^2 \right\} \qquad y_i(\mathrm{w}x_i - \mathrm{b}) \geq 1 \qquad \text{Eq. (27)}$$

Where y_i is the label vector {-1, 1} that determines the class and the optimization problem is seen as the minimization of the reciprocal of the margin.

If data are non-linearly separable the problem is:

$$\min_{w,b} \left\{ \frac{1}{2} \|\omega\|^2 + \lambda \sum_{i=1}^{m} d_i \right\} \qquad y_i(\mathrm{w}x_i - \mathrm{b}) \geq 1 - d_i \qquad \text{Eq. (28)}$$

Where $d_i > 0$ is the error of classification; λ adjusts the relative weight of the generalization capability, which is represented by the reciprocal of the margin, and of the accuracy in respect to the training set, expresses as the sum of the errors.

The optimization problem is solved using Lagrange multipliers $\alpha_i \geq 0$ and $\mu \geq 0$ the multiplier of the constraints:

$$L(w, b, d, \alpha, \mu) = \sum_{i=1}^{m} \alpha_i - \frac{1}{2} \sum_{i=1}^{m} \sum_{k=1}^{m} y_i y_k \alpha_i \alpha_k x'_i x_k \qquad \text{Eq. (29)}$$

With $\alpha \leq \lambda$.

The algorithm was developed in Matlab R2018. Training set and data set were randomly created extracting respectively the 75% and 15% of data. A target array was created to define the correct class of each entry, labeled with {1,0}, where 1 corresponded to correct exercise and 0 to incorrect one. Confusion matrix and accuracy of each testing subset were obtained.

CHAPTER 4
RESULTS AND DISCUSSION

In this Chapter are reported results of simulations and related data analysis. In the first subchapter there are the evolutions of joint angles and joint moments related to correct exercise executions; the second subchapter reports data for comparing kinematics and dynamics coming from correct and wrong techniques of each training exercise. Following, there are results related to weightlessness simulations and optimal BWRs found. In the end, comparison between the two methods of machine learning used to classify performance basing on acceleration signals is reported.

Joint angles and moments are referred to the human body reference system, consisting in three planes (figure 39):

- Sagittal or longitudinal plane: it is perpendicular to the ground and divides body into left and right sides. In this plane, flexion and extension joint angles are considered. Positive values are related to flexion angles.
- Coronal or frontal plane: it is perpendicular to the ground and divides body into posterior and anterior portions. In this plane, adduction and abduction angles are described. Positive values are related to adduction angles.
- Transverse or horizontal plane: it is parallel to the ground and divides body into superior and inferior parts. In this plane, extra-rotation and intra-rotation angles are examined. Positive values are related to intra-rotation angles.

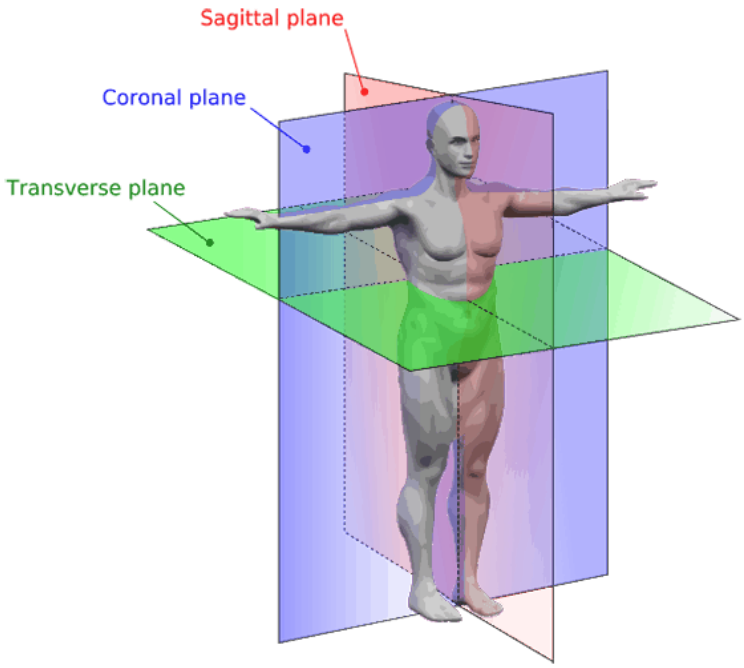

Figure 39: human anatomical planes. In red is shown the sagittal plane in which flex-extension angles are analyzed; in blue, the coronal plane, where abd-adduction movements are considered; in green, the transverse plane that consents to describe intra-extra rotation angles.

Results are focused on joints as follow:

- hip joint: flexion - extension, abduction - adduction and extra-intra rotation
- knee joint: flexion - extension
- ankle joint: plantar - dorsi flexion
- pelvis joint: pelvic tilt (anteversion and retroversion)
- lumbar joint: flexion - extension

Muscles considered are:

- vastus intermedius
- quadriceps femoris
- psoas
- erector spinae
- biceps femoris
- gluteus max
- soleus

4.1 Biomechanics of correct executions

4.1.1 Normal stance squat

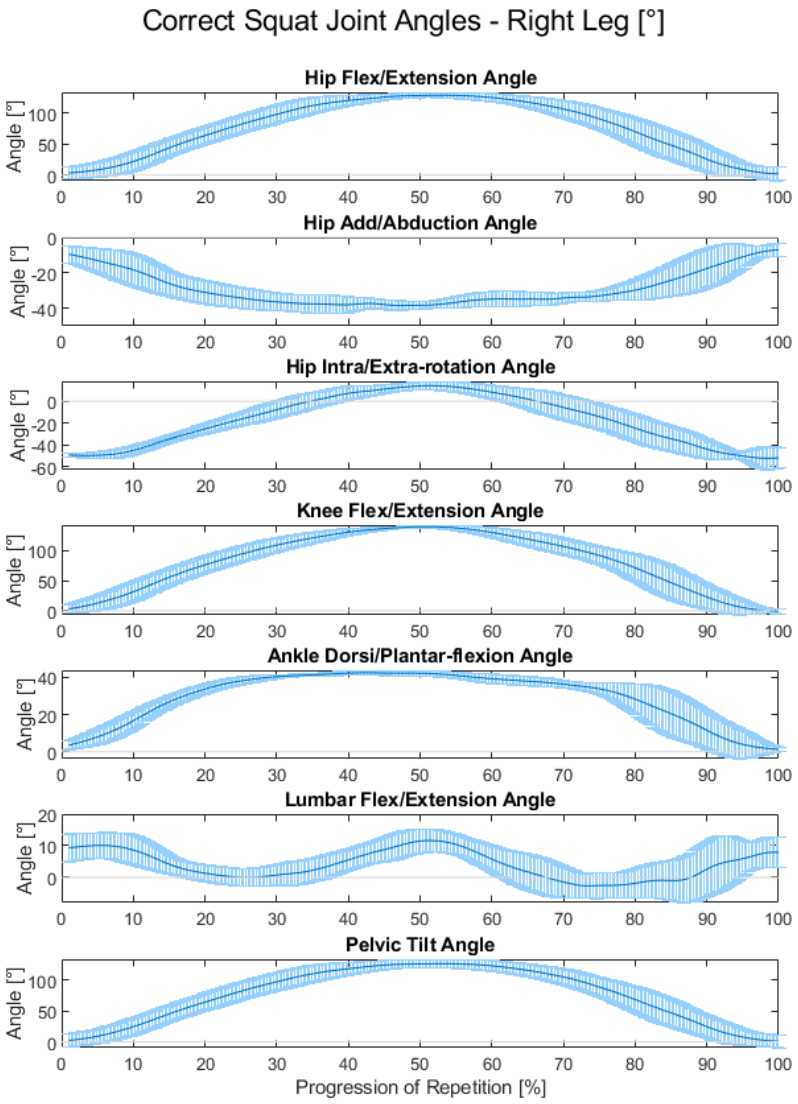

Figure 40: joint angles evolution of correct squat.

Starting position is almost neutral, with a slight lumbar flexion and hip extra-rotated. During squatting, hip, knee and ankle are flexed (ankle dorsi-flexed), hip is abducted with a decrease of the extra-rotation, reaching a small intra-rotation. Pelvis goes in anteversion during the descending phase to come back to 0 in ascending phase. Lumbar oscillates between flexion and a little extension.

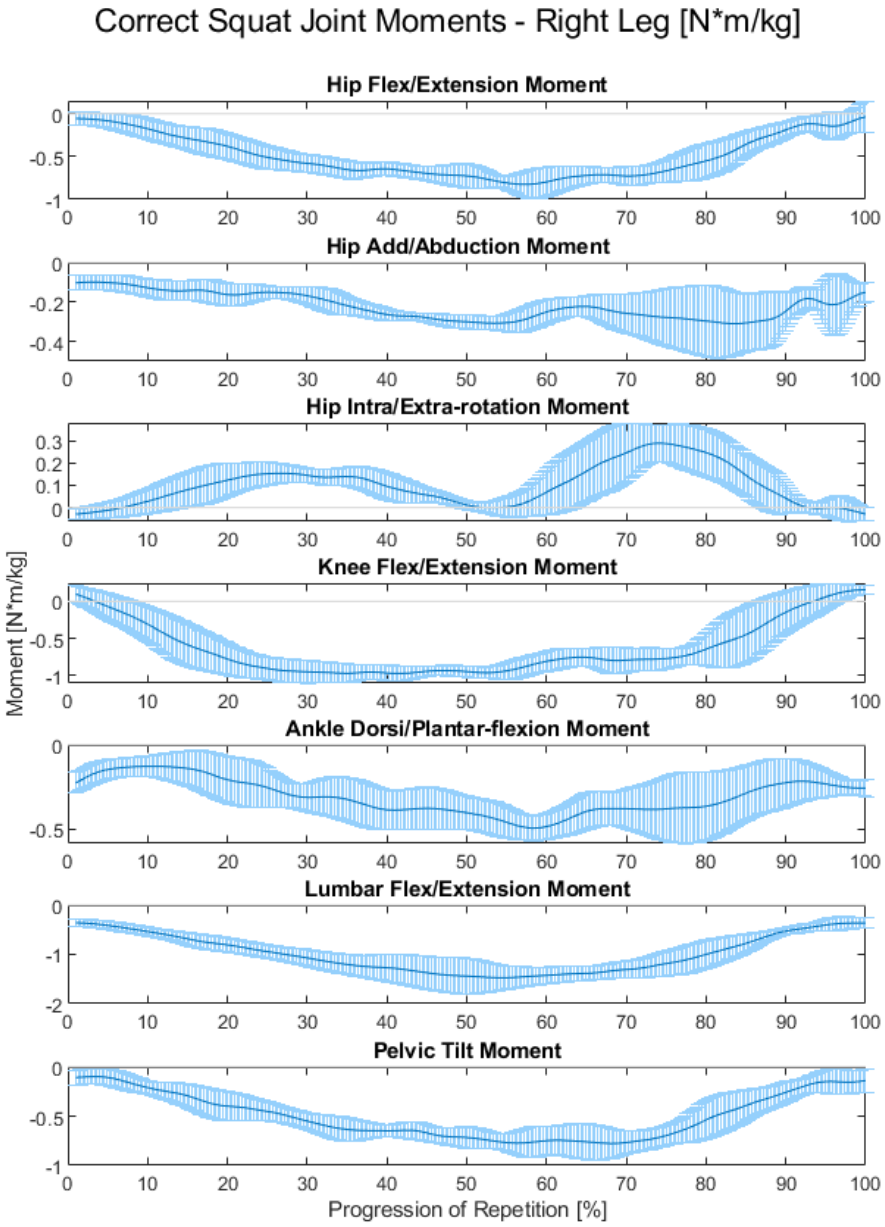

Figure 41: joint moments evolution of correct squat.

In the sagittal plane, trend of each joint shows an increasing internal extensor moment during squatting (plantar-flexion moment for ankle), which decreases by rising up to reach the initial neutral value. Hip is subjected to small increase of abductor moment followed by its decrease. Intra-rotation moment is observed in both descending and ascending phases, with neutral position at max squatting. Pelvis presents retroversion moment, which rises during squatting.

4.1.2 Wide stance squat

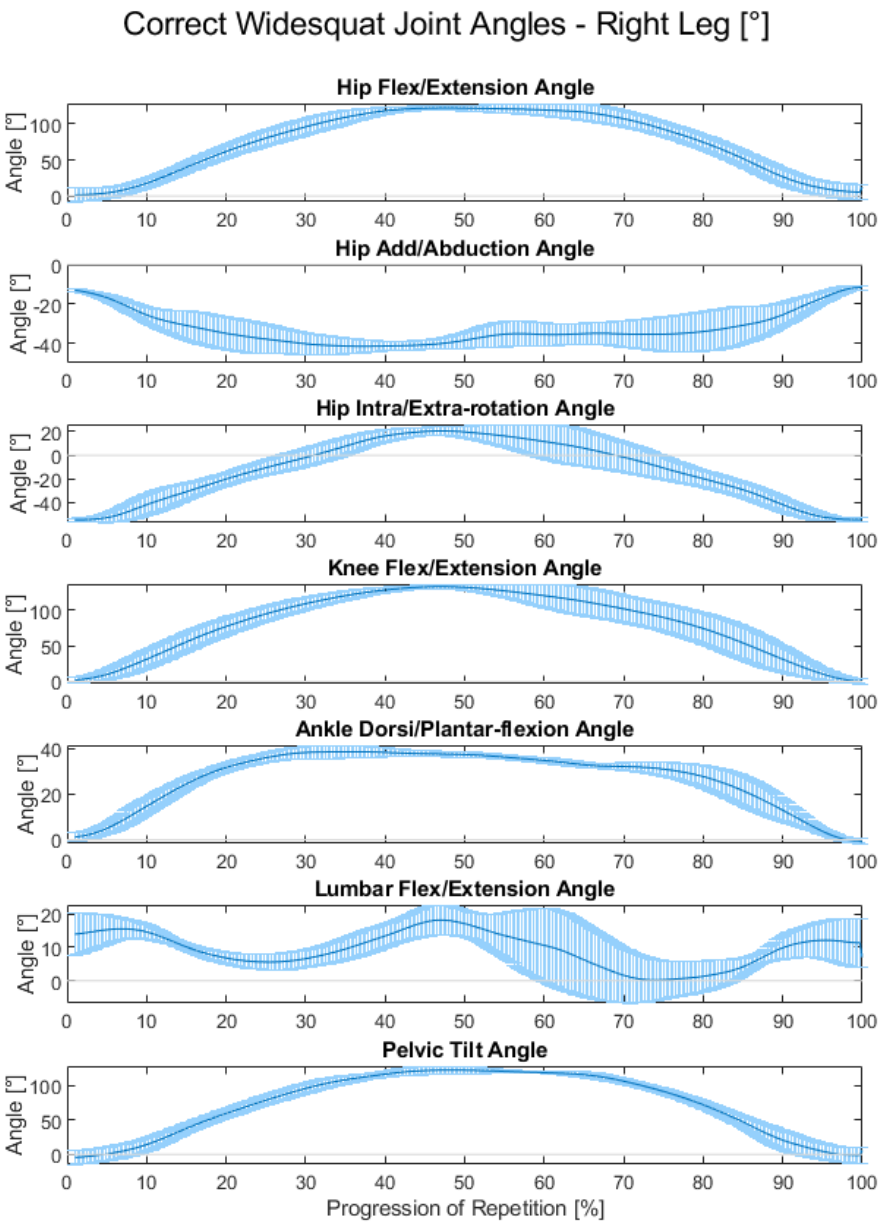

Figure 42: joint angles evolution of correct wide stance squat.

Trends are very similar to those of squat, with greater values of hip intra-rotation angles and lumbar flexion ones.

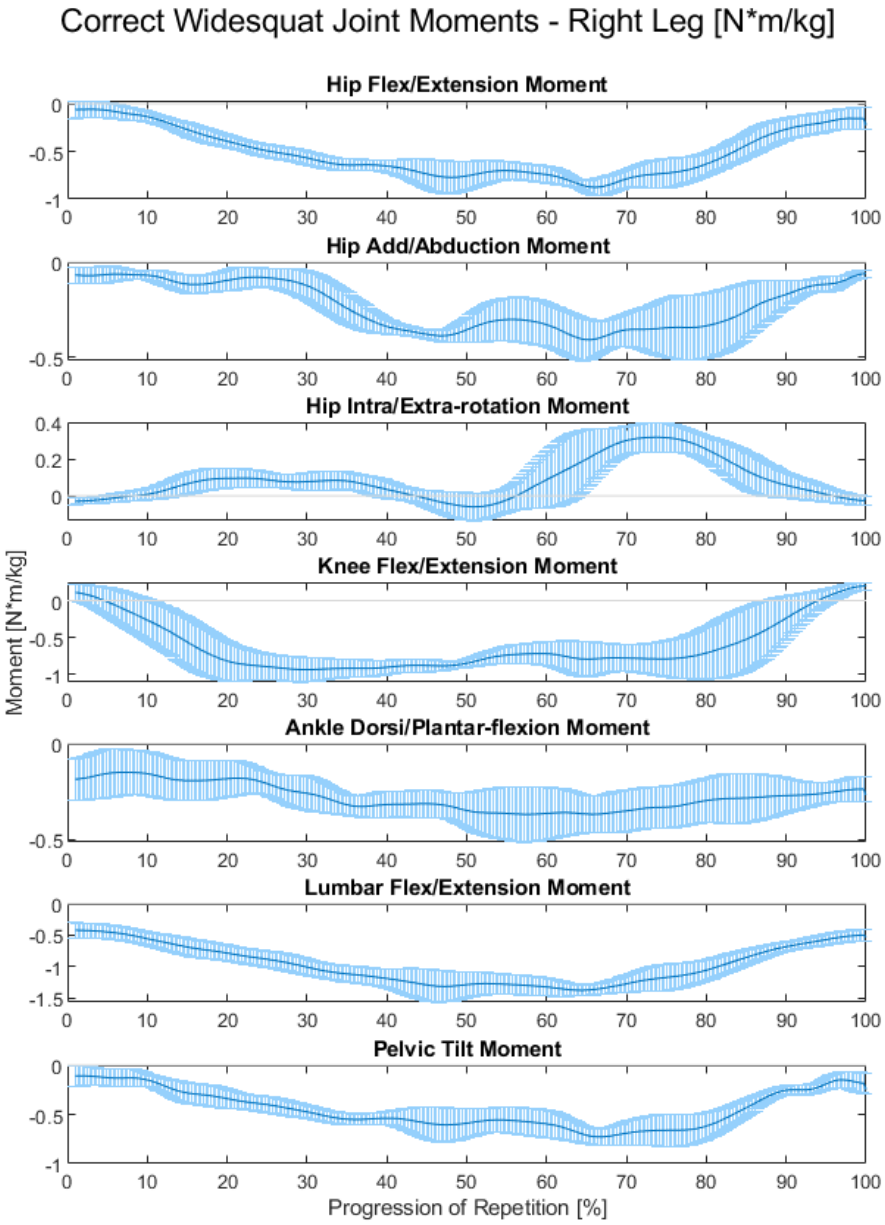

Figure 43: joint moments evolution of correct wide stance squat.

As for joint angles, joint moment trends are almost the same of those of squat.

4.1.3 Deadlift

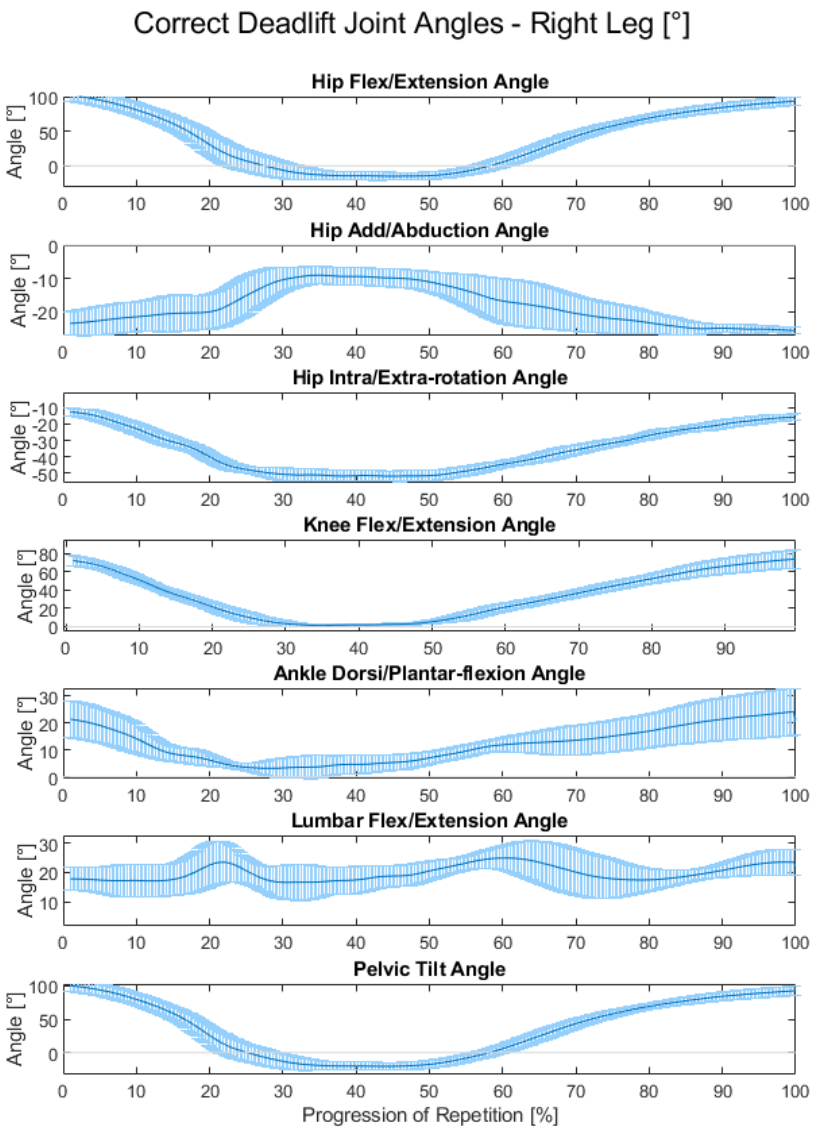

Figure 44: joint angles evolution of correct deadlift.

Deadlift requires starting and ending positions with hip, knee, ankle and lumbar flexed (ankle dorsi-flexed), hip abducted and slightly extra-rotated and pelvis anteverted. Opposite to squat and wide squat, in sagittal plane extension of joints during lifting are observed, followed by their flexion in descendent phase. Abduction of hip decreases and then increases again, as well as its extra-rotation. Lumbar joint oscillates remaining in flexion. Pelvic tilt is subjected to a reduction of anteversion, reaching values in retroversion in the extension phase.

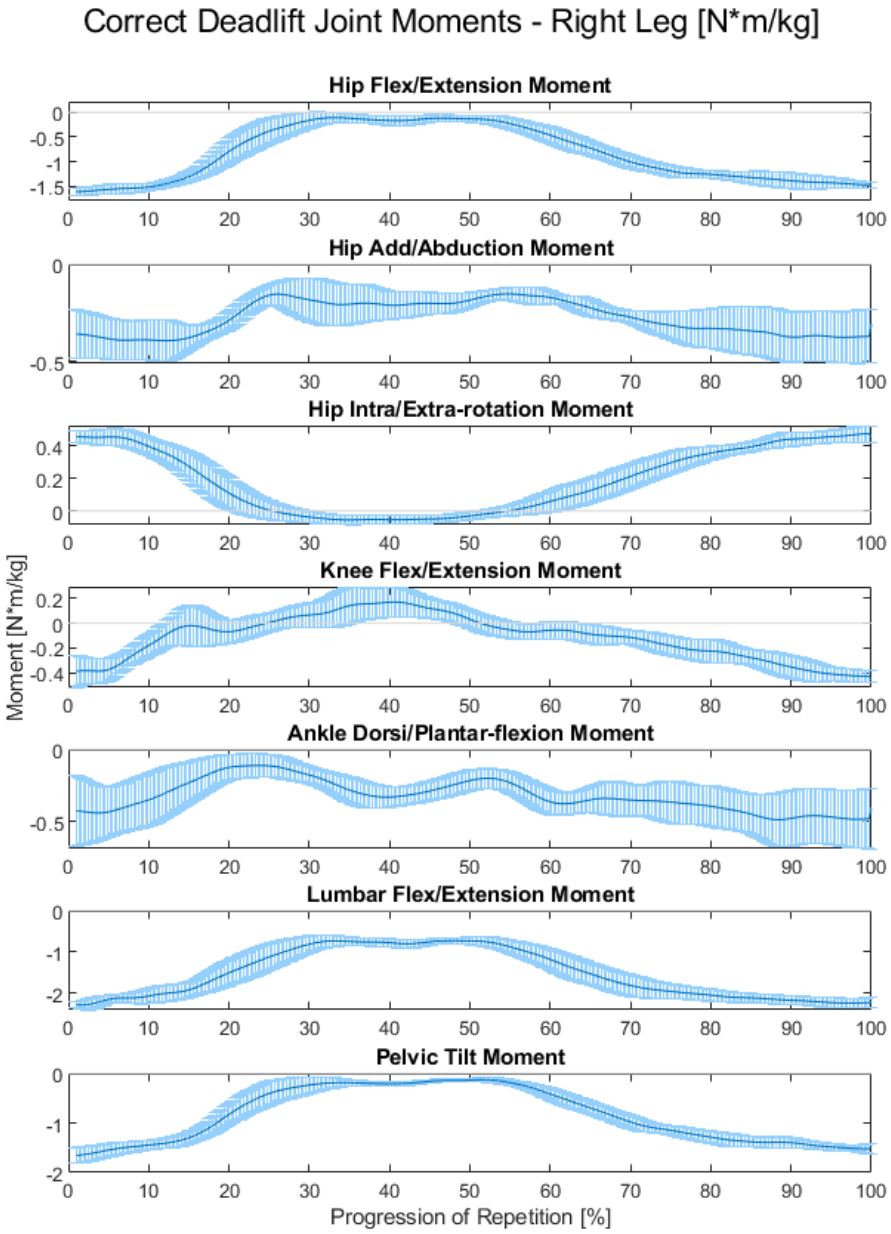

Figure 45: joint moments evolution of correct deadlift.

Also in this case, trends are the opposite than those of squat and wide squat, but while in squat intra-extra rotation hip moment oscillates, in deadlift curve is almost parabolic with vertex in extra rotation.

4.2 Biomechanical comparison between correct and incorrect executions

For each kind of exercise (squat, wide stance squat and deadlift) separated comparisons between joint angles, joint moments and muscle forces are reported. Firstly, symmetry between legs is checked; then, tables containing mean and peak of joint angles and moments are built, with the addition of RoM for joint angles. Furthermore, results of non-parametric Wilcoxon-Mann-Whitney test are specified. In the end, bar graphs showing mean of muscle forces are presented.

To have clear and simply representation to what are the differences between the techniques, angles and moments are represented with positive values. Headers of tables and graphs specify the considered movement (e.g. flexion or extension joint angle/moment). Statistics were computed considering the mid-trend of the whole set of repetitions, as described in 3.3.1.

4.2.1 Normal stance squat

Joint angles

Correlation between sides

Table 5: correlations of joint angles between right and left side of squat.

	Hip Flex-Ext	Hip Abd-Add	Hip Rotation	Knee Flex-Ext	Ankle Flexion
Correct	1,000	0,968	0,993	0,999	0,997
RB	0,999	0,986	0,976	0,998	0,991
KOT	0,999	0,917	0,993	0,998	0,995
VK	0,999	0,983	0,993	0,999	0,997
RH	0,999	0,965	0,997	0,999	0,989
SH	0,999	0,993	0,976	0,998	0,994

Symmetry was demonstrated for each joint and for each angle with a correlation greater than 0.9. Thus, for simplicity, following results are reported considering the right side.

Max joint angles

Table 6: max joint angles of squat [°] (right side).

	Hip Flexion	Hip Abduc	Hip Intrarot	Knee Flexion	Ankle Dorsi-f	Lumbar Flexion	Pelvis Antev
Correct	128,46	38,50	14,17	139,71	42,42	11,64	35,10
RB	129,26	32,46	10,25	130,40	39,91	17,51	57,19
KOT	117,65	31,82	14,61	139,61	49,28	20,57	32,98
VK	120,08	34,73	12,64	131,48	42,76	14,16	32,65
RH	125,70	39,48	22,98	143,44	39,17	19,09	34,85
SH	106,92	29,71	-3,87	108,30	37,05	12,21	33,41

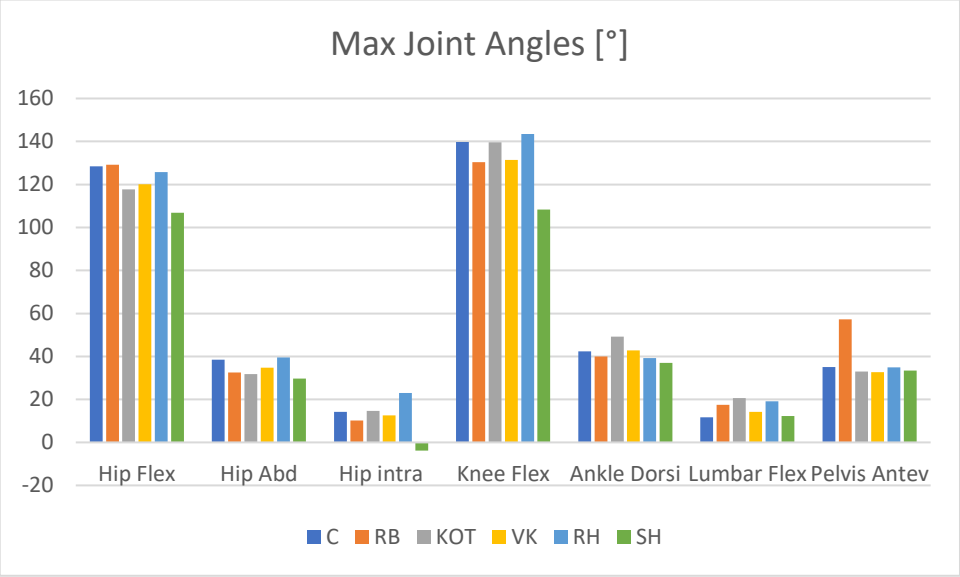

Figure 46: bar graph of max joint angles of squat (right side).

Ranges of motion

Table 7: ranges of motion of squat [°] (right side).

	Hip Flexion	Hip Abduc	Hip Intrarot	Knee Flexion	Ankle Dorsi-f	Lumbar Flexion	Pelvis Antev
Correct	126,24	31,45	66,25	141,13	41,13	14,32	28,97
RB	130,44	23,08	65,14	124,48	34,20	15,40	56,15
KOT	110,24	21,78	60,34	132,10	43,22	14,58	28,40
VK	115,20	25,20	61,93	129,30	39,87	10,92	28,76
RH	124,51	30,91	73,43	141,82	36,62	12,22	30,86
SH	103,60	22,98	47,20	101,57	32,19	14,12	29,77

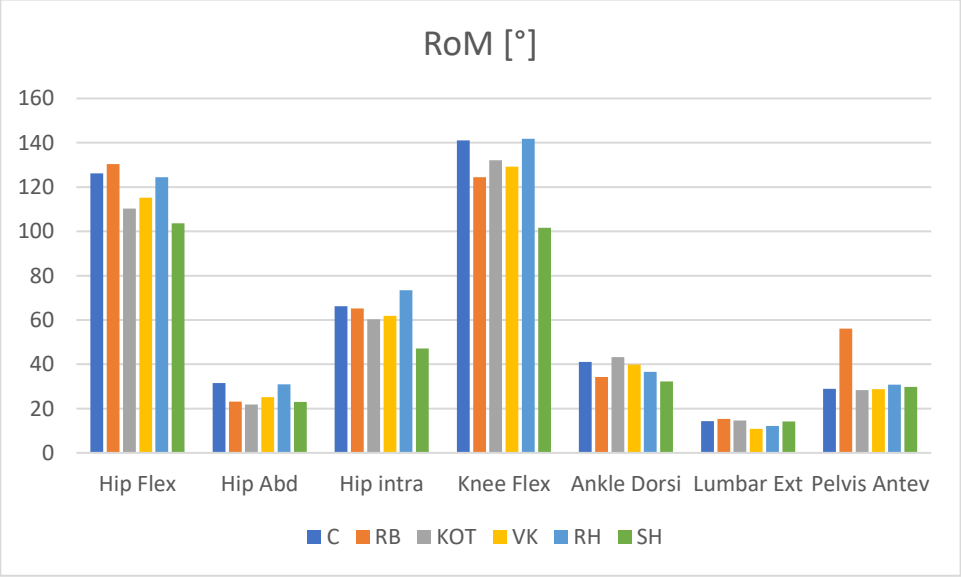

Figure 47: bar graph of ranges of motiom of squat (right side).

Mean joint angles

Table 8: mean joint angles of squat [°] (right side).

	Hip Flexion	Hip Abduc	Hip Intrarot	Knee Flexion	Ankle Dorsi-f	Lumbar Flexion	Pelvis Antev
Correct	76,94	28,95	17,00	82,72	29,58	4,02	23,14
RB	81,66	23,77	19,22	71,17	20,72	11,44	29,57
KOT	78,19	26,12	8,73	93,50	37,65	13,60	20,68
VK	75,35	23,15	11,26	82,63	30,81	8,60	21,96
RH	83,18	29,00	7,26	95,23	29,55	12,68	20,48
SH	65,77	23,46	22,02	70,89	27,05	2,43	22,83

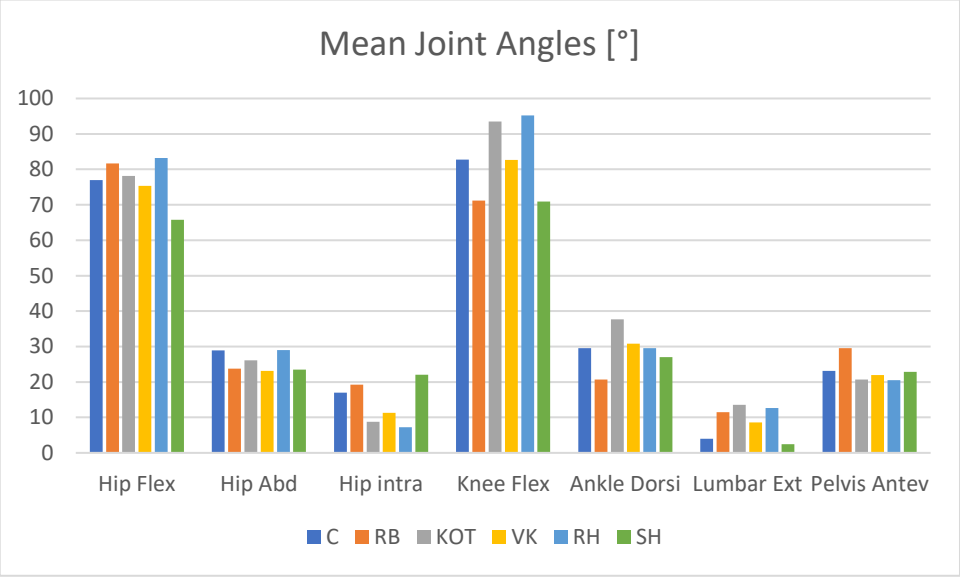

Figure 48: bar graph of mean joint angles of squat (right side).

Wilcoxon-Mann-Whitney

Differences with $p < 0.05$ for each joint were found, except for:

- Hyperextension of KOT
- Knee flexion of VK
- Hip adduction of RH
- Pelvic retroversion of SH

Joint Moments

Correlation between sides

Table 9: correlation of joint moments between right and left side of squat.

	Hip Extension	**Hip Adduction**	**Hip Extrarot**	**Knee Flexion**	**Ankle Plantaflex**
Correct	0,984	0,964	0,968	0,994	0,705
RB	0,997	0,811	0,992	0,989	0,945
KOT	0,985	0,916	0,970	0,986	0,952
VK	0,986	0,884	0,971	0,987	0,936
RH	0,985	0,945	0,969	0,987	0,977
SH	0,979	0,941	0,965	0,993	0,963

Symmetry was demonstrated for each joint and for each angle with a correlation greater than 0.88. Thus, for simplicity, following results are reported considering the right side.

Max joint moments

Table 10: max joint moments of squat [N*m/kg] (right side).

	Hip Extens	Hip Abduc	Hip Intrarot	Knee Extens	Ankle Plant-f	Lumbar Extens	Pelvis Retrov
Correct	0,82	0,31	0,29	0,97	0,49	1,47	0,21
RB	1,47	0,44	0,49	0,93	0,39	2,49	0,40
KOT	0,85	0,28	0,29	0,98	0,57	1,62	0,25
VK	0,78	0,27	0,23	0,95	0,39	1,52	0,23
RH	0,96	0,31	0,39	0,95	0,58	1,75	0,29
SH	0,87	0,30	0,31	0,92	0,41	1,27	0,16

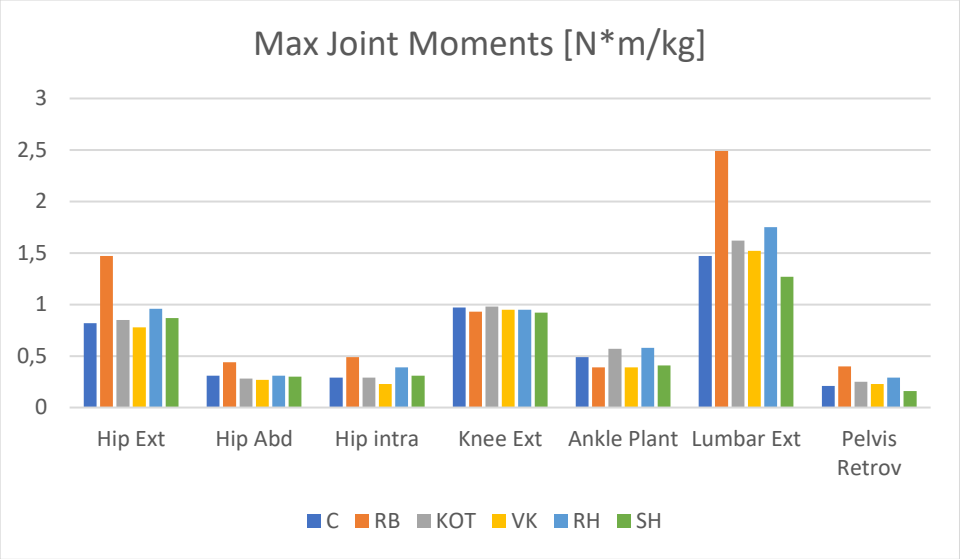

Figure 49: bar graph of max joint moments of squat (right side).

Mean joint moments

Table 11: mean joint moments of squat [N*m/kg] (right side).

	Hip Extens	Hip Abduc	Hip Intrarot	Knee Extens	Ankle Plant-f	Lumbar Extens	Pelvis Retrov
Correct	0,49	0,22	0,10	0,64	0,31	0,98	0,10
RB	0,80	0,25	0,19	0,39	0,25	1,49	0,20
KOT	0,57	0,21	0,11	0,70	0,43	1,20	0,19
VK	0,55	0,19	0,07	0,62	0,30	1,11	0,15
RH	0,57	0,21	0,10	0,60	0,43	1,21	0,17
SH	0,53	0,18	0,15	0,64	0,25	0,88	0,06

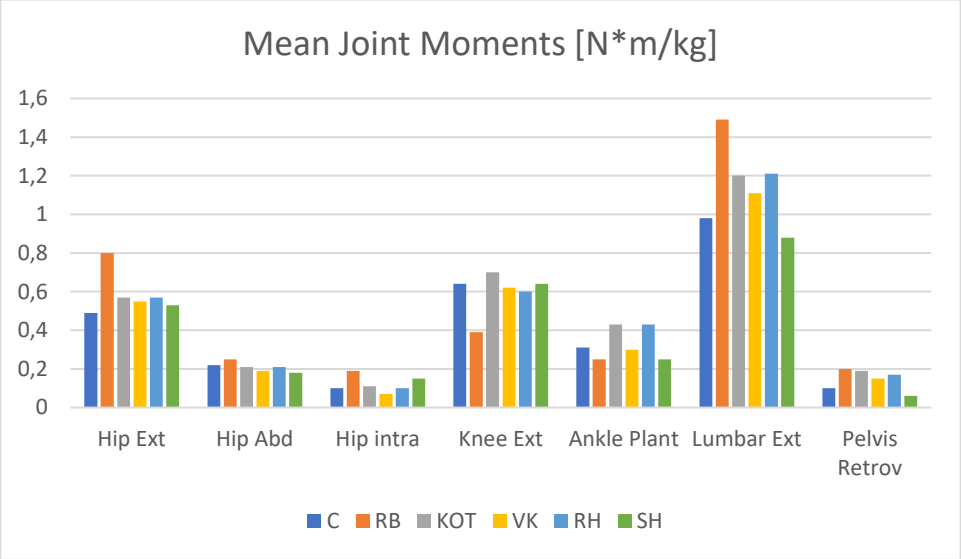

Figure 50: bar graph of mean joint moments of squat (right side).

Wilcoxon-Mann-Whitney

Differences with $p < 0.05$ for each joint moment were found, except for:

- Hip adduction of KOT
- Ankle plantar flexion of VK
- Hip adduction of RH
- Lumbar flexion of SH

Max muscle forces

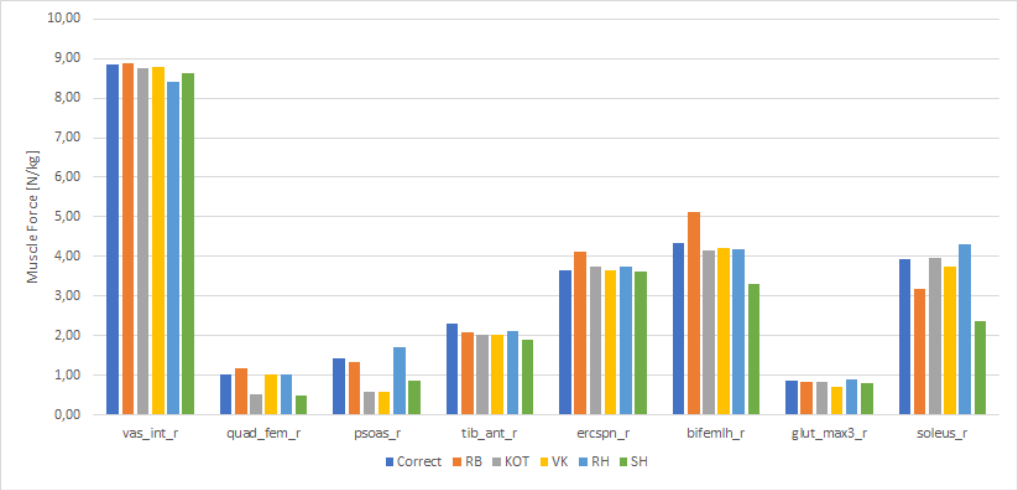

Figure 51: max muscle forces of squat (right side).

It was noticed that performing squat with inappropriate techniques could dangerously increase joint moments, especially in sagittal plane at levels of hip and lumbar joints. Rounding the back during squat showed the most evident changes, reaching values 1.6-1.8 times greater than those obtained with correct squat execution. As a consequence, knee and ankle joints resulted underloaded and this could cause inefficacy of training. Considering lumbar joint, rounding the back, rising heel and overcoming toe with knee revealed critical overloaded, which could cause back pain. Observing muscle forces, in support to these considerations, it was possible to see as rounding the back involved higher force expression of extensor muscle of trunk (erector spinae). Furthermore, shallow squat revealed similar moment joint values, but lower muscle activations of quadriceps femoris, psoas, biceps femoris and soleus, demonstrating its less training ability.

4.2.2 Wide stance squat

Joint angles

Correlation between sides

Table 12: correlations of joint angles between right and left side of wide squat.

	Hip Flex-Ext	Hip Abd-Add	Hip Rotation	Knee Flex-Ext	Ankle Flexion
Correct	1,000	0,984	0,988	0,999	0,996
RB	0,999	0,980	0,984	0,999	0,997
KOT	1,000	0,987	0,988	0,998	0,992
VK	0,999	0,959	0,987	0,999	0,996

Symmetry was demonstrated for each joint and for each angle with a correlation greater than 0.9. Thus, for simplicity, following results are reported considering the right side.

Max joint angles

Table 13: max joint angle of wide squat [°] (right side).

	Hip Flexion	Hip Abduc	Hip Intrarot	Knee Flexion	Ankle Dorsi-f	Lumbar Flexion	Pelvis Antev
Correct	121,99	41,59	20,51	132,43	38,56	18,21	33,42
RB	116,95	43,92	14,21	129,91	40,00	28,83	41,86
KOT	105,94	32,26	6,11	116,78	39,56	26,02	28,38
VK	107,35	37,40	10,62	128,88	41,12	24,15	28,66

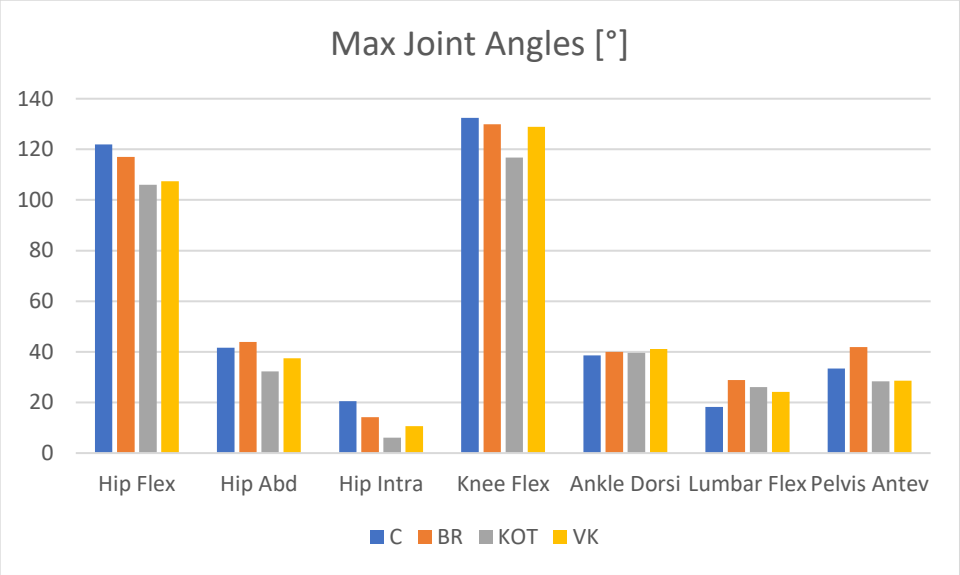

Figure 52: bar graph of max joint angles of wide squat (right side).

Ranges of Motion

Table 14: ranges of motion of joint of wide squat [°] (right side).

	Hip Flexion	Hip Abduc	Hip Intrarot	Knee Flexion	Ankle Dorsi-f	Lumbar Flexion	Pelvis Antev
Correct	120,60	30,18	74,97	132,00	39,59	18,00	30,53
RB	123,56	31,33	64,76	133,01	38,62	17,99	43,67
KOT	112,98	22,85	58,48	115,06	36,11	11,06	33,70
VK	109,23	25,32	58,40	129,90	41,23	15,14	29,76

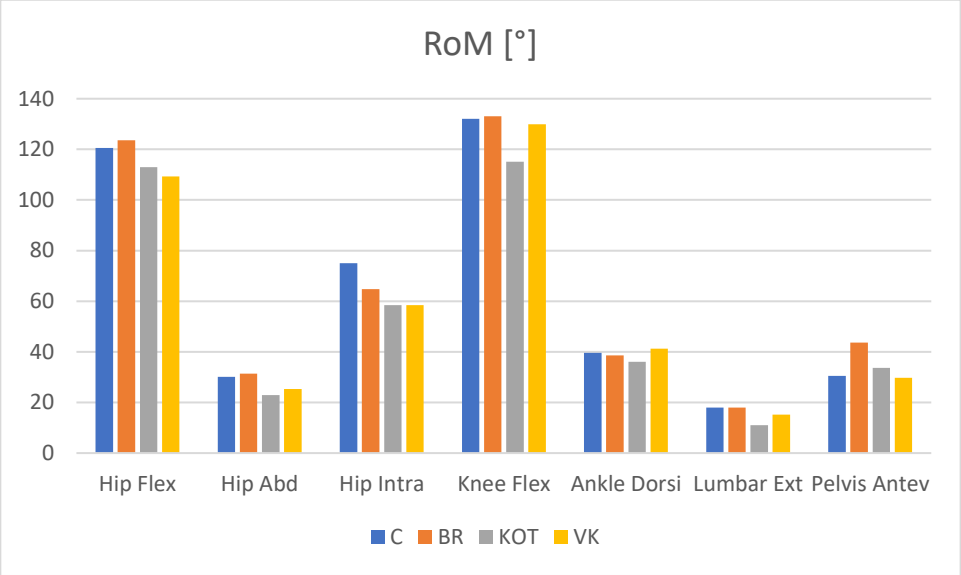

Figure 53: bar graph of ranges of motion of wide squat (right side).

Mean joint angles

Table 15: mean joint angles of wide squat [°] (right side).

	Hip Flexion	Hip Abduc	Hip Intrarot	Knee Flexion	Ankle Dorsi-f	Lumbar Flexion	Pelvis Antev
Correct	75,27	32,43	13,10	81,04	26,96	9,42	18,96
RB	67,94	31,31	20,14	69,89	21,56	19,58	19,49
KOT	64,49	26,39	17,87	74,93	28,40	19,59	16,30
VK	64,54	24,34	12,85	77,30	26,96	17,02	14,40

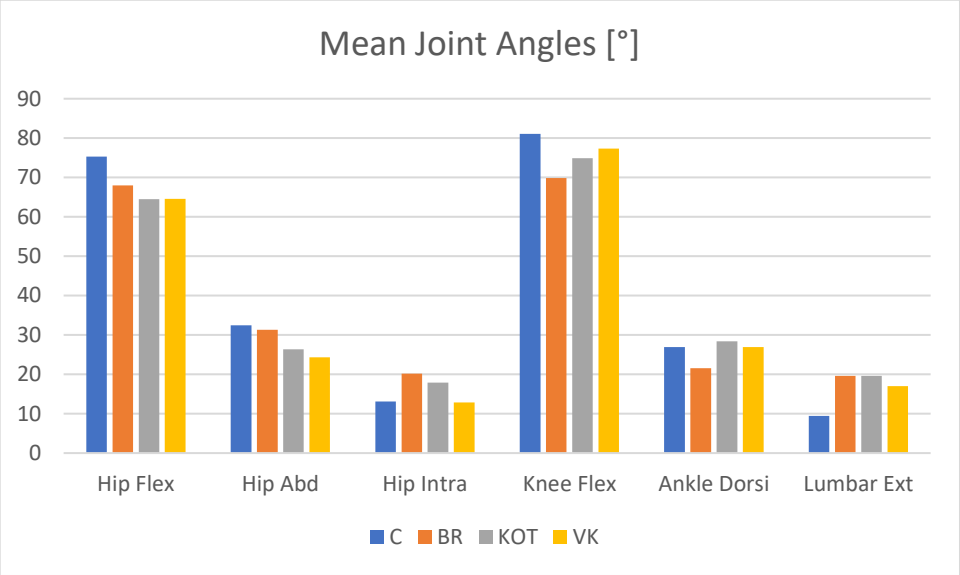

Figure 54: bar graph of mean joint angles of wide squat (right side).

Wilcoxon-Mann-Whitney

Differences with $p < 0.05$ for each joint angle were found, except for hip extension of VK.

Joint Moments

Correlation between sides

Table 16: correlation of joint moments between right and left side of wide squat.

	Hip Flex-Ext	Hip Abd-Add	Hip Rotation	Knee Flex-Ext	Ankle Flexion
Correct	0,986	0,978	0,993	0,995	0,831
RB	0,994	0,905	0,991	0,993	0,769
KOT	0,987	0,835	0,948	0,992	0,940
VK	0,993	0,090	0,953	0,993	0,910

Symmetry was demonstrated for each joint and for each angle with a correlation greater than 0.8, except for ankle flexion of RB (0,769). Thus, for simplicity, following results are reported considering the right side.

Max joint moments

Table 17: max joint moments of wide squat [N*m/kg] (right side).

	Hip Extens	Hip Abduc	Hip Intrarot	Knee Extens	Ankle Plant-f	Lumbar Extens	Pelvis Retrov
Correct	0,88	0,41	0,32	0,93	0,37	1,37	0,20
RB	1,30	0,43	0,50	1,06	0,38	2,27	0,33
KOT	1,12	0,34	0,30	0,83	0,58	1,77	0,57
VK	0,85	0,21	0,19	1,02	0,37	1,53	0,16

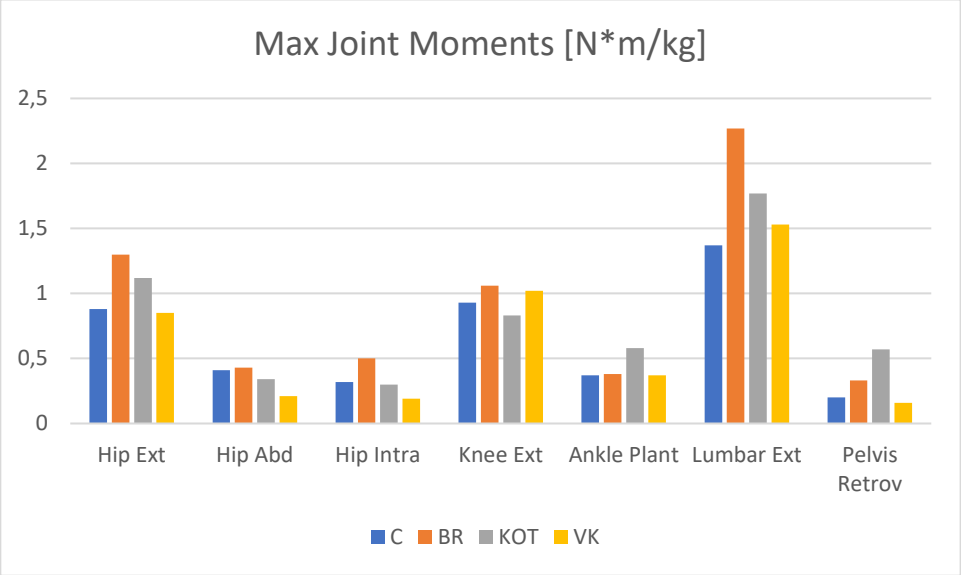

Figure 55: bar graph of max joint moments of wide squat (right side).

Mean joint moment

Table 18: mean joint moments of wide squat [N*m/kg] (right side).

	Hip Extens	Hip Abduc	Hip Intrarot	Knee Extens	Ankle Plant-f	Lumbar Extens	Pelvis Retrov
Correct	0,51	0,23	0,08	0,61	0,28	0,97	0,11
RB	0,67	0,19	0,16	0,47	0,26	1,33	0,16
KOT	0,67	0,23	0,14	0,55	0,36	1,31	0,11
VK	0,55	0,12	0,05	0,61	0,26	1,08	0,11

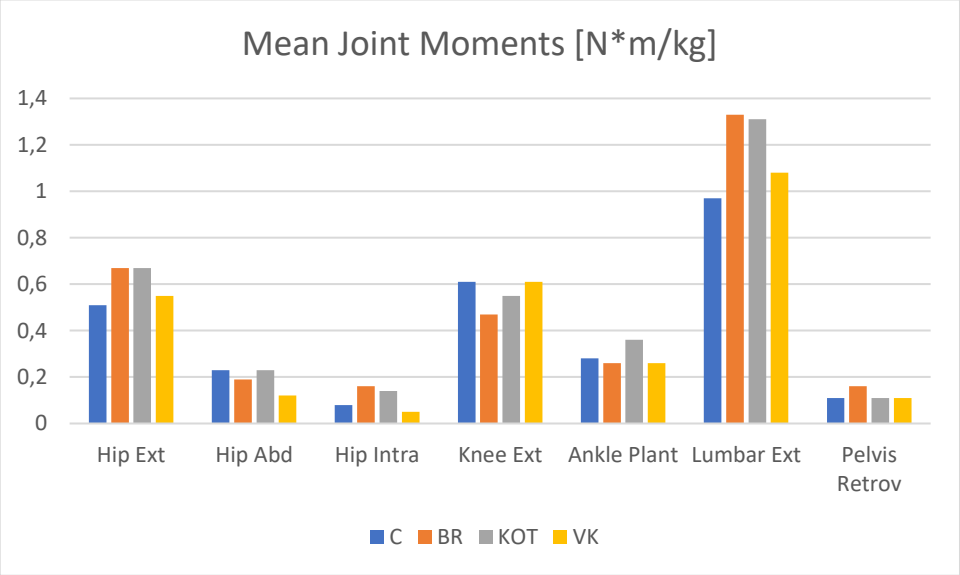

Figure 56: bar graph of mean joint moments of wide squat (right side).

Wilcoxon-Mann-Whitney

Differences with $p < 0.05$ for each joint moment were found, except for:

- hip adduction of KOT
- knee flexion and pelvic retroversion of VK

Max muscle forces

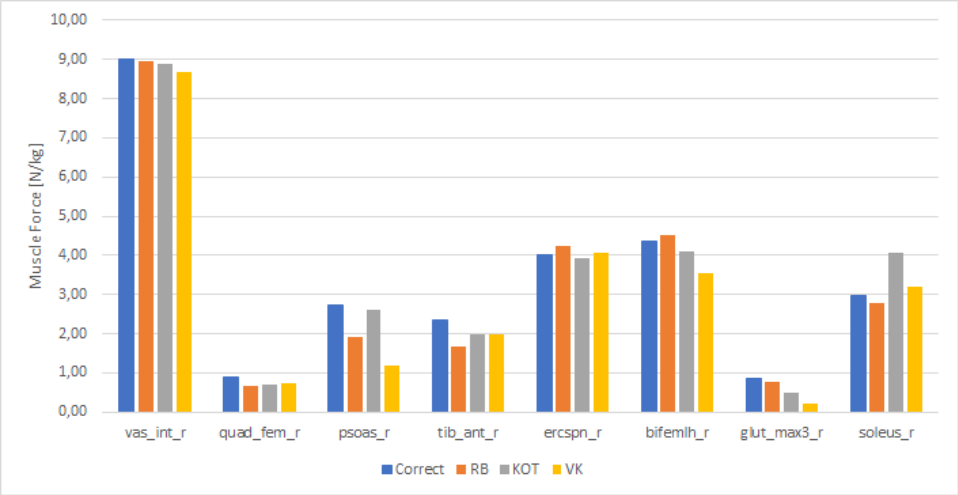

Figure 57: max muscle forces of wide squat (right leg).

Similarly to squat, wide squat alterations were evident especially considering performances with rounded back and overcoming toes with knees. Hip and lumbar joints resulted overloaded, while knee joint underloaded.

4.2.3 Deadlift

Joint angles

Correlation between sides

Table 19: correlations of joint angles between right and left side of deadlift.

	Hip Flex-Ext	Hip Abd-Add	Hip Rotation	Knee Flex-Ext	Ankle Flexion
Correct	0,999	0,929	0,852	0,993	0,968
RB	0,997	0,882	0,984	0,986	0,980
KOT	0,999	0,834	0,945	0,998	0,985
BH	1,000	0,928	0,961	0,996	0,952

Symmetry was demonstrated for each joint and for each angle with a correlation greater than 0.8. Thus, for simplicity, following results are reported considering the right side.

Max joint angle

Table 20: max joint angle reached during lifting of deadlift [°] (right side).

	Hip Flexion	Hip Abduc	Hip Intrarot	Knee Flexion	Ankle Dorsi-f	Lumbar Flexion	Pelvis Antev
Correct	15,26	8,99	51,80	1,26	3,16	16,67	12,40
RB	13,99	7,72	54,60	4,17	2,90	20,79	12,94
SB	8,18	7,25	43,32	0,42	1,86	17,75	6,97
HB	31,59	13,14	51,84	9,01	6,69	14,65	28,90

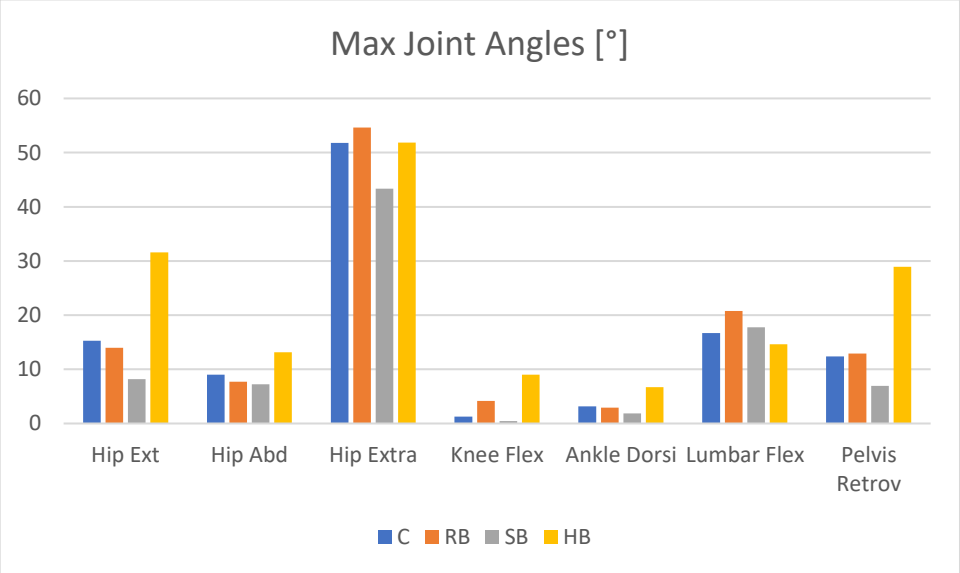

Figure 58: bar graph of max joint angles reaching during lifting of deadlift (right side).

Range of motion

Table 21: ranges of motion of joint of deadlift [°] (right side).

	Hip Flexion	Hip Abduc	Hip Intrarot	Knee Flexion	Ankle Dorsi-f	Lumbar Flexion	Pelvis Antev
Correct	117,48	16,73	39,09	73,15	20,97	8,29	59,62
RB	89,86	15,97	28,36	39,39	9,71	21,56	59,22
SB	90,12	13,31	22,64	50,90	14,36	21,89	61,45
HB	121,47	11,64	34,21	57,33	13,30	12,70	70,80

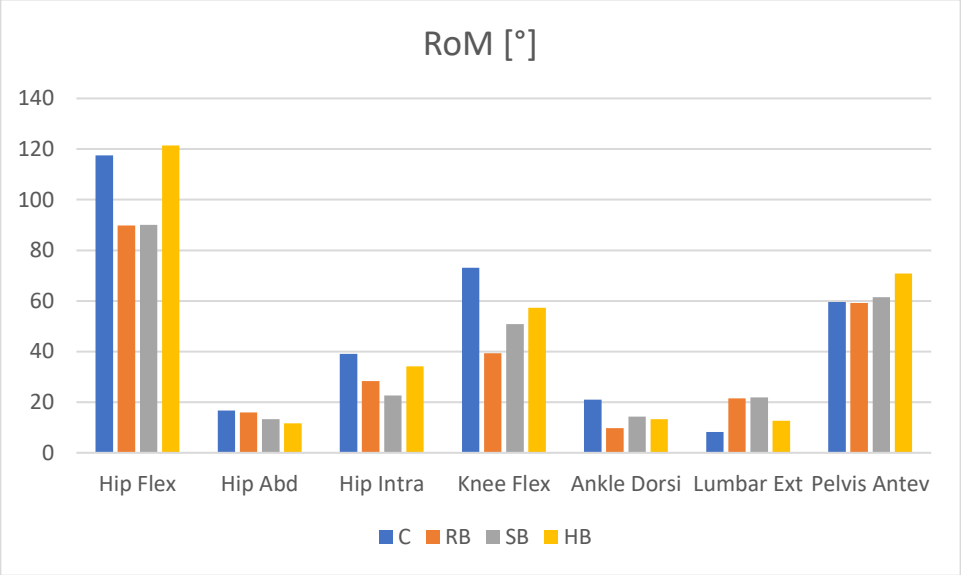

Figure 59: bar graph of ranges of motion of joint of deadlift (right side).

Mean joint angles

Table 22: mean joint angles of deadlift [°] (right side).

	Hip Flexion	Hip Abduc	Hip Intrarot	Knee Flexion	Ankle Dorsi-f	Lumbar Flexion	Pelvis Antev
Correct	37,21	18,10	36,08	33,02	11,98	19,84	15,63
RB	23,96	16,59	41,99	20,20	6,96	32,70	11,33
SB	33,78	13,86	32,95	19,29	7,07	27,75	18,86
HB	20,60	18,42	39,90	27,82	11,23	21,69	4,62

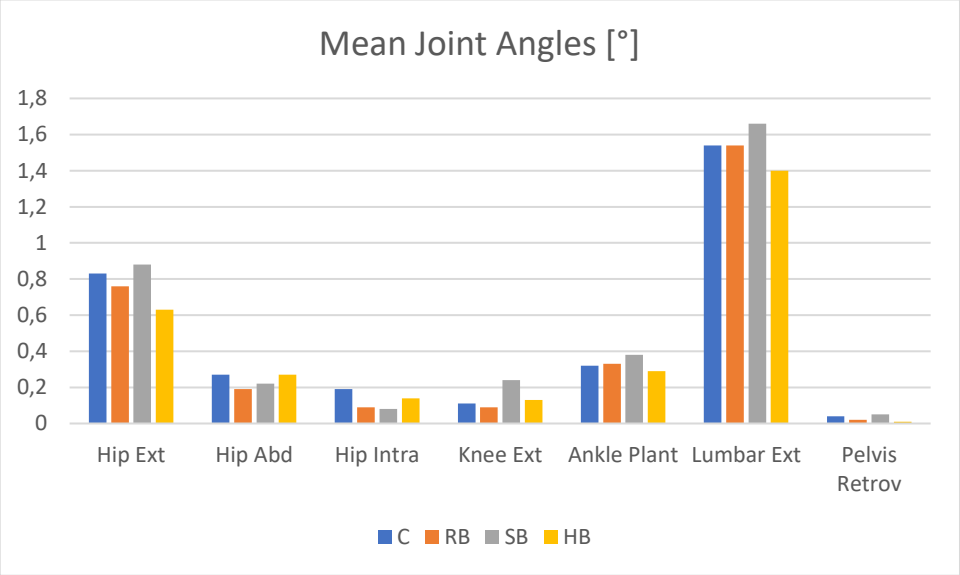

Figure 60:bar graph of mean joint angles of deadlift (right side).

Wilcoxon-Mann-Whitney

Differences with $p < 0.05$ for each joint angle were found, except for:

- hip extension of SB
- hip abduction and ankle dorsi-flexion of HB

Joint Moments

Correlation between sides

Table 23: correlation of joint moments between right and left side of deadlift.

	Hip Extension	Hip Adduction	Hip Extrarot	Knee Flexion	Ankle Plantaflex
Correct	0,997	0,854	0,997	0,942	0,995
RB	0,995	0,852	0,952	0,914	0,962
SB	0,995	0,908	0,978	0,887	0,988
HB	0,993	0,090	0,953	0,993	0,910

Max joint moments

Table 24: max joint moments of deadlift [N*m/kg] (right side).

	Hip Extens	Hip Abduc	Hip Intrarot	Knee Extens	Ankle Plant-f	Lumbar Extens	Pelvis Retrov
Correct	0,11	0,15	0,06	0,17	0,11	0,73	0,04
RB	0,11	0,09	0,04	0,24	0,17	0,75	0,16
SB	0,18	0,12	0,06	0,45	0,13	0,72	0,34
HB	-0,08	0,14	0,05	0,01	0,17	0,66	0,27

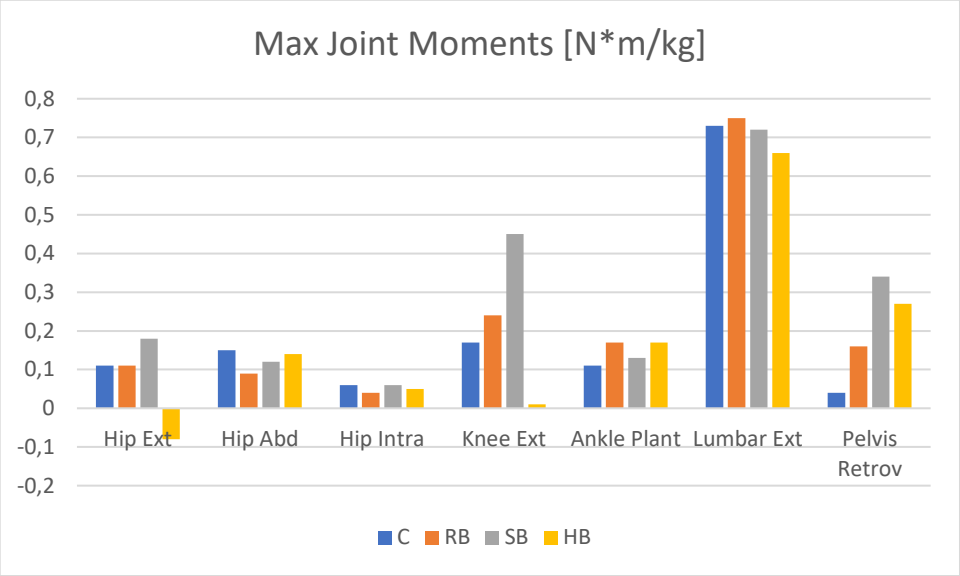

Figure 61: bar graph of max joint moments of deadlift (right side).

Mean joint moments

Table 25: mean joint moments of deadlift [N*m/kg] (right side).

	Hip Extens	Hip Abduc	Hip Intrarot	Knee Extens	Ankle Plant-f	Lumbar Extens	Pelvis Retrov
Correct	0,83	0,27	0,19	0,11	0,32	1,54	0,04
RB	0,76	0,19	0,09	0,09	0,33	1,54	0,02
SB	0,88	0,22	0,08	0,24	0,38	1,66	0,05
HB	0,63	0,27	0,14	0,13	0,29	1,40	0,01

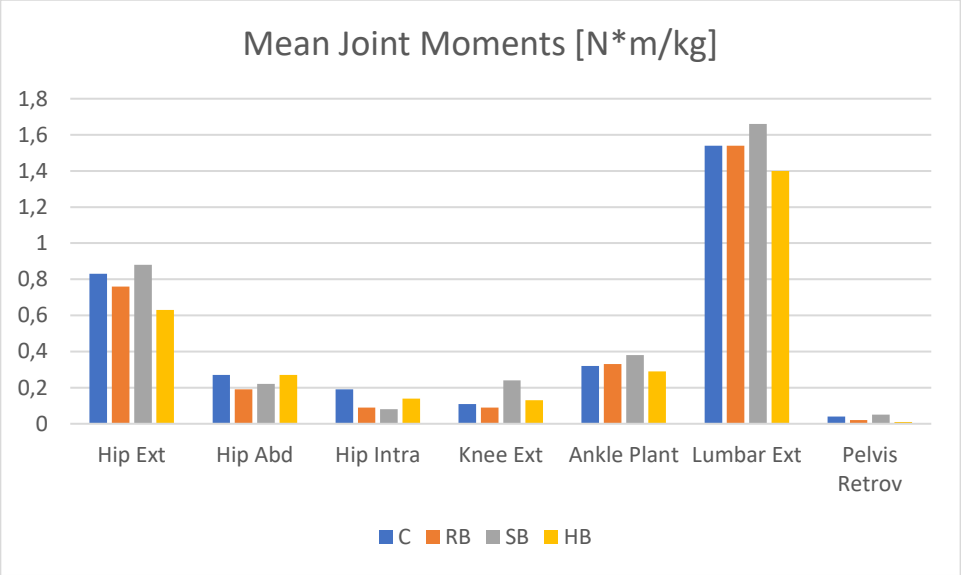

Figure 62: bar graph of mean joint moments of deadlift [N*m/kg].

Wilcoxon-Mann-Whitney

Differences with $p < 0.05$ for each joint angle were found, except for:

- ankle plantar - flexion of RB
- Hip adduction of HB

Max muscle forces

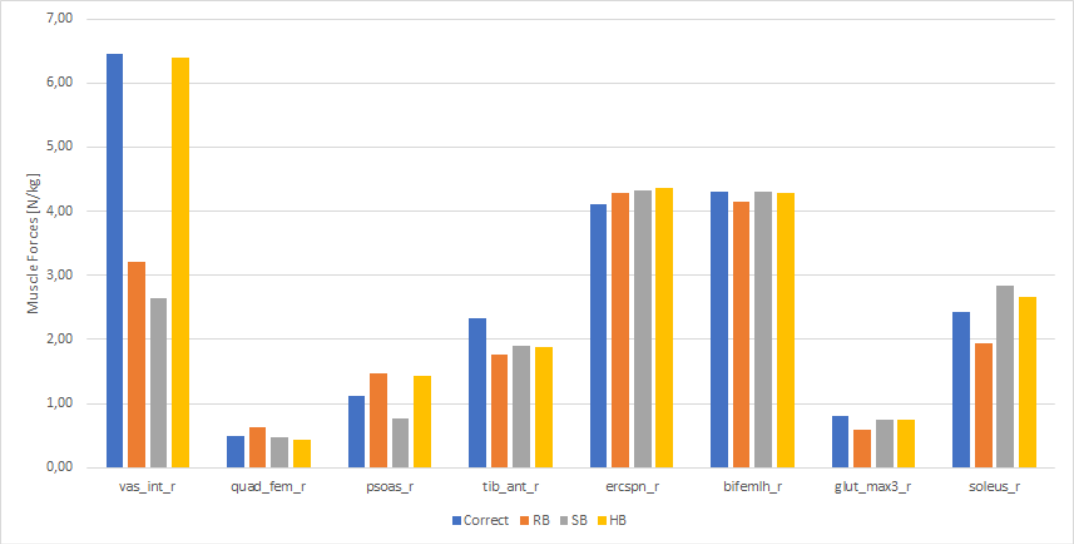

Figure 63: max muscle forces of deadlift (right side).

Comparing deadlift performances, the main differences were seen by starting with the bar detached from the body and hyperextending the back. The first one caused higher hip, knee and lumbar joint moments. Furthermore, HB could lead to decrease hip extension moment until it inverts sign. In fact, as it is possible to see in in figure 62, at the end of lifting internal extensor moment became flexor moment. As concern muscle forces, the main differences are seen for vastus intermediate, whose activations is lower for RB and SB.

4.3 Weightlessness simulation and optimal BWR

Results of weightlessness simulations in zero gravity conditions with different BWRs are now presented. Figures below shown examples about how peak joint moments change in these conditions. Values refer to correct squat, wide squat and deadlift exercises simulated basing on kinematics of subject S1.

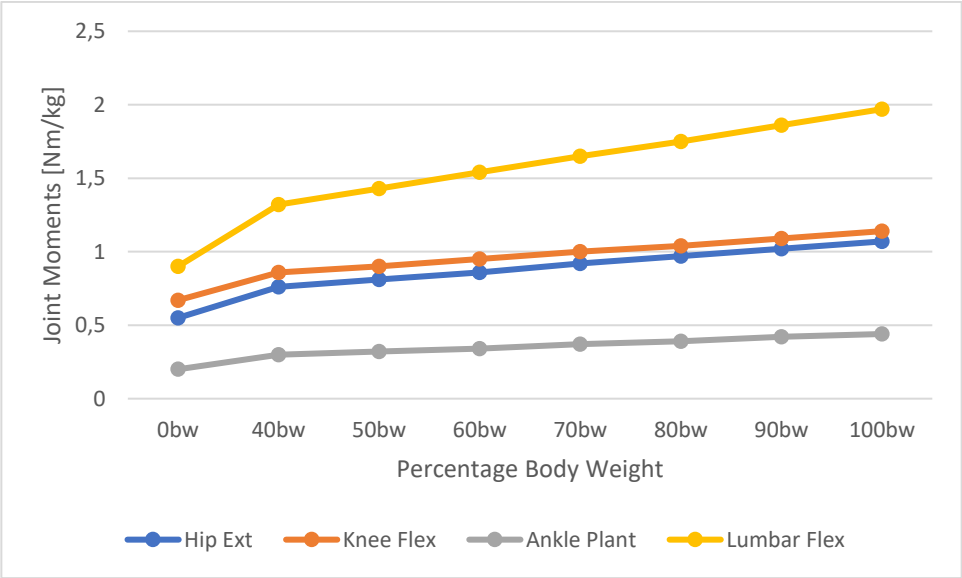

Figure 64: normalized peak joint moments for different BWR of squat.

Figure 65: normalized peak joint moments for different BWR of wide squat

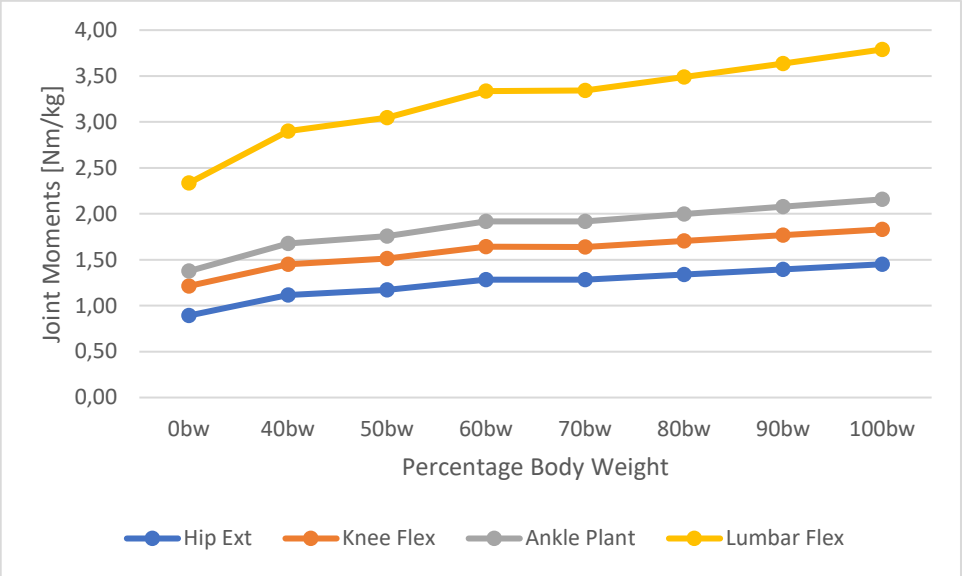

Figure 66: normalized peak joint moments for different BWR of deadlift.

It was possible to see that joint moments in weightlessness increase proportionally to the increment of BWR load on shoulders. Independently from the exercise, lumbar joint had greater slope; this suggested that back is more subjected to injuries and special attention should be paid applying the proper load in 0G. Considering deadlift, it showed greater values of lumbar joint, almost two times the values of squat and wide squat lumbar joint. These results are intuitively related to the fact that deadlift involves the posterior kinematic chain, while squat and wide stance squat the anterior one. Therefore, by applying the same BWR load for each exercise, training effectiveness could be compromised or risk of injuries could be increased.

Following, results of regression models computed in order to find the optimal body weight replacement are reported. Each paragraph refers to one exercise type and contains two tables: one for optimal BWR considering mean joint moments and one considering max joint moments. Values of each subject was computed by averaging results of right and left legs. Please, see the appendix A for tables specifying results obtained for each joint of each subject, with right and left sides separated. The R^2 values were 0.99 for all regression functions found.

4.3.1 Normal stance squat

Table 26: optimal BWR considering mean joint moments of squat [% BW]

	Hip Flexion	Knee Flexion	Ankle Flexion	Lumbar Flexion
S1	65	89	96	40
S2	56	80	96	47
Mean	**60,50**	**84,50**	**96,00**	**43,50**
Std Dev	**6,36**	**6,36**	**0,00**	**4,95**

Table 27: optimal BWR considering max joint moments of squat [% BW]

	Hip Flexion	Knee Flexion	Ankle Flexion	Lumbar Flexion
S1	67	91	97	37
S2	50	86	99	49
Mean	**58,25**	**88,25**	**97,75**	**43,00**
Std Dev	**12,37**	**3,89**	**1,06**	**8,49**

These results were within the ranges found by DeWitt *et al.* (2011): 66.77±4.92% for hip, 88±4.17% for knee and 96.05±1.26% for ankles; only the mean of hip joint was slightly lower. This confirmed as the actual load applied (70-75%) could be suitable for hip joint, but it may underload knee and ankle joints and could be dangerous for lumbar joint.

4.3.2 Wide stance squat

Table 28: optimal BWR considering mean joint moments of wide squat [% BW]

	Hip Flexion	**Knee Flexion**	**Ankle Flexion**	**Lumbar Flexion**
S1	87	100	90	77
S2	71	72	97	33
Mean	**78,75**	**85,75**	**93,25**	**55,00**
Std Dev	**11,67**	**20,15**	**5,30**	**31,11**

Table 29: optimal BWR considering max joint moments of wide squat [% BW]

	Hip Flexion	**Knee Flexion**	**Ankle Flexion**	**Lumbar Flexion**
S1	69	83	95	55
S2	67	90	100	32
Mean	**68,00**	**86,25**	**97,25**	**43,50**
Std Dev	**1,41**	**4,60**	**3,18**	**16,26**

The simulations and the regression model revealed that wide squat would require greater load than squat for hip joint (78.75±11,75 against 60.5±6.36 considering mean joint moments). The same considerations regarding the other joints reported for squat can be extended for wide squat. Furthermore, observing lumbar joint, considerable differences between the subjects could be noticed. This might confirm as training protocol should be properly adapted for each crewmember.

4.3.3 Deadlift

Table 30: optimal BWR considering mean joint moments of deadlift [% BW]

	Hip Flexion	Knee Flexion	Ankle Flexion	Lumbar Flexion
S1	80	97	94	100
S2	82	100	98	28
Mean	**80,50**	**98,25**	**95,50**	**64,00**
Std Dev	**1,41**	**2,47**	**2,83**	**50,91**

Table 31: optimal BWR considering max joint moments of deadlift [% BW]

	Hip Flexion	Knee Flexion	Ankle Flexion	Lumbar Flexion
S1	74	91	95	100
S2	77	78	98	39
Mean	**75,50**	**84,25**	**96,50**	**69,50**
Std Dev	**2,12**	**8,84**	**2,12**	**43,13**

In the end, regression analysis of deadlift supported the considerations done in the previous paragraphs. The current BWR adopted could be too high for lumbar joint and too small for knee and ankle joints. Furthermore, differences between subjects for lumbar joint were evident, suggesting that training protocol could be individually adapted.

4.4 Accelerations analysis

In this subchapter, results of machine learning algorithms for binary classification applied in this work are reported. Each paragraph is dedicated to one exercise type.

4.4.1 Squat

The original dataset, containing 302 features for each entry, was reduced with PCA to 12 features. The hidden layer of ANN was composed by 10 neurons and was trained with 80% of data, validated with 5% of data and tested with the remaining 15%. A single entry corresponded to one repetition that was opportunely labeled as 0 if related to incorrect execution and 1 if correct. A total of 38 observations were used, where correct repetitions were 8 and wrong repetitions were 30. Therefore, the network was tested using 6 entries randomly chosen. SVM was trained and tested with 75% and 25% of data respectively (28 and 10 observations). Below, confusion matrixes of ANN and SVM resulting from testing phase. It was observed a greater accuracy for the second method (88%) than the first one (83.3%).

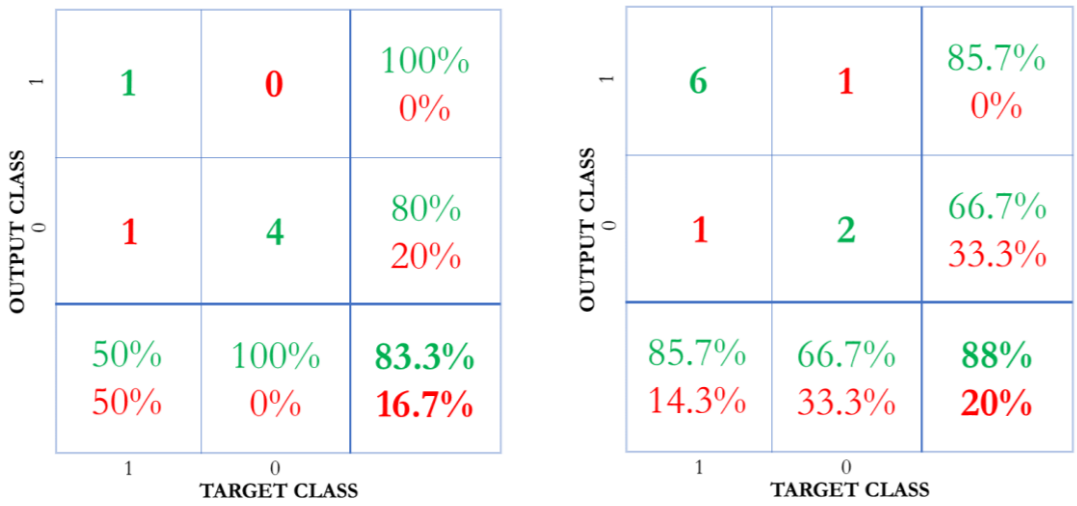

Figure 67: (a) ANN confusion matrix of test set of squat; (b) SVM confusion matrix of test set of squat. Green values refer to correct classification, red values refer to incorrect classification. 1 and 0 are the two classes, which identify correct technique and incorrect one respectively.

4.4.2 Wide stance squat

For wide squat, the original dataset was reduced to 9 features with PCA. The hidden layer of ANN was composed by 5 neurons and was trained, validated and tested with the same percentages used for squat (80%, 5% and 15% respectively). A single entry was opportunely labeled with 0 (incorrect) and 1 (correct). The number of observations utilized was 27, where 8 were correct repetitions and 19 were wrong repetitions. Thus, the network was tested using 4 entries randomly chosen. As done for squat, SVM was trained and tested with 75% and 25% of data respectively (20 and 7 observations). Below, confusion matrixes of ANN and SVM resulting from testing phase. It was observed a similar accuracy comparing the two methods, slightly greater for ANN (75% against 71.4% for SVM).

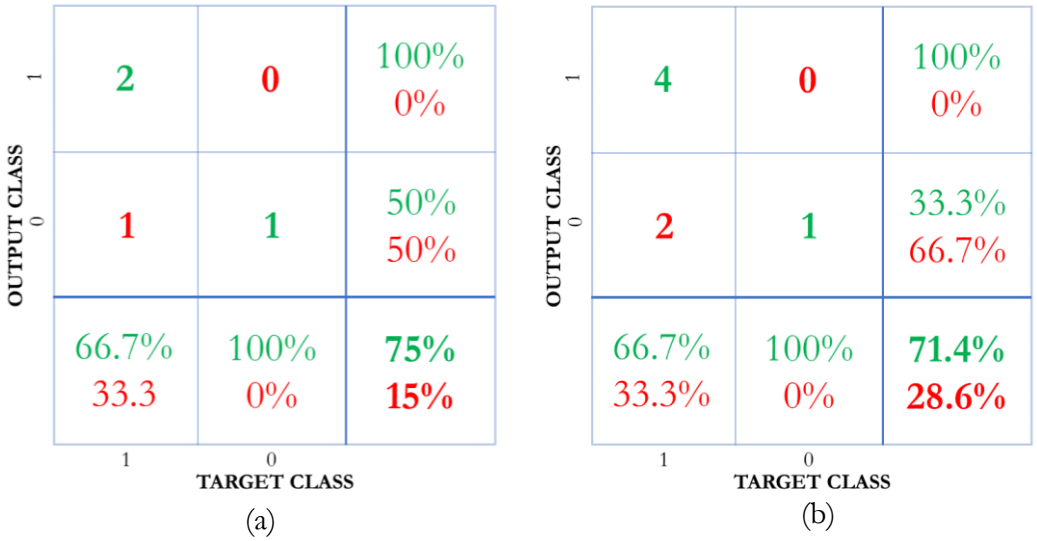

Figure 68: (a) ANN confusion matrix of test set of wide squat; (b) SVM confusion matrix of test set of wide squat. Green values refer to correct classification, red values refer to incorrect classification. 1 and 0 are the two classes, which identify correct technique and incorrect one respectively.

4.4.3 Deadlift

In the end, the same was done for deadlift. PCA consented to reduce the original number of features from 302 to 10. The hidden layer of ANN was composed by 5 neurons and, again, was trained with 80% of data, validated with 5% of data and tested with 15% of data. A total of 25 observations were used, with 7 correct repetitions and 18 wrong repetitions. Therefore, the network was tested using 5 entries randomly chosen. SVM was trained and tested with 20 and 7 examples respectively. Below, confusion matrixes of ANN and SVM resulting from testing phase. As for squat, SVM gave better results in terms of accuracy then ANN (85.7% against 60%).

Figure 69: (a) ANN confusion matrix of test set of deadlift; (b) SVM confusion matrix of test set of deadlift. Green values refer to correct classification, red values refer to incorrect classification. 1 and 0 are the two classes, which identify correct technique and incorrect one respectively.

CHAPTER 5
CONCLUSIONS AND FUTURE WORKS

In this work, an OpenSim biomechanical model was used to simulate countermeasure target exercises performed on ISS by astronauts during missions. Training is essential to reduce the effects of musculo-skeletal system deconditioning due to weightlessness, but it could be equally dangerous or not useful if performed with inappropriate techniques or applying inadequate loads.

Waiting for the transfer of data collected at NASA JSC of six subjects performing exercises with ARED, the model was validated with data collected at Politecnico di Milano during this Thesis. These included kinematics and dynamics data of target exercises (squat, wide squat and deadlift) performed by two subjects in different configurations of execution, correct and incorrect, with a barbell and weights. This permitted to conduct a biomechanical analysis highlighting risks of injuries and inefficacy of training that could occur with wrong performances. Furthermore, the model was used to simulate correct exercises in weightlessness with different percentages of body weight added on the shoulders. With a regression model, it was computed the optimal body weight replacement to use on ISS in order to replicate the joint loads obtained on Earth. In the end, simulation of inertial sensors put on different body points of the model provided accelerations of those points. These data were used to develop the basis of a system based on machine learning algorithm to monitor training of astronauts. Different features in time and frequency domains were extracted from each set of accelerations data, whose

dimension was reduced with principal component analysis. Two supervised learning methods, feed-forward artificial neural network and support vector machine, were used for a binary classification of correct and incorrect executions.

From the results regarding the comparisons between correct and wrong performances of target exercises, the hypothesis of not equality in terms of joint angles and joint moments was statistically demonstrated. Therefore, the chosen categories of incorrectness can be considered suitable to characterize biomarkers, which will anticipate risk of musculo-skeletal damage due to joint overloading and risk of training inefficacy caused by joint underloading. In particular, rounding the back, rising heels and overcoming toes with knees in squat and wide squat showed the most evident increases of hip and lumbar joints, which may evoke classical back pain perceived by astronauts and/or enforce the one due to the natural stretching of spine deriving from weightlessness. Muscle forces estimated with OpenSim partially supported these considerations and induced to endorse the hypothesis of training inefficacy by performing shallow squat. Considering deadlift, the most critical values resulted from exercise performed by starting with the bar away from the body and by hyperextending the back at the end of lifting. These produced higher hip, knee and joint moments than the ones of correct executions, revealing overweight of the joints, with the possible aforementioned consequences.

In order to further support these results, the number of subject tested should be increased. Furthermore, OpenSim estimates muscle forces basing on parameters including maximum contraction speed and optimal force, which could be measured under stress and adapted to the model. Alternatively, analysis can be carried out by using electromyographs.

Considering the evaluations conducted with the regression model to identify the optimal body weight replacement, squat results were compared with the ones found in literature (DeWitt *et al.,* 2011). It is possible to sustain that current BWR (70-75%) used is suitable for hip joint, but it might underload knee and ankle joints. Additionally, in this work evaluations related to lumbar joint were carried out, with the hypothesis that a possible overload could involve incorrect use of muscles of trunk and may induce back pain.

Results revealed as this joint is overstressed, augmenting risk of injuries. Before now, any investigations about optimal BWR for wide stance squat and deadlift were performed. Basing on the related results, wide stance squat has analog needs as squat, with the exception of hip joint that requires slightly higher BWR. Instead, deadlift wants higher BWR load to replicate 1G scenario for all joints, except for lumbar joint. Overall, find a single value could not be adequate in order to have excellent training. Firstly, one subject may need of different percentage in respect to another, so it could be appropriate to create a biomechanical model for each one and to perform simulation to reach the individual optimal load. Furthermore, each joint requires not the same values and the entire weight is applied on the shoulders, which can be too high to be endured and may cause discomfort. Great differences in the optimal BWR between lower body joints and upper body joint (lumbar) were seen, so it could be opportune to think to another way to better distribute the load with the aim to reduce that on the shoulders without underloading leg joint moments.

The acceleration analysis laid the basis for the development of the machine learning algorithm to classify correctness and incorrectness of exercise performances. Combining PCA with ANN or SVM can be considered as a working solution.

The findings of this study have to be considered in the light of some limitations. First of all, the number of subjects should be increased to conduct simulations and further support the final considerations. Furthermore, kinematics and kinetics of exercises performed using a barbell with weights were assumed to be the same of the ones obtainable with ARED. Data collected at NASA JSC, arrived during the final writing phase of this work, will permit to evaluate correlations between data and to prove this hypothesis. Subsequently, the same procedure used in this project to simulate inertial sensors will be adopted to create individual biomechanical models and to extract acceleration data. These data will enlarge the dataset containing correct exercises executions, useful to train the classifier. Then, accelerometers will be bought and used to collect large amount of data related to both correct and wrong exercise executions in order to refine the machine learning algorithm developed.

Some astronauts have already given their approval to conduct in-flight data collection during training in the next missions, once the new MOCAP system will be installed. These data will contribute to improve the weightlessness simulations, to conduct subject specific biomechanical analysis and to test the classifier with real 0G kinematics.

BIBLIOGRAPHY

Abadie, L. J., Lloyd C. W., Shelhamer, M. J. Gravity, NASA Human Research Program, "Who Needs It? NASA studies your body in space". *https://www.nasa.gov/hrp*, Nov. 16, 2015.

Braidot, A. A. A, Brusa, M. H., Lestussi, F. E., Parera, G. P., "Biomechanics of Front and Back Squat exercises". Article in *Journal of Physics Conference Series*, December 2007. DOI: 10.1088/1742-6596/90/1/012009.

Chernbumroong, S., Cang, S., Atkins, A., Yu, H., "Ederly activities recognition and classification for applications in assisted living". *Expert Systems with Applications*. 2013 1662–1674. DOI:10.1016/j.eswa.2012.09.004

Comfort, P., McMahon, J. J., Soychomel, T. J. "Optimizing Squat Technique – Revisited", Article in *Strength and conditioning journal*. May 2018. DOI: 10.1519/SSC.0000000000000398.

Cucinotta F. A., Durante, M., "Cancer Risk from exposure to galactic cosmic rays-implications for human space exploration". *The Lancet Oncol.* 2006 May; 7(5) 431-435. doi.org/10.1016/S1470-2045(06)70695-7.

Cucinotta, F. A., Kim, M. H. Y, Chappell, L. J., Huff, J. L., "How safe is safe enough? Radiation risk for a human mission to Mars". *PLoS ONE*. October 16, 2013. 8: e74988. doi: 10.1371/journal.pone.0074988.

Demontis, G. C., Germani, M. M., Caiani, E. G., Barravecchia, I., Passino, C., Angeloni, D., "Human pathophysiological adaptations to the space environment". *Front. Physiol.*

2017. 8:547. doi: 10.3389/fphys.2017.00547.

DeWitt, J. K., Fincke, R. S., Logan, R. L., Guilliams, M. E., Ploutz-Syder, L. L., "Load variation influences on joint work during squat exercise in reduced gravity". 2011.

Donnelly, E. H., Nemhauser, J.B., Smith, J. M., Kazzi, Z.N., Farfán, E. B., Chang, A.S., Naeem, S. F., "Acute radiation syndrome: assessment and management". *South. Med. J.* 2010 Jun; 103, 541–546. doi: 10.1097/SMJ.0b013e3181ddd571.

Erdas, C. B., Atasoy, I., Koray, A., Ogul, H., "Integrating geatures for accelerometer-based activity recognition". *Procedia Computer Science* 98, 2016, 522 – 527.

Farkas, I., Doran, E., "Activity recognition from acceleration data collected with a tri-axial accelerometer". Acta *Techinca Napocensis. Electronics and Telecommunications*. Volume 52, Number 2, 2011.

Ferchette, A. ARED Photo/TV Reference Document. *ESA Standard Document*. 2017.

Ferrando, A.A., Lane, H.W., Stuart, C.A., Davis-Street, J., Wolfe, R.R., "Prolonged bed rest decreases skeletal muscle and whole body protein synthesis*". AM J Physiol.* 1996. DOI: 10.1152/ajpendo.1996.270.4.E627.

Ferrigno, G., Pedrocchi, A., Baroni, G., Zolesi, V., Bracciaferri, F., Pedotti, A. "Elite S2 – A new instrument for multifactorial movement analysis on the international space station". *54th International Astronautical Congress of the International Astronautical Federation, the International Academy of Astronautics, and the International Institute of Space Law*. 29 September - 3 October 2003.

Fregly, B. j., Fregly, C. D., Kim, B. T., "Computational Prediction of Muscle Moments During ARED Squat Exercise on the International Space Station". *Journal of Biomechanical Engineering*. Decembre 2015, Vol. 137

Hargens, A. R., Bhattacharya, R., Shneider, S. M., "Space physiology VI: exercise, artificial gravity, and conuntermeasure development for prolonged space flight". *Eur J. Appl. Physiol.* 2019, Sept; 113:2183-2192. DOI: 10.1007/s00421-012-2523-5.

J. Kavanagh and H. B. Menz, "Accelerometry: a technique for quantifying movement patterns during walking," *Gait & posture, vol.* 28, no. 1, pp. 1–15, 2008.

Jang, J., Wang, J., Chen, Y., "Using acceleration measurements for activity recognition: An effective learning algorithm for constructing neural classifiers". *Pattern Recognition Letters* 2008 2213–2220.

Kazi, S. B., Sikander, S., Yousafzai, S., Mazhar, S., Khan, G. I., "Fall Detection Using Single Tri-Axial Accelerometer". *ASEE*. April 3-5, 2014

Kramer, L. A., Sargsyan, A. E., Hasan, K.M., Polk, J.D., and Hamilton, D. R., "Orbital and intracranial effects of microgravity: findings at 3-T MR imaging". *Radiology* 2012 Jun; 263(3):819–827, doi: 10.1148/radiol.12111986.

Lang, T., LeBlanc, A., Evans, H., Lu, Y., Genant, H., Yu, A., "Cortical and trabecular bone mineral loss from the spine and hip in long-duration spaceflight". *J Bone Miner Res.* 2004; 19(6):1006–12.

Lorenzetti, S., Ostermann, M., Zeidler, F., Zimmer, P., Jentsch, L., List, R., Taylor, W. R., Schellenberg, F. "How to squat? Effects of various stance widths, foot placement angles and level of experience on knee, hip and trunk motion and loading". *BMC Sport Science, Medicine and Rehabilitation*, 2018. DOI: 10.1186/s13102-018-0103-7.

Macias, B. R., Liu, J., Grande-Gutierrez, N., Hargens, A.R., "Intraocular and intracranial pressures during head-down tilt with lower body negative pressure". *Aviation, Space, and Environmental Medicine*. 2015 January 1; 86(1): 3-7. DOI: 10.3357/AMHP.4044.2015. PMID: 25565526.

Markin, A., Strogonova, L., Balashov, O., V. Polyakov, V., Tigner, T., "The dynamics of blood biochemical parameters in cosmonauts during long-term space flights". *Acta Astronaut*, Volume 42, Issue 1-8, January-April 1998, Pages 247–253.

Mummidivarapu, S. S., Schaffner, G., "A method for determining Body Weight Replacement during Squat Exercise in Weightlessness". *47th International Conference on Environmental Systems* ICES-2017-305 16-20 July 2017.

Myer, M., Kushner, A., Brent, J., Schenfeld, B., Hugentobler, J., Rhodri, Lloyd, Vermeil, A., Chu, D., Harbin, J., McGill, S., "The back squat: A proposed assessment for functional deficits and technical factors that limit performance". *Strength and Conditioning Journal*. December 2014. DOI: 10.1519/SSC.0000000000000103.

O'Reilly, M. A., Whelan, D. F., Ward, T. E., Delahunt, E., Caulfield, B. M. "Classification of deadlift biomechanics with wearable inertial measurement units", *Journal of Biomechanincs* 58 (2017) 155-161.

O'Reilly, M., Whelan, D., Chanialidis, C., Friel, N., Delahunt, E., Ward, T., Caulfield, B., "Evaluating Squat Performance with a Single Inertial Measurement" *IEEE 12th International Conference on Wearable and Implantable Body Sensor Networks (BSN)*. 19 October 2015. 10.1109/BSN.2015.7299380.

Petersen, N., Jaekel, P., Rosenberger, A., Weber, T., Scott, J., Castrucci, F., Lambrecht, G., Ploutz-Snyder, L., Damann, V., Kozlovskaya, I. and Mester, J., "Exercise in space: the European Space Agency approach to in-flight exercise countermeasures for long-duration missions on ISS". *Extrem Physiol. Med.* 2016, 5: 9. DOI 10.1186/s13728-016-0050-4.

Prisk, G. K., "Microgravity and the respiratory system". *Eur. Respir. J.* 2014. 43,1459–1471. doi: 10.1183/09031936.00001414.

Rad, N. M., Kia, S. M., Zarbo, C., Laarhoven, T. V., Jurman,G., Venuti, P., Marchiori, E., Furlanello, C., "Deep learning for automatic stereotypical motor movement detection using wearable sensors in autism spectrum disorders". *Signal Processing*. 14 Sept 2017. DOI: 10.1016/j.sigpro.2017.10.011.

Rizzo, A., Corsetto, P., Montorfano, G., Milani, S., Zava, S., Tavella, S., Cancedda, R., Berra, B., "Effects of long-term space flight on erythrocytes and oxidative stress of rodents", *PLoS ONE*. 012;7(3):e32361. doi: 10.1371/journal.pone.0032361.

Soro, A., Brunner, G., Tanner, S., Wattenhofer, R., "Recognition and Repetition Counting for Complex Physiscal Exercises with Deep Learning". *Sensors*. 2019, 19, 714; doi:10.3390/s19030714.

Sprager, S., Zazula, D., "A cumulant-based method for gait identification using accelerometer data with principal component analysis and support vector machine". *WSEAS Transactions on Signal Processing*. Issue 11, Volume 5, November 2009.

Trappe, S., Costill, D., Gallagher, P., Creer, A., Peters, J. R., Evans, H., Riley, D.A., Fitts, R. H., "Exercise in space: human skeletal muscle after 6 months aboard the International Space Station*". J Appl Physiol.* 2009 Apr; 106(4):1159–68. doi: 10.1152/japplphysiol.91578.2008.

Um, T. T., Babekeshizadeh, V., Kulic, D., "Exercise Motion Classificaion form Large-Scale Wearable Sensor Data Using Convolutional Neural Networks". *Conference: 2017 IEEE/RSJ International Conference on Intelligent Robots and System (IROS)*. September 2017. DOI: 10.1109/IROS.2017.8206051.

Vu, L., Kim, H., Benson, E., Amonette, W., Hanson, A., Perera, J., Rajulu, S., "Development of a Depth Camera-Based Instructional Tool for Resistive Exercise During Spaceflight". © *Springer International Publishing AG*, 2018.

Zhangm, M. and Sawchuk, A. A., "A customizable framework of body area sensor network for rehabilitation," in *Applied Sciences in Biomedical and Communication Technologies*, 2009.

Zwart, S. R., Gibson, C. R., Mader, T. H., Ericson, K., Ploutz-Snyder, R., Heer, M., *et al.* "Vision changes after spaceflight are related to alterations in folateand vitamin B-12-dependent one-carbon metabolism". *J. Nutr.* 2012 Mar, 142, 427–431. doi: 10.3945/jn.111.154245.

APPENDIX A

Input and output OpenSim files explanation

Scale Tool files

- *subject01_model.osim* is the biomechanical model which will be used for the simulation;
- *subject01_static.trc* contains coordinates of markers of a static pose;
- *ScaleMarkerSet.xml* contains coordinates of virtual marker to place on the model, which reproduce exactly the disposition of the experimental markers put on the subject during the data collection;
- *subject01_Setup_Scale.xml* is a file containing all the setting information for the Scale Tool.
- *subject01_scaled_model.osim* is the output of the Tool, so the scaled model of the specific subject.

Inverse Kinematic Tool files

- *subject01_simbody.osim* is the subject specific model obtained with scaling;
- *subject01_walk1.trc* contains experimental marker trajectories;
- *subject01_Setup_IK.xml* is a file containing all the setting information for the Tool;
- *subject01_walk1_ik.osim* is the output of the Tool, so a motion file containing the generalized coordinate trajectories computed by IK (joint angles and/or translations).

Inverse Dynamic Tool files

- *subject01_simbody.osim* is the subject specific model obtained with scaling;
- *subject01_walk1_grf.xml* is a file containing all external load data, including GRFs, moments and Center of Pressure (CoP). This file includes also the name of each force as well the names of the bodies to which they are applied;
- *subject01_walk1.mot* is the result of the IK, so a motion file containing time histories of joint angles;
- *subjec01_Setup_InverseDynamics.xml* is a file containing all the setting information for the Tool;
- *subject01_walk1_InverseDynamics_force.sto* is the output of the Tool, so a storage file containing the time histories of the net joint moments.

Residual Reduction Algorithm Tool files

- *subject01_simbody.osim* is the subject specific model obtained with scaling;
- *subject01_walk1_grf.xml* is a file containing all external load data, including GRFs, moments and Center of Pressure (CoP). This file includes also the name of each force as well the names of the bodies to which they are applied;
- *subject01_walk1.mot* is the result of the IK, so a motion file containing time histories of joint angles;
- *subjec01_Setup_RRA.xml* is a file containing all the setting information for the Tool;
- *gait2354_RRA_Actuators.xml* is a file specifying the residual and reserve actuators to be applied and their parameters, such as maximum/minimum force.
- *gait2354_RRA_Tasks.xml* is a tracking file that specifies which coordinates to track and the corresponding weights, used to determine how well a joint angle will tracks the specified joint angle from IK.
- *subject01_walk1_RRA_Kinematic_q.sto* is the output of the Tool, so a storage file containing the time histories of the net joint moments.
- *Subject01_simbody_adjusted.osim* is a model with adjusted mass properties.

Compute Muscle Control Tool files

- *subject01_simbody_adjusted.osim* is the subject specific model with adjusted mass properties obtained with RRA;
- *subject01_walk1_grf.xml* is a file containing all external load data, including GRFs, moments and Center of Pressure (CoP). This file includes also the name of each force as well the names of the bodies to which they are applied;
- *subject01_walk1_RRA_Kinematic_q.sto* is the output of RRA tool, so a storage file containing the time histories of the net joint moments.
- *subject01_Setup_CMC.xml* is a file containing all the setting information for the Tool;
- *gait2354_CMC_Actuators.xml* is a file specifying the residual and reserve actuators to be applied and their parameters, such as maximum/minimum force.
- *gait2354_CMC_Tasks.xml* is a tracking file that specifies which coordinates to track and the corresponding weights, used to determine how well a joint angle will tracks the specified joint angle from IK.
- *gait2354_CMC_ControlConstraints.xml* is a file which contains limits on model actuators, including muscles, reserve and residual actuators. Control constraints file specifies maximum and minimum excitation for each actuator.
- *subject01_simbody_controls.xml* is the output of the tool containing the excitations to individual muscles as well controls for any residual and reserve actuators.
- *subject01_simbody_forces.sto* (not shown in figure) is a file with muscle forces and reserve or residual forces and torques.

Optimal BWR of each subject and joint

Normal stance squat

Table 32: optimal BWR considering mean joint moments of squat, both sides [% BW]

	R Hip Flexion	R Knee Flexion	R Ankle Flexion	Lumbar Flexion	L Hip Flexion	L Knee Flexion	L Ankle Flexion
S1	63	90	96	40	67	88	96
S2	56	79	96	47	56	81	96

Table 33: optimal BWR considering max joint moments of squat, both sides [% BW]

	R Hip Flexion	R Knee Flexion	R Ankle Flexion	Lumbar Flexion	L Hip Flexion	L Knee Flexion	L Ankle Flexion
S1	67	91	97	37	67	91	97
S2	50	85	99	49	49	86	98

Wide stance squat

Table 34: optimal BWR considering mean joint moments of wide squat, both sides [% BW]

	R Hip Flexion	R Knee Flexion	R Ankle Flexion	Lumbar Flexion	L Hip Flexion	L Knee Flexion	L Ankle Flexion
S1	100	100	100	77	74	100	79
S2	71	70	97	33	70	73	97

Table 35: optimal BWR considering max joint moments of wide squat, both sides [% BW]

	R Hip Flexion	R Knee Flexion	R Ankle Flexion	Lumbar Flexion	L Hip Flexion	L Knee Flexion	L Ankle Flexion
S1	94	100	90	55	44	66	100
S2	64	90	100	32	70	89	99

Deadlift

Table 36: optimal BWR considering mean joint moments of deadlift, both sides [% BW]

	R Hip Flexion	R Knee Flexion	R Ankle Flexion	Lumbar Flexion	L Hip Flexion	L Knee Flexion	L Ankle Flexion
S1	78	93	93	100	81	100	94
S2	81	100	97	28	82	100	98

Table 37: optimal BWR considering max joint moments of deadlift, both sides [% BW]

	R Hip Flexion	R Knee Flexion	R Ankle Flexion	Lumbar Flexion	L Hip Flexion	L Knee Flexion	L Ankle Flexion
S1	74	90	95	100	74	91	95
S2	78	69	98	39	76	87	98